Longshore Sediment Transport

Bulk Formulas and Process Based Models

Proefschrift

ter verkrijging van de graad van doctor
aan de Technische Universiteit Delft,
op gezag van de Rector Magnificus prof. ir. K. C. A. M. Luyben,
voorzitter van het College voor Promoties,
in het openbaar te verdedigen op woensdag 9 maart 2016 om 10:00 uur

door

João Mil-Homens

natuurkundig ingenieur
Instituto Superior Técnico, Portugal
geboren te Caldas da Rainha, Portugal.

This dissertation has been approved by the
promotors: Prof. dr. ir. M.J.F. Stive and Prof. dr. ir. A.J.H.M. Reniers

Samenstelling promotiecommissie:

Rector Magnificus,	chairman
Prof. dr. ir. M.J.F. Stive,	Delft University of Technology, promotor
Prof. dr. ir. A.J.H.M. Reniers,	Delft University of Technology, promotor
Prof. dr. R.W.M.R.J.B. Ranasinghe,	The Australian National University/Unesco-IHE Delft
Independent members:	
Prof. dr. ir. J.A. Roelvink,	Unesco-IHE Delft
Prof. dr. ir. M. Larson,	Lund University, Sweden
Prof. dr. ir. W.S.J. Uijttewaal,	Delft University of Technology
Dr. ir. F. Sancho,	Laboratório Nacional de Engenharia Civil, Portugal

Prof. dr. R.W.M.R.J.B. Ranasinghe has, as supervisor, contributed significantly to the preparation of this dissertation.

The author was funded by Fundação para a Ciência e a Tecnologia (FCT), Portugal, through grant SFRH/BD/65270/2009. This grant was supported by POPH/FSE funds.

Front & Back: "The salt kingdom", Photo by Jon Wright

ISBN 978-94-6186-616-5

An electronic version of this dissertation is available at
http://repository.tudelft.nl/.

SUMMARY

Longshore Sediment Transport (LST) is one of the main drivers of beach morphology. It works at temporal scales ranging from hours to centuries and at spatial scales ranging from tens of meters to hundreds of kilometres. Episodic, large LST rates can result in important physical impacts such as inlet closure, rapid build-up of ebb/flood shoals, headland bypassing of large volumes of sand and rotation of pocket beaches. Persistent alongshore gradients in LST, however small in magnitude, could result in chronic impacts, such as coastline recession, inlet migration and ebb/flood delta depletion/accretion. In general most, if not all, of these impacts are by coastal managers generally considered as negative impacts. Perhaps the most negative impact comes from coastline recession, which poses an immediate threat to populations living in vulnerable coastal areas.

Motivated by these problems, a considerable research effort was invested on developing models to predict LST rates. Two approaches to predict LST can be roughly defined: 1) bulk transport formulas; these are explicit equations based on simplified representations of physical processes, which mostly use empirical coefficients for calibration, and 2) process based models; these include a large number of physical processes attempting to simulate LST in detail.

This research was motivated by a rather generic question: "how do results of LST bulk formulas compare with results of process based models?"The starting point was the evaluation of the most commonly used bulk formulas (CERC, Kamphuis and Bayram). The predictive skill of these bulk LST formulas was rigorously evaluated using an extensive LST data set. As a result, the calibration coefficients of the three formulas were updated resulting in a significant improvement of their predictive skill. Explaining the uncertainty, that was still observed in the predictions of the bulk formulas, was the next step. It was assumed that this uncertainty was not a result of measurement errors alone, and that factors that influence LST were not represented in bulk formulas. The research was focused on profile related factors, such as slope or presence of bars. Using a process based model LST rates were calculated in profiles showing different kinds of features and a significant dependence on several of those features was found. These results led to a new question: "which phenomena lead to the influence of profile features in LST rates?".

To answer this question, the effect of wave breaking induced turbulence on bed shear stresses was investigated and a new LST model that includes the effect of wave breaking generated turbulence was implemented. The model includes a simple turbulence model and uses a novel parametrization for the vertical decay of the wave breaking generated turbulence. Laboratory data, that include test cases with different wave breaking types were used to calibrate the model. The model was able to reproduce the differences in turbulence decay profiles between different wave breaking types and produced realistic cross-shore profiles of LST. A parameter space exploration was performed, using constant slope (“flat”) and real profiles, and it was observed that the results are in the same order of magnitude as the results of bulk formulas, and in agreement to what was expected. The model was applied to field data measured at Vluchtenburg, on the Dutch coast. This survey comprises measurements that detail the evolution of a large scale nourishment. The results of the model follow a trend that is similar to the observed data, showing higher volume losses in the period immediately after the conclusion of the nourishment.

The main results of the research are: 1) the accuracy of the three most commonly used bulk formulas (CERC, Kamphuis and Bayram) was significantly improved, 2) the accuracy is still low for several purposes but there is potential for improvement if the effect of profile features, more specifically, slope related parameters are included, 3) this effect of slope on LST was attributed to wave breaking induced turbulence that reaches the bottom and stirs sediment more efficiently than bed shear stresses caused by orbital velocity, 4) a novel parametrization for the decay of wave breaking induced turbulence, that attempts to account for this phenomenon, was implemented and tested successfully against laboratory data, and 5) an application of an LST model using this parametrization was able to produce similar trends to field data, which is evidence that this approach may be valid.

SAMENVATTING

Kustlangs sedimenttransport (English: LST) is een van de belangrijkste drijfveren van kustmorfologie. LST werkt op een tijdelijke schaal variërend van uur tot eeuw en in de ruimte, variërend van tientallen meters tot honderden kilometers. Een episodisch, hoger LST percentage zou tot belangrijke fysieke effecten kunnen leiden, zoals dichtslibben van een baai, snelle toename zandbanken onder invloed van eb/vloed, grote volumes zand, die een landtong passeren, en rotatie van door landtongen ingesloten baaien. Aanhoudend kustlangs verloop in LST, zelfs klein in grootte, kan tot langdurige effecten leiden, zoals recessie van de kustlijn, migratie van de baaien, en, respectievelijk, eb/depletie of vloed/aanwas van de delta. De meeste, zo niet alle, van deze effecten worden over het algemeen door kustbeheer als negatieve effecten beschouwd. De meest negatieve invloed is recessie van de kustlijn, wat een onvermijdelijke bedreiging vormt voor de bevolking in kwetsbare kustgebieden. Gemotiveerd door deze problematiek, is huidig onderzoek gericht op de ontwikkeling van modellen om LST te voorspellen. Twee benaderingen om LST te voorspellen kunnen grofweg worden gedefinieerd als: 1) “Bulk vervoer” formules; expliciete vergelijkingen op basis van vereenvoudigde representaties van fysieke processen, die over het algemeen gebruik maken van empirische coëfficiënten voor kalibratie, en 2) modellen op basis van processen; deze benadering omvat een groot aantal fysieke processen met behulp waarvan LST wordt gesimuleerd. Dit onderzoek werd ingegeven door een vrij algemene vraagstelling, namelijk: "hoe resultaten van LST bulk formules te vergelijken zijn met de resultaten van op processen gebaseerd modellen?"Het uitgangspunt was de evaluatie van de meest gebruikte bulk formules (CERC, Kamphuis en Bayram). Het voorspellende vermogen van deze bulk LST formules is consequent geëvalueerd aan de hand van een uitgebreide LST-dataset met als resultaat dat een kalibratie van de coëfficiënten van de drie formules is bijgewerkt, wat resulteert in een aanzienlijke verbetering van hun voorspellend vermogen. De volgende stap was de verklaring van de onzekerheid, welke nog steeds werd waargenomen in de voorspellingen van de bulk-formules. Het uitgangspunt was, dat deze onzekerheid niet slechts het gevolg was van meetfouten, en dat factoren die van invloed zijn op LST niet vertegenwoordigd waren in de bulk-formules. Het onderzoek richtte zich op de profiel-gerelateerde factoren, zoals de hellingsgraad of de aanwezigheid van zandbanken. Met behulp van een op proces gebaseerd model werd LST berekend in profielen met verschillende soorten kenmerken, en een grote afhankelijkheid van een aantal van deze functies werd gevonden. Deze resultaten hebben geleid tot een nieuwe vraag: "welke verschijnselen beïnvloeden de mate van LST?". Om deze vraag te beantwoorden werd het effect onderzocht van de turbulentie op bodem-wrijving en een nieuw LST model, met het effect van de turbulentie veroorzaakt door een golfbreker, werd uitgevoerd. Dit model omvat een eenvoudig turbulentie model en gebruikt een nieuwe parametrisatie voor het verticale verval van de door de golfbreker gegenereerde turbulentie. Laboratorium data, met testen van verschillende types golfbrekers, werden gebruikt voor het kalibreren van het model. Het model was in staat om de verschillen in de profielen met turbulentie afname tussen onderling verschillende types golfbrekers te reproduceren, en om realistische 'cross-shore' profielen van LST te produceren. Een onderzoek naar de ruimtelijke parameters, met behulp van constante helling ('vlakke') en realistische profielen, werd uitgevoerd, en de resultaten waren in dezelfde orde van grootte als de resultaten van bulk-formules, en komen overeen met de verwachting. Het model werd toegepast op gegevens gemeten op Vluchtenburg, aan de Nederlandse kust. Dit onderzoek bevatte metingen die gedetailleerd de evolutie van een grootschalige suppletie beschrijven. De resultaten van het model volgen een trend die vergelijkbaar is met de waargenomen gegevens, namelijk een hoger volume verlies in de periode onmiddellijk na de afronding van de suppletie. De belangrijkste resultaten van het onderzoek zijn: 1) de nauwkeurigheid van de drie meest gebruikte bulk formules (CERC, Kamphuis en Bayram) is aanzienlijk verbeterd, 2) de nauwkeurigheid is nog steeds laag voor de verschillende doeleinden, maar er is potentieel voor verbetering wanneer het effect van kenmerken van profielen worden meegenomen, 3) het effect van de hellingsgraad op LST wordt toegeschreven aan de door de golfbreker veroorzaakte turbulentie, die de bodem bereikt en het sediment efficiënter in beweging brengt dan bodem-wrijving veroorzaakt door 'orbital velocity' , 4) een nieuwe parametrisatie voor de vermindering van door turbulentie veroorzaakte golf sterkte, om dit fenomeen te verklaren, werd met succes geïmplementeerd en getest in vergelijking met laboratorium gegevens, en 5) een toepassing van een LST-model met behulp van deze parametrisatie was in staat om vergelijkbare tendensen te produceren in vergelijking met veldgegevens, waaruit blijkt dat deze benadering geldig kan zijn.

Contents

1

INTRODUCTION

1.1. THE PROBLEM

Longshore sediment transport (LST) is one of the main drivers of beach morphology. It works at temporal scales ranging from hours to centuries and spatial scales ranging from tens of meters to hundreds of kilometres (Cowell et al., 2003a,b, Larson and Kraus, 1995). Episodic, large LST rates can result in important physical impacts such as inlet closure (Ranasinghe et al., 1999), rapid build-up of ebb/flood shoals (Oertel, 1972), headland bypassing of large volumes of sand (Short, 2000) and rotation of pocket beaches (Harley et al., 2011, Ranasinghe et al., 2004). Persistent alongshore gradients in LST (even small gradients) could result in chronic impacts such as coastline recession (Cowell et al., 2003a,b, Komar, 1998), inlet migration (FitzGerald, 1988) and ebb/flood delta depletion/accretion (Oertel, 1972). Most, if not all, of these impacts are generally considered as negative impacts by coastal managers/planners. Perhaps the most negative impact comes from coastline recession which poses an immediate threat to populations living in vulnerable coastal areas. This problem affects coasts in all continents and examples of its dramatic effects can be seen in Figures 1.2 and 1.3). For example in Europe, according to EEA (2006) a significant part of coastline displays erosion patterns (Figure 1.1).

The problem of coastal recession will most likely be aggravated with the effects of Climate Change and resulting Sea Level Rise (SLR). According to the last Intergovernmental Panel on Climate Change (IPCC) report (Church et al., 2013), SLR rates are expected to continue (if not increase) with global mean sea levels increasing between 0.4 m and 1 m until the end of this century. A more recent analysis of sea level records (Hay et al., 2015) rectified last century's SLR rates records upwards from the previously estimated and found that SLR rates increased significantly in the last two decades. In face of this new knowledge the IPCC projections are likely to be updated to even higher values. The most obvious impact of Climate Change is the coastal recession directly caused by Sea Level Rise (Kabat et al., 2009) which can be roughly estimated (Stive, 2004) by the Bruun rule (Bruun, 1962). This rule relates Sea Level Rise and profile slope with the length of the recession. As coasts recede they are ever more vulnerable to episodes of shorter time scale recession caused by LST gradients.

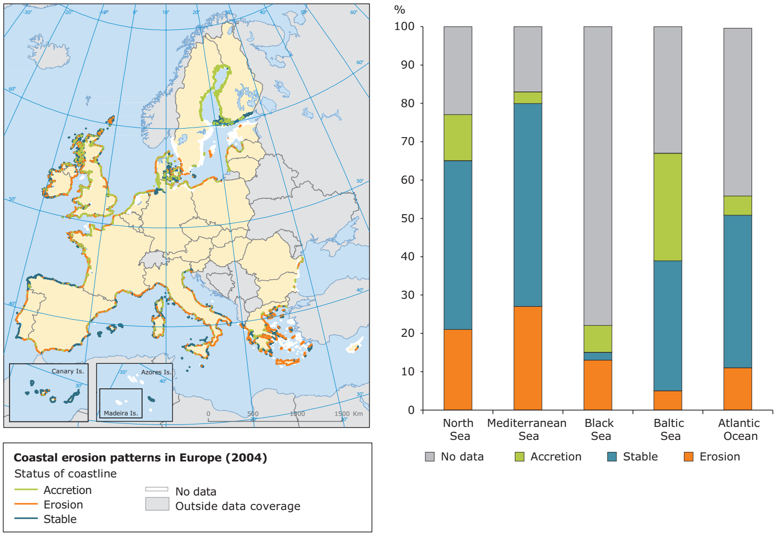

Figure 1.1: Coastal erosion in Europe (European Environment Agency)

(a) Near Aveiro, Portugal (photo by Salette Marques)

(b) Costa da Caparica, Portugal (Photo by Paulo Carriço/LUSA)

Figure 1.2: Examples of coastal erosion

Figure 1.3: Effects of coastal recession in Rhode Island, USA (USGS.gov)

Other Climate Change caused effects, such as the likely frequency increase of extreme wave events in some parts of the globe (Church et al., 2013) or a change in the predominant wave directions (Coelho et al., 2009) may result in impacts of similar or greater magnitude. These effects will induce significant change to LST rates with consequences such as changes in erosion “hot-spots”, reduction of efficiency of existing coastal protection measures, changes in inlet and delta behaviours, etc.

For these reasons, there is an increasing necessity for accurate LST models which are essential to identify risk areas and allow the coastal manager to prepare mitigation measures.

1.2. LST

Sediment transport is the collective movement of sediment grains under the influence of forces within a fluid and gravity. Sediment is set in motion when shear stresses acting on individual grains at the bed exceed a critical value.

Sediment transport occurs in two ways: 1) bed load transport, where particles roll or move in small jumps in a small layer close to the bed and 2) suspended load transport, where particles are suspended in the water without contact with the bed. Bed load transport typically occurs for low bed shear stresses, obviously still above the critical value, while suspended load occurs with higher bed shear stresses. Bed forms such as ripples may enhance sediment suspension via the creation of vortices caused by flow separation at the ripple crest (Toit and Sleath, 1981).

On a coastal context, sediment transport can be separated in two components: a cross-shore (perpendicular to the shoreline) and a longshore component (parallel to the shoreline). Bed load transport has an important role in cross-shore transport but represents only a negligible fraction of LST compared to the fraction of suspended load (Nairn and Southgate, 1993). In coastal waters, two main causes of high bed shear stresses at the bed can be identified: turbulence generated at the bed by wave orbital velocities, that reach a maximum near the breaking point, and turbulence generated at the surface by wave breaking that propagates downward reaching the bed. Both causes depend heavily on the phenomenon of wave breaking.

For a significant amount of LST to occur, besides the presence of suspended sediment, another condition must be met: a longshore current must be present. Longshore currents are forced by a cross-shore gradient in the alongshore shear component of the radiation stress (dS_{yx}/dx), which is in turn driven by obliquely incident breaking waves (Longuet-Higgins, 1970). In some instances, longshore currents may also result from alongshore gradients in breaking wave height (e.g. Monterey Bay; (Orzech et al., 2010)). Longshore currents can also be caused by phenomena that are not related to wave breaking such as tide and wind.

If only one of these two conditions are present, i.e., when waves arrive perpendicular to the coast bringing sediment into suspension but no longshore current is generated, or when a longshore current exists (e.g. a tidal or wind generated current) but no waves stir the sediment, LST will be minimal. In any case, most of the times both phenomena occur at the same time as both are mainly caused by the breaking of incoming wind generated gravity waves. Due to the large dependence of both longshore current and sediment suspension on wave breaking properties, LST models have wave parameters as main inputs.

1.2.1. PREDICTING LST

Motivated by the problems caused by coastal erosion, there has been, over the last half century, a large research effort expended on developing models to predict LST rates (Wellen et al., 2000, van Rijn, 1993, Watanabe et al., 1991, Kamphuis, 1991, Deigaard et al., 1986, Bailard, 1981, Ackers and White, 1973, Bijker, 1971, Komar and Inman, 1970, Bijker, 1967, Engelund and Hansen, 1972, Duncan, 1981, Savage, 1962). The approaches to predict LST can be roughly divided in two:

- Bulk transport formulas; these are explicit equations based on simplified representations of physical processes which generally use empirical coefficients for calibration. Bulk formulas provide an estimate of the total (integrated over the whole profile) LST rate with relatively few and easily available input parameters. Two of the most commonly used formulas are the so-called CERC formula (CERC, 1984a) and the Kamphuis formula (Kamphuis, 1991). These formulas account for all transport (including swash zone transport).

- Process based models; these include a large number of physical processes (wave breaking, radiation stresses, bed shear stress, entrainment, suspension, wave-current interaction, etc), and attempt to simulate LST in detail. In general these models use a wave propagation model to calculate wave parameters along the profile and thus take into account bathymetric features. These models usually need a large number of input parameters and also need to be calibrated per application.

Examples of such models are: the model described in Deigaard et al. (1986) and UNIBEST-LT (WL|Delft Hydraulics, 1992, Stive and Battjes, 1984).

Both approaches are useful in Engineering practice. Bulk formulations are often used to make a first estimate based on limited information while process-based models are generally expected to yield more accurate estimates and more spatio-temporal information. The latter approach is, however, far more labour intensive due to its reliance on relatively detailed input data and modelling expertise.

1.3. OBJECTIVES AND PATH OF RESEARCH

This research started with a rather generic question: "how do results of LST bulk formulas compare with results of process based models?". From such a generic question the research took its own path cascading into ever more specific questions. While accessing the state-of-the-art in bulk formulas a possibility for improvement was identified and implemented. An extensive data set was used to derive new or update coefficients and statistical tools were used to improve the calibration/validation process. Next, the research focus turned to the explanation of the uncertainty still observed in the predictions of the bulk formulas. Assuming that this uncertainty could not be explained only by measurement errors, I looked for inputs that could influence LST but were not explicitly accounted for in bulk formulas, e.g., three-dimensional variation in bathymetry and profile features. I opted to focus on the influence of profile features, such as slope and presence of bars, on LST rates. Using a process based model I calculated LST in profiles showing different kinds of features and found a significant dependence on some of those features. These results led to a new question: "which phenomena lead to the influence of profile features in LST rates?". To answer this question the effect of wave breaking induced turbulence on bed shear stresses was investigated and a new process based LST model was implemented. In the end I performed a parameter space exploration of the results of the model and investigated if the model could explain the bathymetry evolution observed at a large scale nourishment.

1.4. THESIS OUTLINE

The thesis is organized as follows. In Chapter 2 three of the most used bulk LST formulas were applied to an extensive dataset and their coefficients improved and/or updated. In Chapter 3 one of the possible explanations for the remaining uncertainty observed in Chapter 2, the influence of profile features in LST was studied. In Chapter 4 a new LST process based model is implemented as an attempt to better account for wave breaking induced turbulence effects. In Chapter 5 the parameter space of the results was explored and the model was applied to a field case. Finally, conclusions drawn from the study are presented in Chapter 6.

2

BULK LST FORMULAS

ABSTRACT

Longshore sediment transport (LST) is one of the main drivers of beach morphology. Bulk LST formula are routinely used in coastal management/engineering studies to assess LST rates and gradients. Over 50 years of research has resulted in several bulk LST formulas that have been tested with varying levels of rigour. In this study, the predictive skill of three of the most commonly used bulk LST formulas (CERC, Kamphuis and Bayram) is rigorously evaluated using the most extensive LST data set presently available. The calibration coefficients in the three formulas are improved using a least-squares optimization algorithm, resulting in a significant improvement in the predictive skill of all three formulas. The generality of the improved formulas is verified via the statistical methods of bootstrapping and cross-validation. While the performance of all three improved formulas is very similar, the improved Kamphuis formula performs best, followed by the improved Bayram formula. [a]

[a]This chapter is an extended version of the article "Re-evaluation and improvement of three commonly used bulk longshore sediment transport formulas", published in the Journal of Coastal Engineering (Mil-Homens, 2013)

2.1. INTRODUCTION

The main objective of this chapter is to investigate whether the predictive skill of three of the most widely used bulk LST formulas, i.e., the CERC (CERC, 1984a), Kamphuis (Kamphuis, 1991) and Bayram(Bayram et al., 2007) formulas can be improved. To this end the most extensive LST data set presently available (as presented in Bayram et al. (2007)) is used to assess and improve the above three formulas.

The chapter is organized as follows. Section 2.2 describes the data set used in this study. The three bulk LST formulas investigated herein are described in Section 2.3. Next, in Section 2.4 the performance of the bulk formulas with the data set presented

Table 2.1: Data set composition

Publication	Type	Location	Number of points
Schoonees and Theron (1993)	Field data	Diverse locations	123
Smith et al. (2003)	Large scale laboratory data	Large-scale Sediment Transport Facility, Vicksburg, USA	4
Miller (1999)	Field data	Duck, North Carolina, USA	10
Kumar and Anand (2003)	Field data	Karwar, India	81
Wang et al. (1998)	Field data	East and Gulf Coast, USA	29

in Section 2.2 is assessed, while in Section 2.5, the methods used to improve the performance of the formulas are described. Section 2.6 presents the results obtained with the improved formulas. Finally, conclusions drawn from the study are presented in Section 2.8.

2.2. DATA SET

This study exclusively uses the data set presented in Bayram et al. (2007) (Table 2.1). The data set consists of several sub-sets, which were collected from 1953 to 2004. The duration of the various sub-sets and the temporal and spatial resolution of measurements vary substantially. In addition, a wide variety of observation methods has been used in acquiring the data, ranging from visual observations of wave heights, to sophisticated optical and acoustic backscatter devices to measure suspended sediment concentrations. In this analysis a data sub-set is only taken into account when the most important input parameters for the bulk LST formulations and the surfzone integrated LST are available. These include measurements of significant wave height and angle at the break point, peak period, and mean grain diameter (D_{50}). The beach slope, which is an input parameter in the Kamphuis formula is, when not available, calculated from the mean grain diameter assuming a Dean profile (Dalrymple, 2004).

To assess the representativeness of the data set and the LST regimes for which limited data points are available an overview of the data set is generated via histograms (Figure 2.1).

Figure 2.1a shows that the significant wave height at the break point is smaller than 1 m for more than 70% of the data points and that there are only few observations of wave heights above 2 m. This is probably due to the logistical difficulties associated with acquiring field measurements under high breaking wave conditions. The peak period

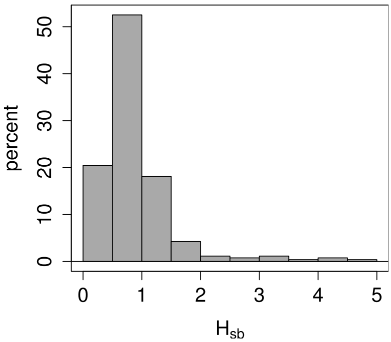

(a) Histogram of significant wave height at the break point

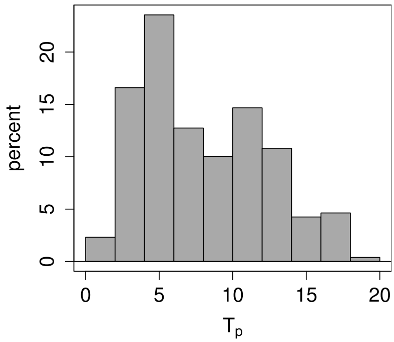

(b) Histogram of peak period

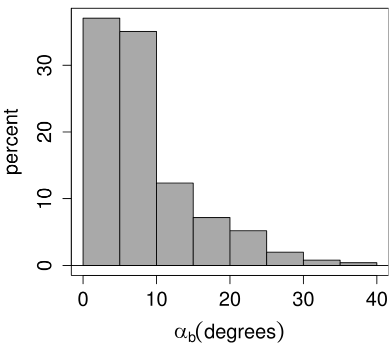

(c) Histogram of wave angle at the break point

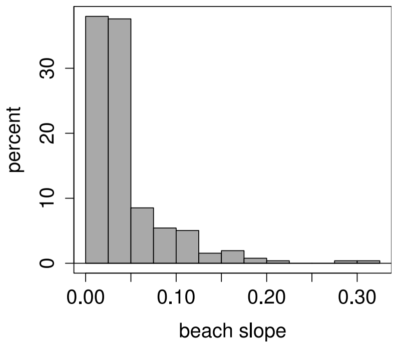

(d) Histogram of beach slope

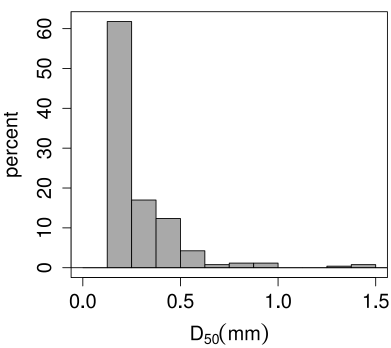

(e) Histogram of mean grain diameter

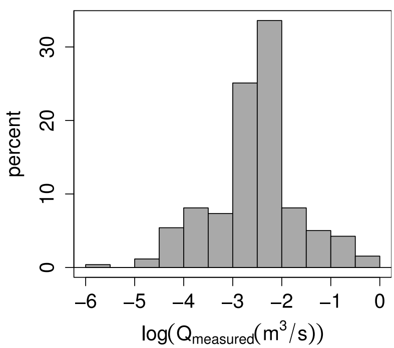

(f) Histogram of measured transport

Figure 2.1: Histograms of (a) significant wave height, (b) peak period, (c) breaker angle, (d) beach slope, (e) mean grain diameter and (f) measured LST

histogram (Figure 2.1b) shows a bimodal distribution, with peaks around 5 s and 11 s. Figure 2.1c shows that about two thirds of the measured angles are below 10 degrees. More than 70% of the data points are from beaches with slopes smaller than 0.05 (Figure 2.1d) and fall in Wright and Short's dissipative and intermediate beach states region (reflective beaches are considered to have slopes steeper than 0.1 (Wright and Short, 1984)). Approximately 52% of the data points correspond to fine sand with a D_{50} smaller than 0.2 mm and 42% fall in the category of medium sand with a D_{50} between 0.2 mm and 0.5 mm (Figure 2.1e). The LST rates (Figure 2.1f) are concentrated between 10^{-3} and 10^{-2} m³/s and the distribution gradually tails off for smaller and higher orders of magnitude. The main shortcomings of the data set are the limited number of data points for (coarse sand) reflective beaches and for the higher transport regime (e.g. between 0.1 and 10). The latter shortcoming is particularly unfortunate because it is more likely than not that it is the higher LST rate occurrences that are more damaging to the coastal zone.

2.3. BULK FORMULAS

2.3.1. CERC FORMULA

The CERC formula is based on the assumption that the LST rate is directly proportional to the alongshore component of wave power. Considering values at the breaker line and using significant wave height, the LST rate (expressed in m³/s) is given by:

$$Q_l = k \frac{\rho g^{\frac{1}{2}}}{16\sqrt{\gamma_b}(\rho_s - \rho)(1-p)} H_{sb}^{\frac{5}{2}} \sin 2\alpha_b \tag{2.1}$$

The k coefficient was first determined by linear regression on field measurements of sediment transport obtained at Silver Strand, California, and El Moreno, Mexico by Komar and Inman (1970) who obtained a value of $k_{K\&I,H_{rms}} = 0.77$ (using the $H_{b,rms}$ - *root mean square* breaking wave height). In CERC (1984a), some other data sets were added, and the value of k was updated to $k_{SPM,H_s} = 0.39$ (using significant wave height at the breaker - H_{sb}). The corresponding value using $H_{b,rms}$ is $k_{SPM,H_{rms}} = 0.92$. Although the sediment transport predictions followed a clear correlation with observations, there was considerable scatter, which may suggest that k is a function of some other physical parameters (Rosati et al., 2002).

Several other studies attempted to find a more robust value or formulation for k. Kamphuis and Readshaw (1978) observed a relationship between k and the surf similarity parameter, also known as Iribarren number (eq. 2.2):

$$\xi_b = \frac{m}{\sqrt{H_b/L_0}} \tag{2.2}$$

were m represents the beach slope and L_0 the wavelength in deep water. The laboratory data analysed in Kamphuis and Readshaw (1978) suggested the relation $k_{K\&R} = 0.7\xi_b$ for $0.4 > \xi_b > 1.4$ (relative to H_{rms}). Outside this interval no dependency on ξ_b was observed. This relation, suggests that LST increases as more energy is dissipated in the breaking process, ranging from spilling breakers (low energy) to plunging and collapsing (high energy).

An energetics based model for the transport coefficient k was developed in Bailard (1984, 1981). In this model, k (relative to H_{rms}) was presented as a function of the wave angle at the breaking point and the ratio of the orbital velocity magnitude and the sediment fall velocity (eq.2.3).

$$k_B = 0.05 + 2.6 \sin^2(2\alpha_b) + 0.007 \frac{u_{mb}}{w_s} \tag{2.3}$$

where $u_{mb} = 0.5\gamma_b\sqrt{gd_b}$ is the maximum oscillatory velocity magnitude, obtained from shallow-water wave theory, w_s is the sediment fall velocity and $\gamma_b = {}^{d_b}/{}_{H_b}$ is the breaker index.

Komar (1988) evaluated some previous experiments and concluded that some of the previous relations were based on erroneous data. Komar found that k was only slightly dependent on grain size and interpreted this as an indication of the bad quality of the available data.

By extending Komar's data set with data from the Adra River Delta, Spain, that covers a range of median sediment grain sizes from 0.40 mm to 1.5 mm, del Valle et al. (1993) presented an empirically based relationship for the k parameter as a function of the median grain diameter (relative to H_{rms}) given by:

$$k_{VM\&L} = 1.4\, e^{(-2.5\, D_{50})} \tag{2.4}$$

Schoonees and Theron (1994) tested various formulations with a large data set. The best result was obtained with the formulation presented in Kamphuis and Readshaw (1978).

In Smith et al. (2009), formulations for the k coefficient were evaluated against laboratory data (comprising just 4 data points). Again, the best results were obtained with a k coefficient formulation dependent on the surf similarity as suggested in Kamphuis and Readshaw (1978).

2.3.2. KAMPHUIS FORMULA

Kamphuis (1991) presented an LST formula that performed well on an extensive data set, mainly comprising small scale laboratory data. By performing a dimensional analysis along with some physical assumptions, eq.(2.5) was derived (valid for regular waves):

$$\frac{I_m}{\left(\frac{\rho H^3}{T}\right)} = k^* \left(\frac{H}{L_{o*}}\right)^p m_b^q \left(\frac{H}{D_{50}}\right)^r \sin^s(2\alpha_b) \tag{2.5}$$

where I_m is the immersed mass of sediment transported alongshore expressed in ${}^{kg}/{}_{s}$. I_m is related to the volume rate (Q in ${}^{m^3}/{}_{s}$) via:

$$Q_l = \frac{I_m}{(\rho_s - \rho)(1-p)} \tag{2.6}$$

H represents the wave height, T the wave period, d the water depth, ρ the fluid density, m the beach slope, p, q, r and s are exponents (empirically determined) and k^* a calibration coefficient (also empirically determined). L_{o*} is the deep water wavelength (for regular waves). The nominal grain size adopted was D_{50} and the beach slope considered was that within the surf zone: $m_b = {}^{d_b}/_{\lambda_b}$ where λ_b is the distance from the shoreline to the break point.

For irregular waves, considering significant wave parameters at the break point, Kamphuis (1991) presents the formula:

$$\frac{I_m}{\left(\frac{\rho H_{sb}^3}{T_p}\right)} = 1.3 \times 10^{-3} \left(\frac{H_{sb}}{L_o}\right)^{-1.25} m_b^{0.75} \left(\frac{H_{sb}}{D_{50}}\right)^{0.25} \sin^{0.6}(2\alpha_b) \tag{2.7}$$

where H_{sb} is the significant wave height at the breaker, T_p is the peak period and $L_o = {}^{gT_p^2}/_{2\pi}$, i.e. the deep water wave length corresponding to the peak period. This formula can be written in a simplified form, considering $k = k^* \rho \left({}^{g}/_{2\pi}\right)^{1.25} = 2.27$:

$$I_m = 2.27 H_{sb}^2 T_p^{1.5} m_b^{0.75} D_{50}^{-0.25} \sin^{0.6}(2\alpha_b) \tag{2.8}$$

Using their extended data set, Schoonees and Theron (1996) presented a new value for the calibration coefficient k^*. The value that provided the best fit was $k^* = 50000$, expressed in ${}^{m^3}/_{y}$. The equivalent value, with Q_l in ${}^{m^3}/_{s}$ is $k_{S\&T} = 2,77$.

2.3.3. BAYRAM FORMULA

The Bayram formula (Bayram et al., 2007) assumes that sediment becomes suspended by the action of breaking waves, and thereafter gets transported by any type of longshore current (tidal, wave driven, etc). Furthermore, the Bayram formula also assumes that a majority of the transported sediment remains in suspension (suspended load). Bayram et al. (2007) reason that the wave breaking stirs up the sediment and maintains an average concentration distribution $c(x,z)$ in the surf zone. Thus, the total work required to keep the sediment in suspension (W) is given by the product of the concentration, submerged weight and the sediment fall speed (w_s).

$$W = \int_0^{x_b} \int_{-h(x)}^{0} c(x,z) \left(\rho_s - \rho\right) g w_s dz dx \tag{2.9}$$

where x is a cross-shore coordinate with the origin at the shoreline and positive in the offshore direction, the subscript b refers to the breaking point, z is the vertical coordinate with origin at the still water level and negative underwater and d is the water depth. The total work W is considered to be a fraction of the flux of wave energy ($F = EC_g$), i.e. $W = \varepsilon F$.

LST rate (Q_l) is defined as the product of the suspended concentration and longshore current velocity (V):

$$Q_l = \int_0^{x_b} \int_{-d(x)}^{0} c(x,z) V(x,z) dz dx \tag{2.10}$$

When a representative longshore current velocity is considered, eq.(2.9), $W = \varepsilon F$, and eq.(2.10) are combined into:

$$Q_l = \frac{\varepsilon}{\left(\rho_s - \rho\right)(1-a) g w_s} F\overline{V} \tag{2.11}$$

where $\overline{V}$ is the mean (or representative) longshore current velocity over the surf zone, a is the porosity and ε is a non-dimensional transport coefficient that represents the efficiency of the waves in keeping sand grains in suspension. Bayram et al. (2007) estimated this crucial coefficient by performing a dimensional and error analysis, which led to the following transport coefficient ε:

$$\varepsilon = \left(9 + 4\frac{H_{sb}}{w_s T_p}\right).10^{-5} \tag{2.12}$$

where H_{sb} represents the significant wave height at the breaking point.

WAVE-ENERGY FLUX (F)

Considering obliquely incident waves, the cross-shore component of the wave energy flux at the break point is given by:

$$F_b = E_b C_{gb} \cos\alpha_b \tag{2.13}$$

where E_b is the wave energy per unit crest and C_{gb} is the group velocity, both defined at the break point and obtained from linear wave theory. For irregular waves, as was done for the CERC formula, H_b can be replaced by H_{sb}, which results in the expression:

$$F_b = \frac{2^{\frac{5}{4}}}{8} \frac{g^{\frac{3}{2}}}{\sqrt{\gamma_b}} \rho H_{sb}^{\frac{5}{2}} \cos\alpha_b \tag{2.14}$$

with the reasonable assumption that energy dissipation before the break point (due to i.e. bottom friction) is negligible, $F = F_b$ is assumed.

MEAN (OR REPRESENTATIVE) LONGSHORE CURRENT ($\overline{V}$)

Ideally, to use the Bayram formula, measured longshore current data should be available. Otherwise, $\overline{V}$ can be calculated from wave characteristics and beach profile data. Bayram et al. (2007) adopted a simple longshore momentum equation which assumes linearised friction and neglects lateral mixing (Larson and Kraus, 1991), such that:

$$\frac{2}{\pi}\rho c_f u_0 V = \frac{dS_{xy}}{dx} \tag{2.15}$$

where c_f is the friction coefficient, u_0 is the bottom orbital velocity and S_{xy} is the radiation stress directed alongshore and transported onshore. Assuming that shallow water conditions hold and that the beach profile can be approximately represented by a Dean's equilibrium beach profile ($h = Ax^{2/3}$, being A a shape parameter (Dalrymple, 2004)), an expression for the longshore current is obtained as:

$$V = \frac{5}{24} \frac{\pi\gamma_b\sqrt{g}}{c_f} A^2 \frac{x^{1/3}}{\sqrt{h_b}} \sin\alpha_b \tag{2.16}$$

The shape parameter A is related to the fall velocity w_s with eq.(2.17).

$$A = \frac{9}{4}\left(\frac{w_s^2}{g}\right)^{1/3} \tag{2.17}$$

The surf zone average $\overline{V}$ in eq.(2.11) is obtained by cross-shore integration of eq.(2.16) over the surf zone width to obtain:

$$\overline{V} = \frac{1}{x_b}\int_0^{x_b} V\,dx = \frac{5}{32}\frac{\pi\gamma_b\sqrt{g}}{c_f}A^{3/2}\sin\alpha_b \tag{2.18}$$

Eq.(2.18) assumes that the friction coefficient is time/space constant at 0.005, while the wave climate is represented by a single representative wave.

2.4. PERFORMANCE COMPARISON OF THE CERC, KAMPHUIS AND BAYRAM FORMULAS

The three bulk LST formulas were applied to the comprehensive data set presented in Section 2.2. To quantify the overall performance of the formulas, the *root mean square error* ($RMSE$) and the *bias* were computed, which were calculated as:

$$RMSE = \sqrt{\frac{\sum_{i=1}^{n}\left(\log(Q_{p,i}) - \log(Q_{m,i})\right)^2}{n}} \tag{2.19}$$

$$bias = \frac{\sum_{i=1}^{n}\left(\log(Q_{p,i}) - \log(Q_{m,i})\right)}{n} \tag{2.20}$$

The $RMSE$ value is a commonly used error measure. The sum of squares gives more weight to higher error values, and consequently higher error variances. The *bias* provides insight on any systematic offset of the data. Because logarithmic values (base 10) are considered in both statistical measures, the values indicate errors in terms of magnitude order, e.g., an $RMSE$ value of 1 would mean that the predicted values are roughly, on average, 10 times larger or smaller than the measured ones. Logarithmic values were chosen because the data range extends through several orders of magnitude. Another performance measure of the formulas is the percentage of calculated transport values that are within a factor of 2, with respect to measurements (see for example Schoonees and Theron (1993)).

The performance of the three formulas with various associated coefficients is presented in Table 2.3. Based on the $RMSE$ and "factor 2" performance indicators, the CERC formula with $k_{K\&R}$ gives the best results. The performance of the bulk formulas when applied to the new data set, is consistent with that obtained with Data Set 1 (Section 2.2) presented in Schoonees and Theron (1996, 1994). The only difference between the results of the present analysis and that presented by Schoonees and Theron (1996) is that that the Kamphuis formula with $k_{S\&T}$ fares better than the CERC formula with $k_{K\&R}$, probably due to the inclusion of the newest data.

Where *bias* is concerned, the Bayram formula shows a *bias* that is very close to zero, while the CERC formula with $k_{K\&R}$ also results in a small *bias*. Other combinations of formulas and coefficients show considerable *bias*.

2.5. IMPROVEMENT LST COEFFICIENTS AND FORMULATIONS

2.5.1. DEPENDENCY OF CALIBRATION COEFFICIENTS ON PHYSICAL PARAMETERS

The CERC and Bayram formulas are based on simplified models that attempt to represent basic physical processes governing LST. The calibration coefficients are thus expected to take into account effects that are not included in the basic models (or that are poorly represented therein). The various values of the non-dimensional coefficient (k) in CERC formula presented in Section 2.3.1 have been derived with considerably smaller data sets than the one used in this study. Therefore, it is reasonable to expect the larger data set used in the present study may result in a new empirical coefficient which will improve the predictive skill of the formula. On the other hand, the Bayram formula coefficient (ε) was derived with the same data set used in this study. However it is hypothesized, that the error analysis can be improved using logarithmic values and a non-linear function can be used to establish an improved relation between the calibration coefficient and a dimensionless parameter. The Kamphuis formula was already determined from a set of dimensionless parameters. It seems therefore more appropriate to update the numerical values of the $k*$, p, q, r and s coefficients in the Kamphuis formula (eq.(2.5)) with the more extensive data used herein rather than obtaining a transport coefficient which is also a function of non-dimensional parameters. For this reason, the procedure described in this section was not applied to the Kamphuis formula. The update of the Kamphuis formula coefficients is treated in the following section (Section 2.5.2).

In the previous sections, the notation used for each formula was the same as in the original publications. In this section a more general notation is used for consistency. Equations (2.11) and (2.1) can be expressed in the form:

$$Q = kX \tag{2.21}$$

where Q is the total transport (in $\mathrm{m^3/s}$), k is the non-dimensional transport coefficient and X represents the formula without the calibration factor. For the Bayram formula ε is now represented by k and X is defined by eq.(2.22).

$$X = \frac{F\overline{V}}{\left(\rho_s - \rho\right)(1-a)\, g w_s} \tag{2.22}$$

For the CERC formula, X is defined by eq.(2.23).

$$X = \frac{\rho g^{\frac{1}{2}}}{16\sqrt{\gamma_b}(\rho_s - \rho)(1-p)} H_{sb}^{\frac{5}{2}} \sin 2\alpha_b \tag{2.23}$$

For each data point i a comparison was made in terms of the differences between the logarithms (base 10) of X and measured values: $\Delta_i = \log(X_i) - \log(Q_{m,i})$. The Δ_i values will be henceforth called *deltas*.

To obtain the optimal k coefficient, it is necessary to find a dependency between the *deltas* and some physical parameter. Since k is non-dimensional by definition, the desired dependency will also be related to one or more non-dimensional parameters, or with a non-dimensional combination of these parameters. The parameters were selected from the dimensional analysis made by Kamphuis (1991) and Bayram et al. (2007). In addition, the surf similarity parameter was also considered as a candidate as it is directly related to breaker type which influences LST (Kamphuis and Readshaw, 1978). The chosen parameters were: breaking wave height to deep water wavelength ratio H_{sb}/L_o, the breaking wave height to grain diameter ratio H_{sb}/D_{50}, surf similarity $m/\sqrt{H_{sb}/L_0}$ and the Dean number (also known as non-dimensional fall velocity) $H_{sb}/w_s T_p$.

In order to visualize a correlation and investigate the data distribution, the *deltas* were plotted against the above mentioned non-dimensional parameters. The results show considerable scatter (Figures 2.3 and 2.4).

The (*y-axis*) *deltas* distributions were analyzed. These distributions, given the existence of a sufficient number of data points, can give an insight about the nature of the scatter. Uniformly distributed *deltas* may indicate that the scatter results from a failure of the formula to capture important processes while normally distributed *deltas* around a peak may indicate that the formula is adequate and the scatter is a result of measurement errors. To analyze the evolution of these distributions along the *x-axis* one needs to divide it in sections and calculate the *deltas* distribution in each section. This approach has a problem: in order to have a good resolution on the *x-axis* (a function on the width of the sections), the number of points in each section must be low. With the goal of having a good *x-axis* resolution and enough points to calculate statistically meaningful distributions, a *moving window* method was used. The method can be summarized in the following steps:

1. Sort the N data points along the *x-axis*.

2. Pick the first set (or window) of n points $(1,2,3...n)$ and calculate an histogram (with a number b of bins) of the distribution along the *y-axis*. The x position attributed to this distribution will be the mean x value of the n points.

3. Repeat step 2 starting at $m \times p$, being p the number of points that the window moves in each step and $m = 1,2,3,...,q$. The process will be repeated $q = (N-n)/p$ times. Each one of the q sets has the points $(m \times p+1, m \times p+2, m \times p+3, ...m \times p+n)$.

Figure 2.2 shows a scheme illustrating the steps described above, using a scatter plot of the deltas (calculated with the CERC formula) vs. H_{sb}/L_o. In this figure the distance between histograms is exaggerated for visualization purposes.

After the application of the *moving window*, a contour of the *deltas* distributions evolution along the *x-axis* could be plotted. Figures 2.3 and 2.4 show the contours of the distributions for the dimensionless parameters considered: the Dean number, surf similarity, H_{sb}/L_o and H_{sb}/D_{50}, using the CERC and Bayram formulas. For these plots, the values used in the *moving window* method were: $N = 245$ points (total number of data points), $n = 60$ points, $b = 15$ bins, $p = 5$ points and $q = 37$. In these figures, contours representing the *x-axis* evolution of the *y-axis* data distribution were included. From these figures, two important observations can be made: the first is that the point density varies along the *x-axis*, where *deltas* for the breaking wave height to deep water wavelength ratio H_{sb}/L_o are most uniformly distributed. The second is that the distribution with

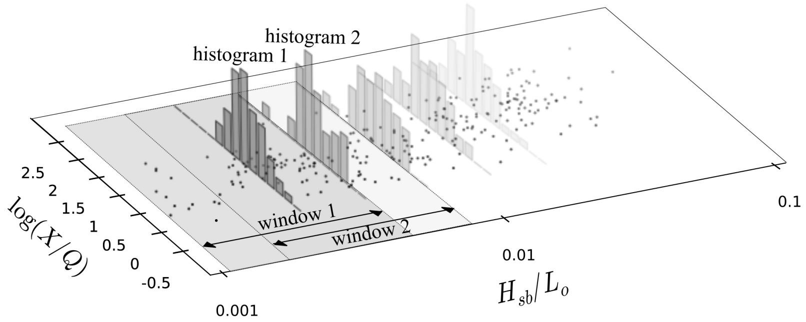

Figure 2.2: *Moving window* method to estimate the evolution of the distribution along the *x-axis.* Histogram 1 refers to the points contained on window 1 and Histogram 2 to window 2.

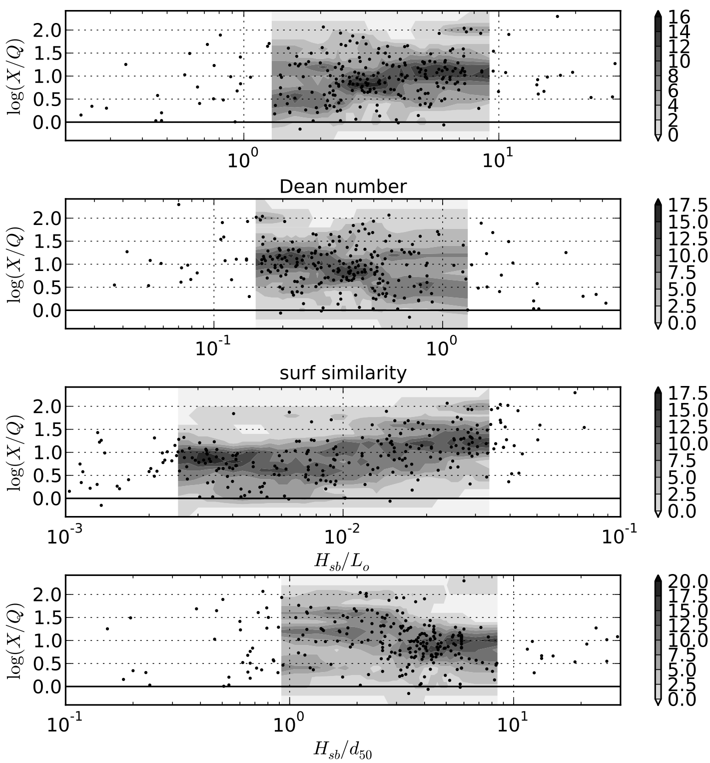

Figure 2.3: Distribution of *deltas* for the non-dimensional parameters considered: Dean number, surf similarity, H_{sb}/L_o and H_{sb}/D_{50} (using the CERC formula). The grey scale filled contours indicate the observation density and assist in determining possible trends in the deltas

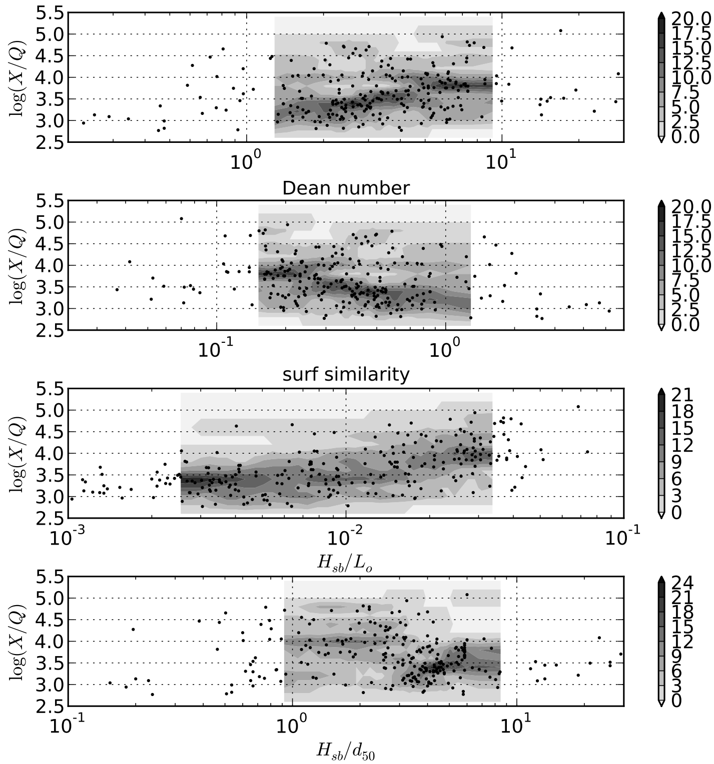

Figure 2.4: Distribution of *deltas* for the non-dimensional parameters considered: Dean number, surf similarity, H_{sb}/L_o and H_{sb}/D_{50} (using the Bayram formula). The grey scale filled contours indicate the observation density and assist in determining possible trends in the deltas

the H_{sb}/L_o parameter follows a more or less clear trend for both the CERC and Bayram formulas, while for the others parameters, the existence of a trend seems less clear.

An important feature of the *deltas* distributions is their normality along the *y-axis*, i.e., the probability that the sample of n points used to build each histogram came from a normal distribution. As referred above, the normal distribution along the *y-axis* can be interpreted as an indication that the observed scatter is a result of measurement errors. To assess this in an objective way, an Andersen-Darling (Anderson and Darling, 1952) test was used. In this test, a statistic A^2 is calculated. If A^2 is above the critical value for a given significance level, the null hypothesis (the sample is taken form a population normally distributed) can be rejected. The chosen value for the significance level was 5%. Figure 2.5 shows the values obtained for the statistic A^2, along with the critical value for the chosen significance level, using the CERC formula. All parameters show statistics that are mostly under the critical value which indicates normality of the distributions. It is noticeable that for the H_{sb}/L_o parameter, the statistic is in general lower than for the other parameters. The mean values of the statistics were: 0.52 for the Dean number, 0.54 for the surf similarity, 0.36 for H_{sb}/L_o and 0.53 for H_{sb}/D_{50}.

In the case of the Bayram formula, similar considerations as for the CERC formula can be made. In Figure 2.6, it can be seen that only the H_{sb}/L_o parameter show A^2 values that are mostly under the critical value. For this parameter, the statistic is in general much lower than for the other parameters. The mean values of the statistics were: 1.20 for the Dean number, 1.19 for the surf similarity, 0.46 for H_{sb}/L_o and 0.83 for H_{sb}/D_{50}.

There is a substantial difference between the mean values of the A^2 statistics obtained with the CERC and Bayram formulas. With the CERC formula the distributions show lower A^2 statistics values. This means that the CERC formula results seem to be more normally distributed along the y axis than the results obtained with the Bayram formula.

For the reasons exposed in this section: 1) higher likelihood that the distribution along the *y-axis* is normal, which indicates that it is more likely that a significant part of scatter is a result of measurement errors and 2) *deltas* distributions along the domain, it is apparent that the deltas are better described by a function of the H_{sb}/L_o parameter.

2.5.2. LEAST-SQUARES OPTIMIZATION

To obtain a new transport coefficient as a function of a non-dimensional number, a least-squares algorithm was used to calculate the coefficients of a non-linear function that best fits the *deltas*.

All optimization calculations were undertaken using a modified Levenberg-Marquardt (Levenberg, 1944) least-squares optimization method. The method takes a vector of data points y_i and attempts to find the set of parameters x for the function $g(t,x)$ such that the squared sum of residuals is minimized. The residuals are defined as $f_i(x) = y_i - g(t_i,x)$, where t is the available input data. The Levenberg–Marquardt algorithm is an iterative method. It starts with an initial guess x_0, and in each iteration the algorithm determines a correction p to x_n that produces a sufficient decrease in the residuals calculated with the new parameter set $x_{n+1} = x_n + p$. The solution will converge to x^*, being $g(t,x^*)$ the function that minimizes the squared sum of residuals. The calculation of the correction p is described in detail in More et al. (1980). This method allows for non-linear

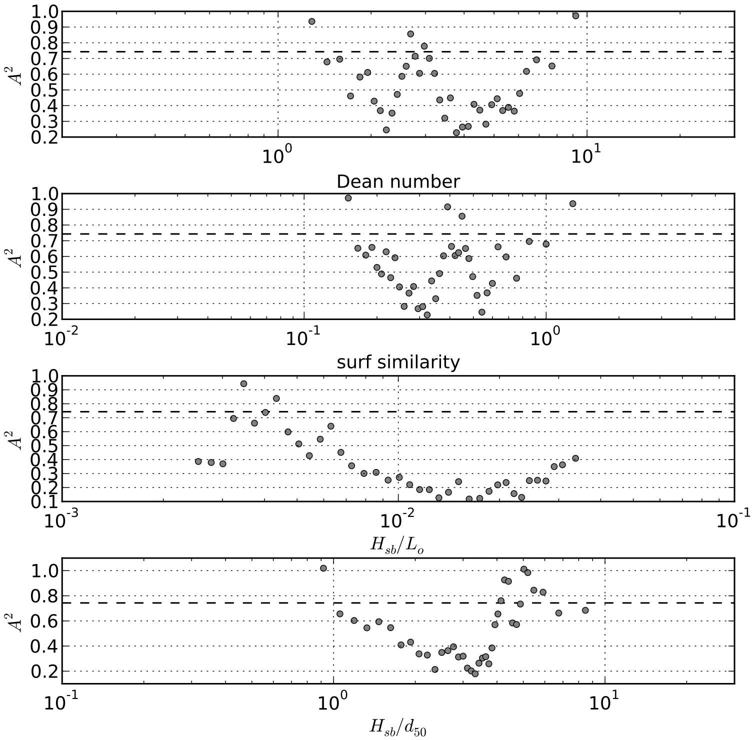

Figure 2.5: Anderson-Darling statistic for the dimensionless parameters considered: : the Dean number, surf similarity, H_{sb}/L_o and H_{sb}/D_{50} (using the CERC formula). The horizontal dashed line represents the critical value correspondent to a significance value of 5%.

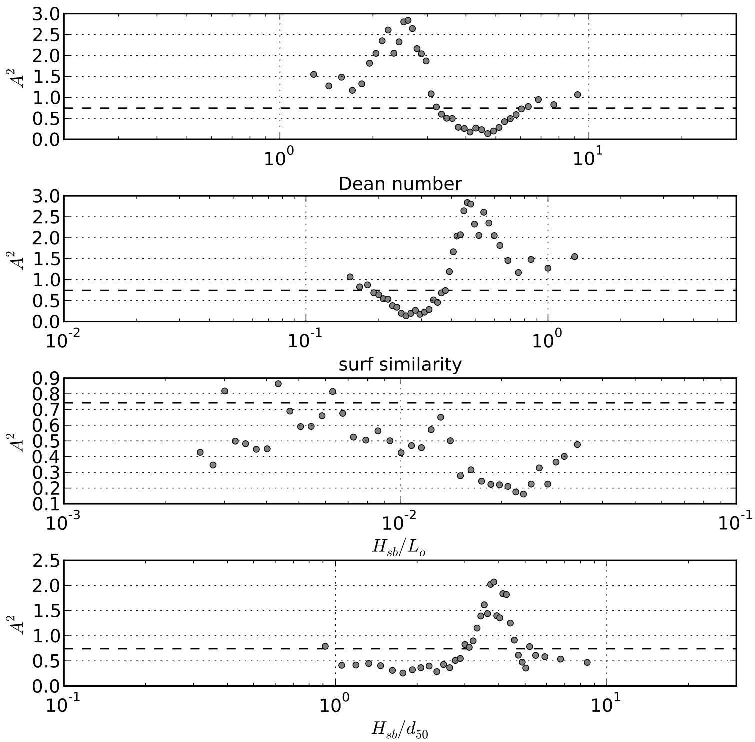

Figure 2.6: Anderson-Darling statistic for the dimensionless parameters considered: : the Dean number, surf similarity, H_{sb}/L_o and H_{sb}/D_{50} (using the Bayram formula). The horizontal dashed line represents the critical value correspondent to a significance value of 5%.

Table 2.2: *RMSE* values obtained with the optimization for the different non-dimensional parameters and function types

		H_{sb}/L_o	H_{sb}/D_{50}	surf similarity	Dean number
CERC	exponential	0.414	0.479	0.470	0.475
	polynomial	0.413	0.479	0.469	0.469
Bayram	exponential	0.408	0.500	0.491	0.495
	polynomial	0.407	0.498	0.490	0.490

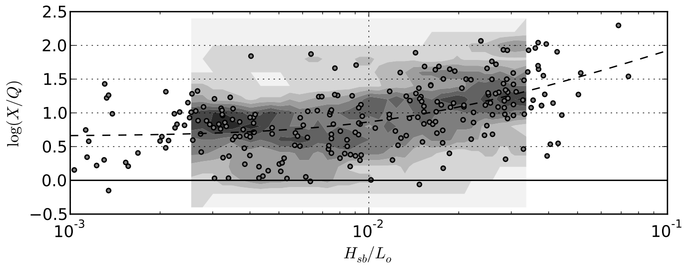

Figure 2.7: Best fitting function (dashed line), point scatter and distribution contour for the CERC formula

models to be tested. However, depending on the initial guess, the Levenberg–Marquardt algorithm can converge to local minima, failing to find the absolute minimum.

Taking into account the apparent trend in Figures 2.3 and 2.4, two candidate non-linear functions were considered: one polynomial and the other exponential. The expressions for the *deltas* take the form: $\Delta_i(x) = log[f(x)]$ where $f(x) = ax^b + c$ (polynomial function) or $f(x) = ae^{bx} + c$ (exponential function) and a, b and c are the coefficients that need to be calculated. The calibration coefficient becomes: $k = [f(x)]^{-1}$, as can be seen from eq.(2.21) with: $\log\left(\frac{X}{Q}\right) = \log[f(x)]$. The optimization was carried out for the non-dimensional parameters considered in the previous section. Table 2.2 shows the *RMSE* values obtained in each optimization, confirming the observation in the previous section that the H_{sb}/L_o parameter provides the best fit regardless of the function or formula used.

The best fit for the CERC formula was achieved with the polynomial function described by:

$$k_{CERC} = \left[2232.7\left(\frac{H_{sb}}{L_o}\right)^{1.45} + 4.505\right]^{-1} \tag{2.24}$$

The exponential function gave a slightly higher *RMSE* (0.414 as opposed to 0.413 obtained with the polynomial function), and thus the polynomial expression was chosen (note that both functions have the same number of free parameters). The function $f(x)$ is shown in Figure 2.7.

Similarly, for the Bayram formula, the best fit (also with the polynomial function) is:

$$k_{Bayram} = \left[7.862\times10^5\left(\frac{H_{sb}}{L_o}\right)^{1.283} + 1672.2\right]^{-1} \tag{2.25}$$

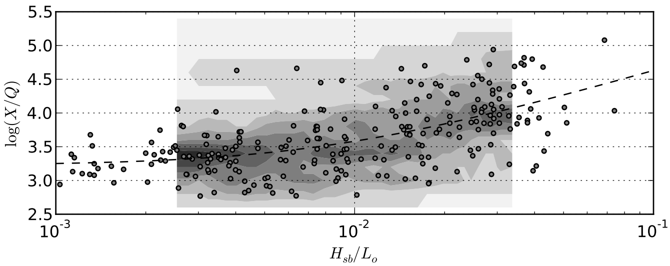

Figure 2.8: Best fitting function (dashed line), point scatter and distribution contour for the Bayram formula

Also in this case, the exponential function gave a slightly higher $RMSE$ (0.408 against 0.407 of the polynomial).

As mentioned before, a different approach was taken for the Kamphuis formula. The least-squares optimization algorithm was used to calculate the new $k*$, p, q, r and s values in eq.(2.5) that better fitted this data set. The best fit was found with:

$$I_{m,new} = 0.149 H_{sb}^{2.75} T_p^{0.89} m_b^{0.86} D_{50}^{-0.69} \sin^{0.5}(2\alpha_b) \tag{2.26}$$

The breaking wave height to deep water wavelength ratio H_{sb}/L_o (which is similar to the wave steepness), present in Eqs. (2.24) and (2.25) may affect LST in more than one way. Smaller wave steepness is usually result of a large T_p, which can have opposite effects on the LST. A larger period gives more time for the sediment to settle between waves and yields smaller wave breaking angles, due to more intense refraction. Both these effects would result in a reduction of the LST relatively to shorter period waves. On the other hand, a larger wave period also corresponds to an higher surf similarity parameter which is known to be associated with more intense plunging breakers (Battjes, 1974). This type of breakers dissipate energy in a concentrated area, stirring more sediment from the bottom, thus resulting in higher LST. The present analysis however suggests that the latter effect is more important than the former, as LST increases with T_p in Eqs. (2.24), (2.25) and (2.26) .

2.6. MODEL PERFORMANCE

2.6.1. PERFORMANCE COMPARISON BETWEEN PREVIOUS AND NEW COEFFICIENTS

The results obtained with the previous and new coefficient formulations are plotted against measured transport values in Figures 2.9, 2.10 and 2.11. The improvement is visible for all formulas. With the new coefficients, the LST values predicted by the CERC and Kamphuis formulas are visibly closer to the measured LST values (i.e. data points are closer to the diagonal line representing $Q_{predicted} = Q_{measured}$), while the LST values predicted by the Bayram formula with new coefficients show considerably less scatter. In general, the results with the new coefficients are concentrated around the diagonal in the $Q_{predicted}$ vs. $Q_{measured}$ plots. However, it is a concern that the CERC and Bayram formulas underestimate higher LST rates. This underestimation of high LST values is

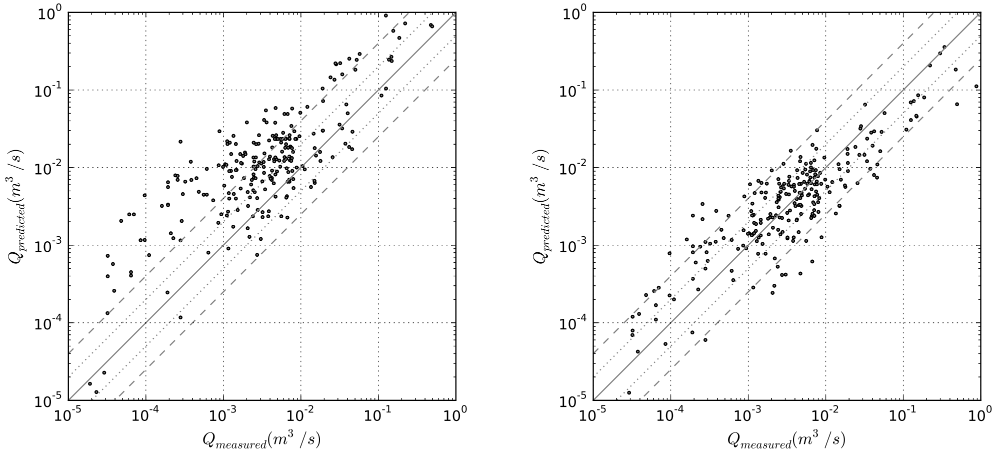

(a) Previous (b) New

Figure 2.9: $Q_{predicted}$ vs. $Q_{measured}$ using the CERC formula with previous and new coefficients (Solid line: $x = y$, dotted lines: $x = 0.5y$ and $x = 2y$, dashed lines: $x = 0.25y$ and $x = 4y$)

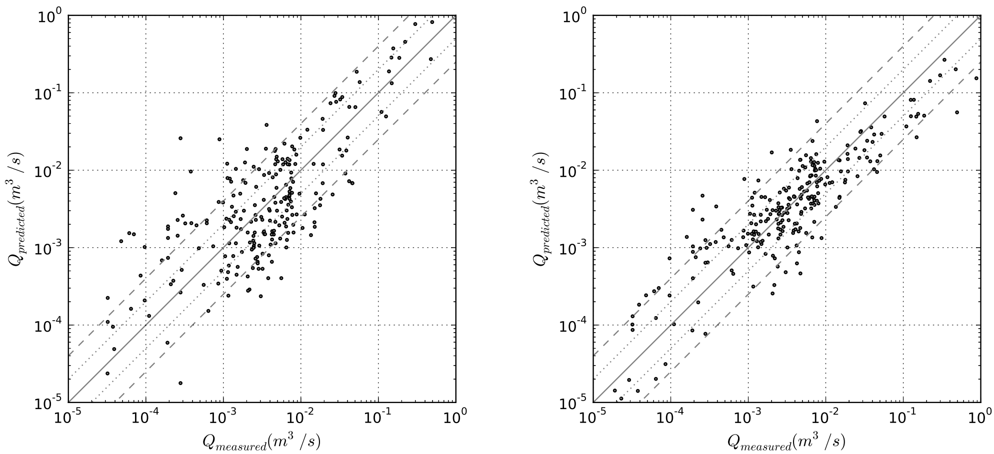

(a) Previous (b) New

Figure 2.10: $Q_{predicted}$ vs. $Q_{measured}$ using the Bayram formula with previous and new coefficients (Solid line: $x = y$, dotted lines: $x = 0.5y$ and $x = 2y$, dashed lines: $x = 0.25y$ and $x = 4y$)

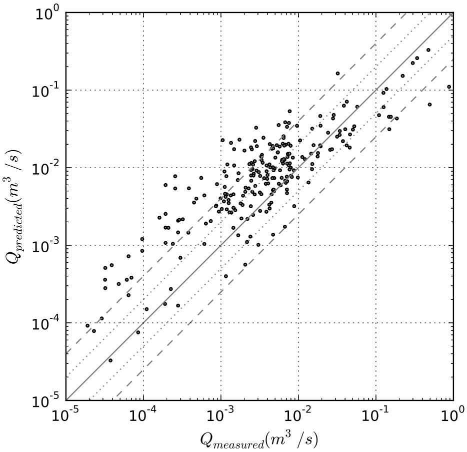

(a) Previous

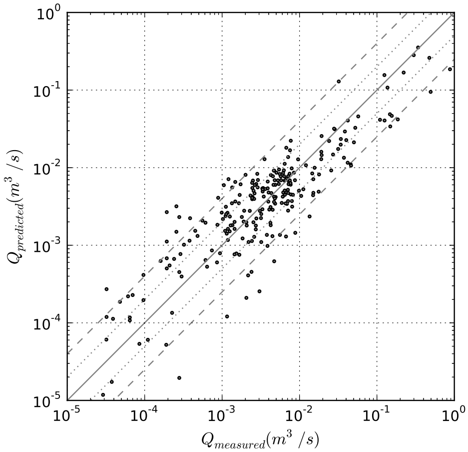

(b) New

Figure 2.11: $Q_{predicted}$ vs. $Q_{measured}$ using the Kamphuis formula with previous and new coefficients (Solid line: $x = y$, dotted lines: $x = 0.5y$ and $x = 2y$, dashed lines: $x = 0.25y$ and $x = 4y$)

most likely due to scarcity of measured high LST values, which will inevitably lead to high LST region being assigned less weight in the optimisation procedure described in Section 5.2. The Kamphuis formula with new coefficients also shows this behaviour, but in a less significant level, as is apparent in Figure 2.11.

The various error statistics associated with the three bulk formulas with the improved calibration factors (Eqs. 2.24-2.26) are shown in Table 2.3.

Table 2.3 indicates that the *RMSE* and the "factor 2" indicator values are significantly lower and higher, respectively, for the improved formulas, while the *bias* values are approximately zero. All three improved formulas have very similar *RMSE* values around 0.4. The percentage of points between a factor of 2 with respect to the observations is also similar and ranging between 53% and 56%. The Kamphuis formula performs best, followed by the Bayram formula, but the differences in performance are relatively small. The fact that the three formulas have almost identical *RMSE* suggests that this value is close to the statistical noise inherent in the data. Considering these observations, it appears that the new calibration coefficients significantly improve the predictive skill of all three formulas.

It should however be noted that there is still considerable scatter in Figures 2.9b to 2.11b, which show plots of $Q_{predicted}$ vs. $Q_{measured}$ with the improved formulas. This is probably because of the complex nature of the processes involved and the difficulty of measuring the LST related parameters, and LST rates. The simplified bulk formulations fail to take into account factors such as the existence of submerged nearshore bars and other morphological features on the beach that will influence wave breaking, current patterns and thus LST. For example, the existence of a bar may drastically influence the value of the beach slope at the break point, when compared with the beach slope values calculated using a representative Dean profile (as assumed in the Bayram formula). It is

Table 2.3: Relative performance of the bulk formulas with the previous and new calibration factors

	formula	$RMSE$	$bias$	% between 0.5 and 2
previous	CERC with k=0.39	0.719	0.534	28%
	CERC with $k_{K\&R}$(Kamphuis and Readshaw, 1978)	0.518	0.192	48%
	CERC with k_B (Bailard, 1984)	0.619	0.344	36%
	CERC with $k_{VM\&L}$ (del Valle et al., 1993)	0.681	0.378	25%
	Kamphuis with original coefficients	0.609	-0.417	40%
	Kamphuis with $k_{S\&T}$ (Schoonees and Theron, 1996)	0.554	-0.331	41%
	Bayram with original k	0.570	0.010	32%
new	CERC with new coefficient	0.413	0	53%
	Bayram with new coefficient	0.407	0	56%
	Kamphuis with new coefficients	0.398	0	56%

also not unlikely that the data includes LST due to currents generated by forcing mechanisms other than wave breaking (e.g. wind and tide). Another source of uncertainty is the use of representative wave conditions to simulate the effect of a wave climate over a period of time. This is applicable mainly for longer term measurements.

2.6.2. DIFFERENCES BETWEEN RESULTS USING COMMONLY OBSERVED WAVE INPUTS

To quantify differences between new and previous coefficient formulations, the three formulas were applied with a range of plausible wave inputs. Because the new coefficients in the Bayram and CERC formulas depend only in H_{sb} and T_p (through L_o), the wave inputs were chosen to represent a range of these parameters. All other inputs to the formulas were kept constant. Table 2.4 shows the percentage differences between the LST values predicted with the previous and new formulations ($f = {}^{100*(Q_{new}-Q_{previous})}/{}_{Q_{previous}}$).

The differences are significant for all formulas. For the Bayram formula the differences range from -91% to 202%, with these values corresponding to the highest and lowest wave steepness values considered (i.e., $H_{sb} = 0.5m$ with $T_p = 14s$ and $H_{sb} = 2m$ with $T_p = 6s$). In the case of the CERC formula, the new coefficient decreases the predicted LST values by between 45% and 88%, with the larger decrease being associated with higher waves and smaller periods. The Kamphuis formula shows differences between -75% and 18%, that correspond to the lowest and highest steepness values considered. It is noted that the Kamphuis formula also depends on other parameters, i.e., m, D_{50} and α_b. However, the differences obtained varying H_{sb} and T_p were already substantial, and therefore the variation with the other parameters was not investigated.

Table 2.4: Percentage differences between LST values predicted with previous and new coefficients for combinations of different H_{sb} and T_p values and with α_b =10°

	Bayram			CERC			Kamphuis		
T_p	$6s$	$10s$	$14s$	$6s$	$10s$	$14s$	$6s$	$10s$	$14s$
H_{sb} =0.5m	-2%	119%	202%	-63%	-49%	-45%	-58%	-70%	-75%
H_{sb} =1m	-67%	5%	75%	-77%	-57%	-49%	-30%	-49%	-58%
H_{sb} =2m	-91%	-62%	-21%	-88%	-70%	-57%	18%	-14%	-30%

2.7. GENERALITY

The generality of a model expresses its reliability when applied to a data set different than the one used for calibration. In this study, both *bootstrapping* and *cross-validation* methods were used to assess the generality of the improved formulas presented above.

The *bootstrapping* method involves calculating the coefficients and statistics of a number of samples that are taken from the available data set. The method can essentially be summarized as follows: 1) a sample with random points (picked with replacement from the data set, i.e. the same point can be picked more than one time) is selected. This so called *bootstrap sample* has the same size as the data set. 2) A least-squares fitting is performed using the *bootstrap sample*, and the coefficients and statistics are stored. 3) The process is repeated many times for different bootstrap samples (in this case 10000) in order to have a meaningful statistic. 4) the distributions of the estimated parameters and error statistics are calculated from the results obtained with the different *bootstrap samples*. The histogram with the distribution of fitting parameters, and the histogram of *RMSE* values obtained with the new CERC formula, is shown in Figures 2.12 and 2.13.

In the *cross-validation* method the data set is randomly divided in two groups: a calibration group and a validation group (in this case I used a 50/50 division). The calibration group is used to calculate the coefficients, using the least-squares algorithm. The validation group is used to test the predictive skill of the model. The process is repeated many times to have a meaningful statistic (in this case I repeated the process 10000 times), and the resulting coefficients and statistics are stored. Finally, as with the *bootstrapping* method, the distributions of the estimated parameters and error statistics are calculated using these stored values.

The results obtained with the *cross-validation* and *bootstrapping* methods are similar and no advantage to either method could be found. For that reason only the results obtained with the *bootstrapping* method are presented.

The values obtained for the performance measures considered in this study: *RMSE* and *bias*, are shown in Table 2.5 for the *bootstrapping* method. In this table one can observe that the median *RMSE* values are in the vicinity of 0.4, and have a small standard deviation (around 0.02). The 95$^{\text{th}}$ percentile is equal or less than 0.45, for all formulations and for both methods. This means that more than 95% of the samples have an *RMSE* value well under the one obtained with the previous best performing coefficient (Table 2.3). The *bias* values obtained for the all the formulations and methods are indistinguishable from zero and for that reason I chose not to show them. The low *RMSE* variability indicates that the improved coefficients have a good generality and are expected to result

Table 2.5: Median, standard deviation and 95th percentile of the *RMSE* distributions obtained with the *bootstrap* method. All formulas use the new coefficients

formula	$\tilde{x}$	σ	95th PCTL
CERC with new coefficient	0.410	0.018	0.440
Bayram with new coefficient	0.404	0.0191	0.435
Kamphuis with new coefficients	0.392	0.0186	0.423

Table 2.6: Coefficients obtained with the calibration groups using the *bootstrap* method. All formulas use the new coefficients

coefficients	a		b		c		d		e	
	$\tilde{x}$	σ	$\tilde{x}$	σ	$\tilde{x}$	σ	$\tilde{x}$	σ	$\tilde{x}$	σ
CERC	2303	11992	1.46	0.32	4.45	0.92	-	-	-	-
Bayram	8×10^5	3.1×10^6	1.29	0.27	1653	321	-	-	-	-
Kamphuis	0.012	0.0205	-0.94	0.07	0.89	0.35	0.70	0.26	0.50	0.11

in good predictions with different data sets.

The statistics of the coefficients show that for all formulations the median values are very similar to the ones found via the least-squares algorithm (Eqs.2.24, 2.25 and 2.26). This demonstrates that even if the model was calibrated using only part of the data set, it would still give good predictions on the other part, regardless of the division made. This is an indication that the model has good generality, i.e. the accuracy of the predictions on other data sets will be similar to the accuracy observed on this one.

2.8. CONCLUSIONS

A comprehensive analysis of three of the most commonly used bulk longshore sediment transport (LST) formulas (CERC, Kamphuis and Bayram) has been undertaken using the most extensive LST data set presently available. The analysis resulted in new calibration coefficients (and also new exponents for the Kamphuis formula), using a least-squares optimization algorithm that allow the use of non-linear functions. The predictive skill of all three improved formulas (RMSE ~ 0.4-0.41, *bias* ~ 0, % within factor 2 ~ 53-56) was significantly better than their previous versions (RMSE ~ 0.52-0.56, *bias* ~ -0.4-0.5, % within factor 2 ~ 32-48). The generality of the improved formulas was examined by applying the *bootstrapping* and *cross-validation* statistical methods, both of which returned similar results and confirmed the generality of the formulations. While the performance of all three improved formulas are very similar, the improved Kamphuis formula performs best, followed by the improved Bayram formula.

It is important to notice that despite the significant improvement in the prediction skills of the LST formulations, there is still considerable scatter. About 42% of the predictions (by all three improved formulas) deviate more than a factor 2 with respect to

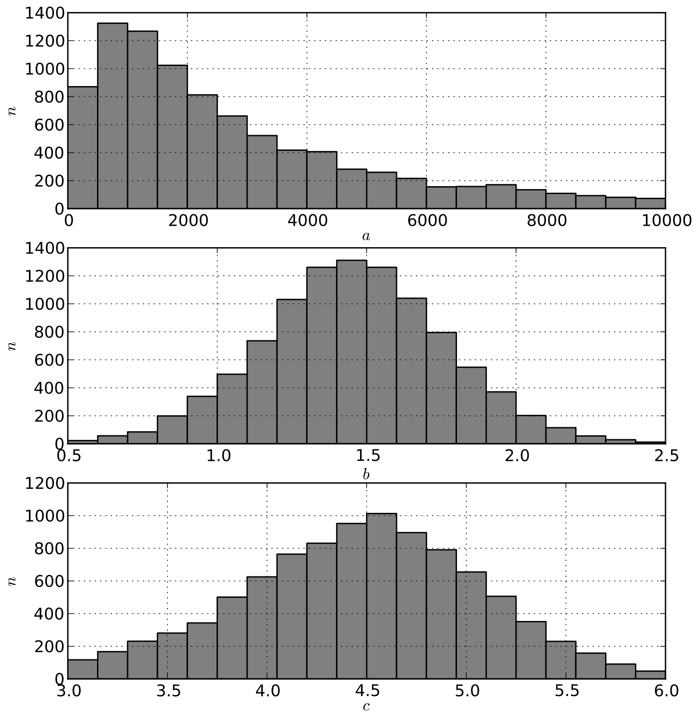

Figure 2.12: distribution of the fitting parameters a, b, and c for the CERC formula with $k_{CERC,a} = k\left(\frac{H_{sb}}{L_o}\right)$, using the *bootstraping* method

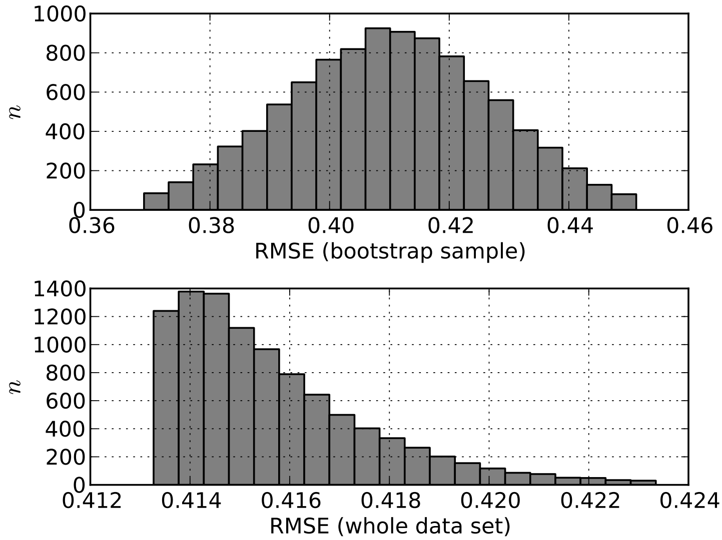

Figure 2.13: distribution of the statistical parameters: bias related to the *bootstrap sample*, bias related to the whole data set,RMSE related to the *bootstrap sample* and RMSE related to the whole data set, for the CERC formula with $k_{CERC,a} = k\left(\frac{H_{sb}}{L_o}\right)$,using the *bootstraping* method.

observations. This may be due to the several reasons including: the non-consideration of parameters that may influence LST such as cross-shore profile features, 3 dimensional morphological features, tidal range and wind conditions in bulk LST formula; experimental errors that may have compromised data quality and insufficient data for high LST conditions. Another important shortcoming is the underestimation of LST in the higher energy region. This is most visible in the results of the CERC and Bayram formulas with the new coefficients. It would be desirable to have more data points in this region.

2.9. ACKNOWLEDGEMENTS

The authors wish to express their gratitude to Dr. Atilla Bayram (Halcrow, Inc.) and Prof. Magnus Larson (Lund University, Sweden) for kindly providing the invaluable data set used herein. The authors also acknowledge the contribution of Pieter van Gelder for his help and insights in the statistical analysis.

3

INFLUENCE OF PROFILE FEATURES ON LST

ABSTRACT

Longshore sediment transport (LST) is one of the main drivers of beach morphology. Bulk LST formulas are routinely used in coastal management/engineering studies to assess LST rates and gradients. However, there is still great uncertainty in LST estimation with these bulk formulas. This uncertainty may have two sources: 1) experimental errors in the measured values and 2) the effect of physical processes that are not part of the formulas. In this study, I attempt to find the influence of profile related features on LST rates, which are not yet accounted for in the bulk formulas. These features influence the location and type of wave breaking and by that the cross-shore distribution of alongshore flow and the local sediment stirring.

A process-based model (UNIBEST-LT) is used to calculate LST rates on a large number of profiles measured at the Dutch coast using the same realistic wave climate. I found that the LST rates vary with the profiles. The value corresponding to the 95th percentile of the resulting distribution is 50% higher than one correspondent to the 5th percentile. The root mean square downward slope parameter showed the best correlation with LST rates.[a]

[a]This chapter is based on the article published in the Proceedings of the 7th International Conference on Coastal Dynamics, Arcachon, France, with the title: "Influence of profile features on longshore sediment transport" (Mil-Homens et al., 2013b)

3.1. INTRODUCTION

Wave breaking generates turbulence that can propagate downwards in the water column and reach the bed, as observed by Melville et al. (2002).This turbulence can contribute for stirring the sediment from the bed. It has been shown in laboratory that the type of wave breaking influences the amount of suspended sediment: Ting (2001) concluded that plunging wave breakers generate considerably larger downward velocities when compared to spilling breakers and Smith et al. (2009) measured Longshore Sediment Transport (LST) under spilling and plunging wave conditions and concluded that the latter was able to stir significantly larger amounts of sediment from the bed and generated larger LST rates.

Wave breaking influences LST in more than one way. It causes cross-shore gradients in the radiation stresses, which result in a net force on the water column that drives the alongshore flow. In addition, wave breaking controls the local wave height and consequently the stirring capacity due to local orbital velocity. Sediment can also become suspended by wave breaking induced turbulence that travels down the water column and reaches the bed. However, this last effect is not included in any of the LST bulk formulas or process-based models. The simultaneous combination of sediment stirring and alongshore current causes LST.

The gradients in LST dictate to a large extent whether shores erode, accrete or remain stable. In addition, large and/or persistent LST rates may have various other impacts, such as: inlet closure/migration, ebb/flood delta erosion/accretion, rotation of pocket beaches and headland sand bypassing. The calculation of LST rates is therefore a key component on most coastal engineering/planning studies. The main approaches to estimate LST can be divided in two groups: bulk transport formulas which are basic models that assume a simplified representation of the physical processes and generally use empirical coefficients for calibration (e.g. the CERC (CERC, 1984b), the Kamphuis (Kamphuis, 1991) and the Bayram (Bayram et al., 2007) formulas) and process-based models which intend to include a large number of physical processes such as shear stress, pickup, suspension, wave-current interaction, etc. (e.g. Deigaard et al. (1986), UNIBEST (WL|Delft WL|Delft Hydraulics, 1992) and GENESIS (Hanson, 1989)).

In the present, bulk formulas show great uncertainty. Using an extensive data set, Mil-Homens et al. (2013a) (chapter 2) concluded that about 42% of the predictions obtained by the CERC, Kamphuis and Bayram formulas differ by a factor greater than 2 with respect to measured values. As input, bulk formulas usually require wave characteristics at the edge of the surf zone (e.g. breaking wave height, direction and period) and in some cases basic morphological variables (e.g. mean grain diameter, beach slope). The effects of more complex hydrodynamics associated with morphological features in the surf zone are not taken into account.

The objective of this study is to investigate whether there are any significant correlations between LST rates and cross-shore surf zone features such as beach slope, the presence and number of bars, and others. It is hypothesised that profile features may influence LST rates significantly, mainly by dictating the location and type of wave breaking and by that the cross-shore distribution of alongshore flow and the local sediment stirring. This hypotheses is motivated by the results in Smith et al. (2009) where plunging breakers resulted in considerably higher LST rates when compared to spilling breakers. For this reason, I investigate profile features that may be related to the type of breaker, i.e., that are related with the bed slope at the breaking point. To accomplish this, LST rates are calculated in a large set of profiles surveyed on the Dutch coast using a process-based model, UNIBEST-LT (WL|Delft Hydraulics, 1992). Correlations between the results obtained and profile related parameters will be examined.

3.2. BED SLOPE AND LST

Bed slope can influence LST rates in two ways: through controlling the wave breaking type and through the cross-shore distribution of the alongshore current.

3.2.1. WAVE BREAKING TYPE

In order to include the effect of the wave breaking type on LST rates it is necessary to parametrise it. The Iribarren number (eq.2.2), also known as surf similarity, is the most used indicator for the type of breaker. Battjes (1974) found that ξ_b is typically less than 0.4 for spilling breakers and typically ranges from 0.4 to 2.0 for plunging breakers. When wave height and period are held constant, breakers become increasingly more plunging with increasing slope. Intuitively, larger LST rates are expected as waves become more plunging as an increasingly strong jet of water is ejected from the wave crest and creates turbulence that more easily reaches the bed and stirs more sediment.

A possible relationship between LST rates and the Iribarren number has been discussed in several studies, e.g., Kamphuis and Readshaw (1978), Vitale (1981) and Bodge and Dean (1987) . Kamphuis and Readshaw (1978), Kamphuis et al. (1986) and others, attempted to incorporate the Iribarren number into the empirical coefficient in the CERC formula. The Kamphuis formula (Kamphuis, 1991) includes the slope at the breaker as a factor.

For irregular waves the beach slope is usually computed as the average over the breaking zone, i.e., the breaking depth divided by the (cross-shore) distance from the still water line to the breaker position. However, this average bed slope may be a misleading indicator for the dominant breaker type. Waves with different heights break at different locations and the slope at the breaker position can be very different from the average slope. If bars are present, it is likely that waves break over the seaward slope of the bar where the slope can be much steeper than the average.

3.2.2. CROSS-SHORE DISTRIBUTION OF ALONGSHORE CURRENT

The bed slope may also influence LST through a different mechanism. On a steeper slope the surf zone is more concentrated, i.e. waves with different heights have breaking points that are closer to each other. Consequently, the energy dissipation occurs over a smaller area. The rate of energy dissipation (proportional to the cross-shore gradient of the shear stress component S_{xy} of the radiation stress) is responsible for driving wave generated alongshore currents (Longuet-Higgins, 1970). In a shorter surf zone, and under the same wave forcing, a more localized and stronger current will be generated in same the area where more sediment is in suspension.

3.3. UNIBEST-LT MODEL

The process-based model UNIBEST-LT computes the tide and wave induced alongshore currents and resulting sediment transport for a given cross-shore beach profile assuming that the beach is uniform in alongshore direction. The longshore sediment transport and its cross-shore distribution can be calculated using various transport formulas.

3.3.1. WAVE PROPAGATION AND SURF ZONE DYNAMICS

UNIBEST-LT computes the surf zone dynamics through a built-in wave propagation and decay model (Stive and Battjes, 1984). This model takes into account the main processes affecting wave propagation: refraction, shoaling and dissipation due to wave breaking and bottom friction. The wave induced time-averaged alongshore current distribution is derived from a simplified momentum equation that reduces to a balance between cross-shore gradient of the alongshore momentum flux and alongshore bottom stress.

3.3.2. LST RATES CALCULATION

LST rates are calculated according to several total-load sediment transport formulations for sand and shingle. All formulas use a threshold for initiation of motion and a limitation of the flow capacity to carry sediment. The sediment transport is assumed to respond to local wave and current conditions in an instantaneous quasi-steady way. The formulation identified as Van Rijn 2004 (van Rijn, 2007a,b, van Rijn et al., 2007, van Rijn, 2007d)(van Rijn, 2007a,b, van Rijn et al., 2007, van Rijn, 2007d) is used in this study. It accounts for most of the physical processes known to be involved in sediment transport. The main features of this model are:

- intra-wave approach to bed-load transport with initiation of motion and estimation of effective bed-roughness (accounts for the effect of bed forms such as ripples)
- suspended-load transport calculation using a vertical concentration distribution (including effects like sediment mixing due to currents and waves, flocculation, hindered settling and stratification)
- consideration of sediment grading in the bed

3.3.3. MODELLING WAVE BREAKING AND SEDIMENT SUSPENSION

It is important for this study to understand how the model UNIBEST-LT simulates wave breaking and its contribution to sediment suspension. The wave propagation model includes wave breaking through a dissipation term added to the wave energy balance equation (eq.3.1).

$$\frac{d}{dx}\left(\frac{E}{\omega_r}c_g\cos\alpha\right)+\frac{D_b}{\omega_r}=0 \tag{3.1}$$

In eq.2 E is the wave energy per unit area, ω_r is the relative wave peak frequency, α is the wave angle, c_g the group velocity and D_b represents energy dissipation due to wave breaking (eq.3.2). The adopted referential uses x and y for the cross-shore and alongshore directions respectively.

$$D_b=\frac{1}{4}\rho g a_c Q_b\left(\frac{\omega_r}{2\pi}\right)H_{max}^2 \tag{3.2}$$

In eq.3.2 ρ is the density of water, g is the acceleration of gravity, a_c is a coefficient for wave breaking, Q_b is local fraction of breaking waves and H_{max} is the depth limited wave height. The alongshore current, when tide generated currents are not taken in to account is only forced by the cross-shore gradient of the shear stress component S_{xy} of the radiation stress (eq.3.3):

$$\frac{dS_{xy}}{dx} + \rho \frac{g}{C^2} V |V_{tot}| = 0 \tag{3.3}$$

where $S_{xy} = En \sin\alpha \cos\alpha$, which is directly dependent on D_b (eq.3.1), C is a Chezy friction coefficient, V is the longshore current component and $V_{tot} = \sqrt{V^2 + U_{rms}^2}$ where U_{rms} is the root mean squared orbital velocity. The suspension of sediment is simulated within the sediment transport formulation that takes the form of a time averaged advection-diffusion equation (eq.3.4).

$$c w_s + \varepsilon_{s,cw} \frac{dc}{dz} = 0 \tag{3.4}$$

where c is the sediment concentration and w_s the fall velocity of suspended sediment. The effect of wave breaking on the Van Rijn 2004 formulation is accounted for by the sediment mixing coefficient $\varepsilon_{s,cw}$ (eq.3.5) that results from contributions of waves and currents:

$$\varepsilon_{s,cw} = \sqrt{\varepsilon_{s,c}^2 + \varepsilon_{s,w}^2} \tag{3.5}$$

where $\varepsilon_{s,c}$ and $\varepsilon_{s,w}$ are the current and wave sediment mixing coefficients. The wave mixing coefficient is different for the bed (eq.3.6) and upper (eq.3.7) parts of the water column:

$$\varepsilon_{s,w,bed} = 0.018 \gamma_{br} \beta_w \delta_s U_{\delta,r} \tag{3.6}$$

$$\varepsilon_{s,w,max} = \min\left(0.035 \gamma_{br} h \frac{H_s}{T_p}, 0.05\right) \tag{3.7}$$

β_w is a coefficient dependent on the sediment fall velocity, δ_s is the thickness of the mixing layer (also dependent on γ_{br}), $U_{\delta,r}$ is the representative near-bed peak orbital velocity based on significant wave height, h is the water depth, H_s is the significant wave height, T_p the peak period and γ_{br} is an empirical coefficient related to wave breaking (eq.3.8).

$$\gamma_{br} = 1 + \left(\frac{H_s}{h} - 0.4\right)^{0.5} \tag{3.8}$$

3.3.4. SLOPE INFLUENCE ON LST CALCULATED BY UNIBEST-LT

The influence of the profile slope on the results of the UNIBEST-LT can be two-fold: 1) a steeper slope results in a shorter surfzone with higher wave breaking dissipation per distance unit and therefore a higher value of $\frac{dS_{xy}}{dx}$, which forces locally higher longshore currents; and 2) the coefficient γ_{br} (eq.3.8) is a function of H_s/h that has been accepted as a good indication to whether waves are breaking or propagating as bores (Ting and Kirby, 1995), with higher values for the former. This means that on a steeper slope waves of different heights start breaking closer to each other yielding higher H_s/h values, and consequentially higher γ_{br}. These two effects combine in a way that the highest sediment mixing occurs at the same zone where the highest longshore current is forced.

Some test runs using “flat” profiles, i.e, profiles with a constant slope, were made with different slopes from 0.005 to 0.05. A single wave condition was used: H_s =1 m,

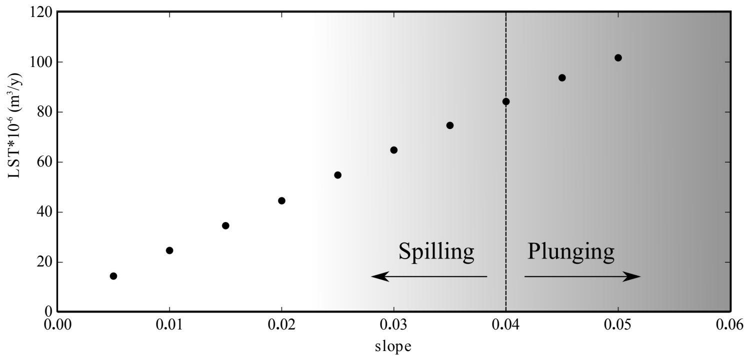

Figure 3.1: LST results from UNIBEST-LT using "flat" profiles with different slopes and transition between spilling and plunging breakers.

T_p= 10 s and α=10 degrees, and the default values for the coefficients on the Van Rijn 2004 formula. The results (figure 3.1) show a linear variation of LST with the slope. The transition between spilling and plunging wave breaking types referred to in section 3.2 is also represented in figure 3.1. Considering the reasons presented in the previous paragraph, LST rates were expected to increase with slope.

These perfectly "flat" profiles and single wave conditions do not occur in nature. In the next sections, the UNIBEST-LT model will be applied to real profiles, with a real wave climate in order to see how this trend transfers to real conditions.

3.4. DATA

The numerical model inputs are the cross-shore bathymetry profiles and the wave climate data in deep water offshore of the studied area. The bathymetry profiles used in this study are part of the JARKUS data set. This data set comprises profiles surveyed every year since 1965, along the entire Dutch coast. The profiles are separated by 250 m in the alongshore direction. In the cross-shore direction the points have a grid spacing of 5 m in the beach area and surf zone. In earlier measurements it is common to find a cross-shore grid spacing of 10 m in the points below NAP[1]. The profiles start inland after the first dune row, and extend to depths of up to 18 m NAP in the most recent surveys. In general, profiles measured earlier stop at smaller depths and have lower quality data (less data points, more fluctuations). For this reason, only profiles that reach at least 8 m of depth are used. I considered the 8 m depth also to be the limit of the active profile. This limit was chosen based on Hinton and Nicholls (1998), that found the depth of closure in the Holland coast to be between 5 m and 8 m, for a time scale of 20 years.

For this study, I only considered profiles that: 1) are located between IJmuiden and Hoek van Holland (South-Holland coast), 2) have its most offshore point deeper than 8 m NAP, 3) have at least 30 points with elevation below NAP, 4) reach at least the level 3 m above NAP and that are at least 4 km away from the breakwaters at Hoek van Holland or

[1] Nieuw Amsterdams Peil – reference level in the Netherlands

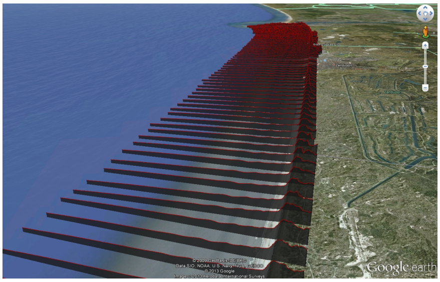
(a) Jarkus profiles rendered on Google Earth

(b) South-Holland coast

Figure 3.2: Jarkus profiles and area used in this study

IJmuiden. The total number of profiles that satisfy these conditions is 3085. These profiles show a large degree of variability as it can be observed in figure 3.3. A more detailed analysis of the variability of slope and shape of the profiles is presented in section 3.5.2. Sediment in this area has grain sizes between 200 μm and 250 μm.

As input, the model used a wave climate that is composed of 1 year of conditions distilled from 10 years of wave observations. The wave data was measured by Rijkswaterstaat near IJmuiden, at IJmuiden munitiestortplaats, located at 52°33'00" East and 4°03'30" North. The water depth at this location is 21 m. The data was collected with intervals of 1 hour and values for significant wave height, mean zero-crossing period (T_{m02}) and direction amongst others were measured. The measurements were divided in three-dimensional bins according to H_s (from 0 m to 7 m in 0.5 m increments), T_{m02}(from 2 s to 10 s in 2 s increments) and direction (0 to 360 degrees in 20 degrees increments). Figure 3.4 shows the total histograms (comprising all directions) of H_s and T_{m02}. Figure 3.5 shows the directional histograms of H_s and T_{m02}.

Using UNIBEST-LT, each three-dimensional bin condition was propagated from a 21 m depth to an 8 m depth assuming a slope similar to what is observed at those depths close to IJmuiden (approximately 0.004). Because UNIBEST-LT uses as input the peak period (T_p) instead of T_{m02}, I needed to perform a conversion. Lecture notes from Prof. Battjes (personal archive) state that the conversion factor should be $T_p = T_{m02}$ for swell and $T_p = 1.4T_{m02}$ for locally generated wind waves. Based on this information a factor that varied linearly from 1.4 at $T_{m02} = 4$ s to 1 at $T_{m02} = 16$ s was used.

The propagated wave parameters were re-classified into the same three-dimensional bins. For T_p the bins were set from 4 s to 12 s in 2 s increments. The results are shown in Figure 3.6. At the depth of 8 m the waves come from two predominant directions: around NNW and WSW, that account for approximately 55% of all waves. In general NNW waves can be associated with larger periods, typically above 6 s, while WSW waves typically have smaller period values. In terms of wave heights, WSW waves present slightly higher waves.

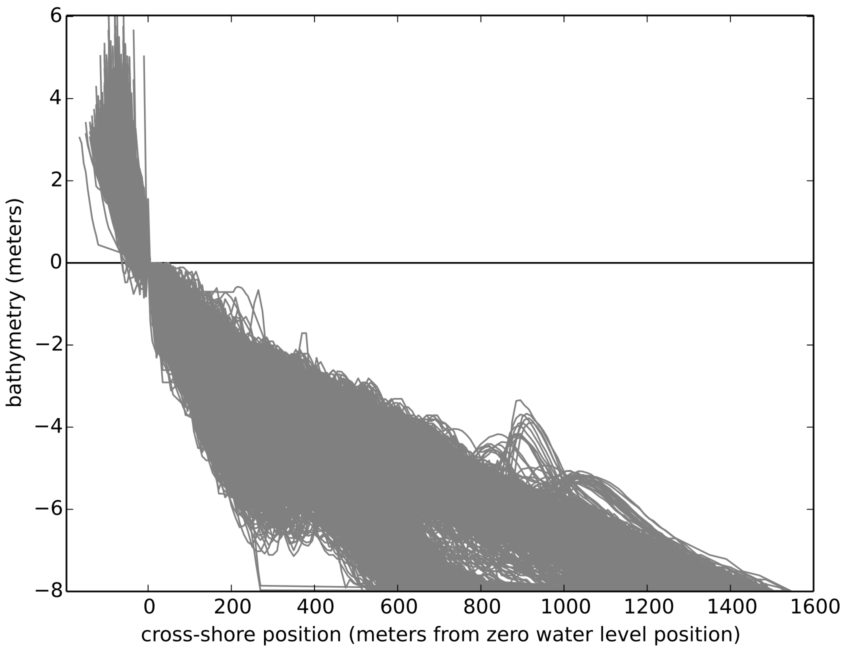

Figure 3.3: "Cloud" of all the profiles used showing the high variability in slope and shape

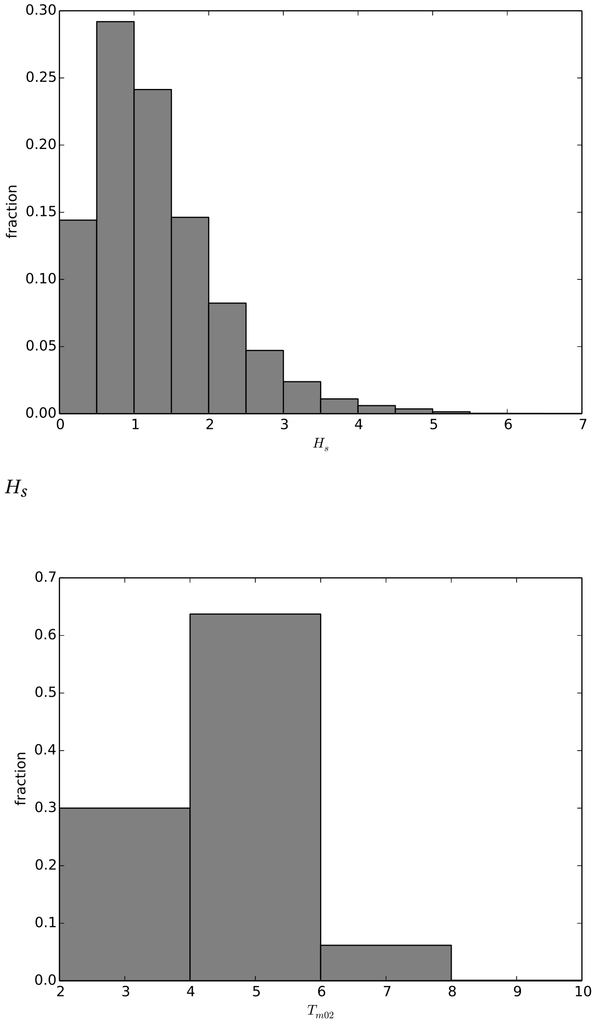

(a) H_s

(b) T_{m02}

Figure 3.4: Histograms of H_s and T_{m02} at 21 m depth.

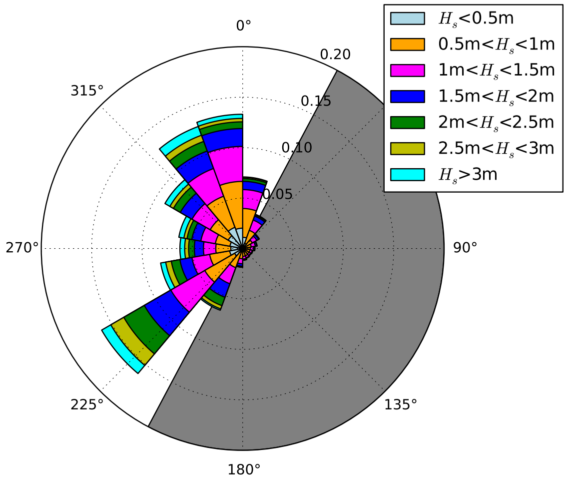

(a) H_s

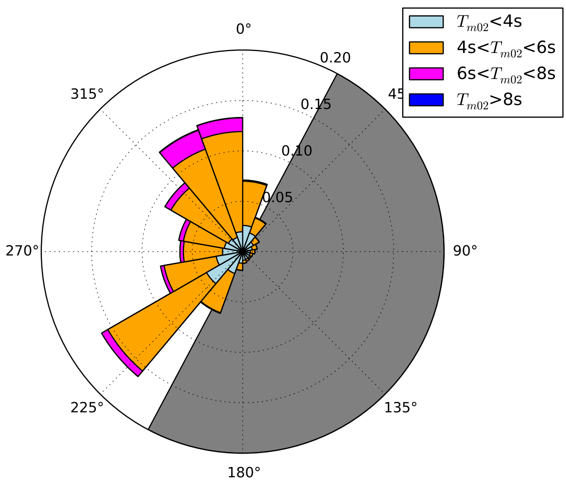

(b) T_{m02}

Figure 3.5: Directional histograms of H_s and T_{m02} at 21 m depth. The grey area represents the coastal orientation.

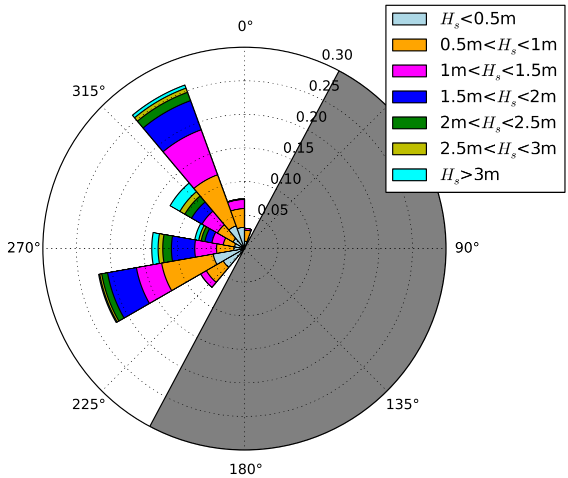

(a) H_s

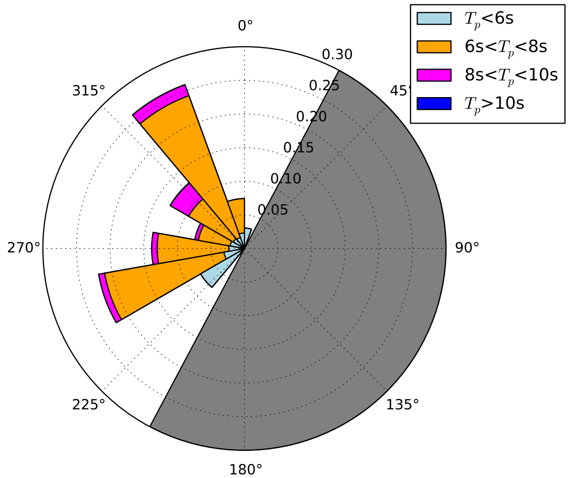

(b) T_{m02}

Figure 3.6: Directional histograms of H_s and T_p at 8 m depth. The grey area represents the coastal orientation.

Table 3.1: Values used for the Van Rijn (2004) formula

D_{10}	D_{50}	D_{90}	D_{ss}	ρ_{water}	$\rho_{sediment}$	Porosity	Temperature	Salinity
μm				kg/m³		-	°C	ppm
140	225	280	200	1025	2650	0.4	15	30

Table 3.2: Values used for the wave parameters in UNIBEST-LT

γ	α	k_b
0.8	1	0.1 m

3.5. METHOD

The UNIBEST-LT model was used to calculate LST rates for all the 3085 JARKUS profiles considered valid under the same wave forcing. For each profile used, I tried to identify and parametrise the most important profile features.

3.5.1. MODEL SETUP

In all computations the same input coefficients and wave forcing were used. The only difference between computations was the profile used. Tables 3.1 and 3.2 show the model parameters adopted in the simulations. The sediment properties used are typical values for the Dutch coast. Because the aim of this work is to study the differences between results and not the absolute values of LST rates, the value of the input parameters is not crucially important. Nevertheless, I took care that sediment related parameters have realistic values.

In Tables 3.1 and 3.2: D_{10}, D_{50} and D_{90} are the 10^{th}, 50^{th} and 90^{th} percentiles of the grain size distribution, D_{ss} is the median size of suspended sediment, ρ_{water} and $\rho_{sediment}$ are the densities of water and sediment, γ is a wave breaking coefficient, α is another wave breaking coefficient and k_b is the bottom roughness. Input files for the model were created with Python scripts. In this step, the grid that the model uses, the transport truncation point and dynamic boundary were defined. The model uses a flexible grid that allows the use of smaller cells near the shoreline and larger cells in deeper positions. Table 3 shows the reference grid sizes used in our simulations.

3.5.2. PROFILE FEATURES

The profile features chosen to be tested are: average slope, root mean square slope, average downwards slope, root mean square downwards slope and the number of bars. Smoothed profiles were used to calculate these parameters because measurement fluc-

Table 3.3: Reference grid sizes used in the computations (cross-shore position is positive in the onshore direction, and zero represents the shoreline)

Cell size (m)	40	2	4	5	50	100
Cross-shore position (m)	10	0	-300	-500	-1000	-1800

tuations or even ripples can influence heavily these parameters.

The average slope was calculated with the formula: $m = x_{max}/h_{max}$ where x_{max} is the cross-shore position at a depth of h_{max}=8 m.

The root mean square slope was calculated with eq.3.9 where m_i are the slope values in each grid cell. Only cells over the active profile (until the 8 m depth) are considered. The root mean square accounts for variations of the slope value. Profiles with high slope variation have higher root mean square values.

$$m_{rms} = \sqrt{\frac{\sum_{i=0}^{N} m_i^2}{N}} \tag{3.9}$$

The average downwards slope is the average slope value of the grid cells that have a negative slope (cells in the seaward slope of a bar, for example), over the active profile (until the 8 m depth). Because waves start to break where the slope is negative, it is expected that only the slope of those locations influences the type of breaker.

The root mean square downwards slope is obtained taking the root mean square of the slope value on the grid cells that have a negative slope.

The detection of bars is not straightforward. There is some ambiguity in what is considered a bar. In order to have an objective measure, the following method was used: 1) the profile was interpolated in a 5 m grid (to avoid problems of missing values), 2) using a moving average method, the profile was smoothed to eliminate fluctuations due to measurement errors, 3) all local maxima (crests) and minima (troughs) were listed, 4) a relative height parameter r_{ct} was calculated using eq.3.10, where d_{crest} and d_{trough} are the depths at the crest and at the trough respectively and 5) a threshold value for the ratio r_{ct} was set. Local maxima that have a relative height greater than the threshold are considered bars. The threshold adopted (via trial and error) was 0.1, but other values were also tested. Figure 3.7 shows an example of the results of the method.

$$r_{ct} = \frac{d_{crest} - d_{trough}}{d_{crest}} \tag{3.10}$$

Figure 3.8 shows the distribution of the values obtained for these measures for all valid profiles. The distribution of average slope values is bimodal, with two distinct peaks clearly visible on figure 3.8a. These two peaks correspond to profiles in the most northern part of the domain (smaller average slopes) and the most southern part (higher average slopes). This bimodal character is in part caused by the existence of more valid profile measurements in these regions, in contrast with the area in between where fewer valid profiles are available and consequently is less represented in the histogram. For the other profile features, the bimodal character of the distributions becomes more attenuated.

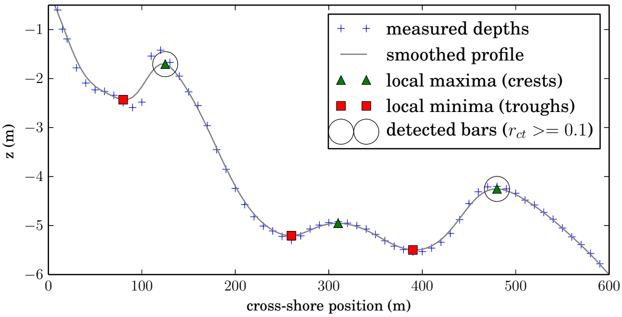

Figure 3.7: Example of the results obtained with the bar detection method. Notice that the second maximum is not considered a bar.

Table 3.4: r^2values for all the profile features

Profile feature	r^2
average slope	0.50
rms slope	0.66
average downwards slope	0.72
rms downwards slope	0.77
Number of bars	0.06

3.6. RESULTS

3.6.1. LST RATES

Figure 3.9 shows the distribution of LST rates obtained. LST rates range from 100 000 to more than 400 000 m³/y, and approximately 50% of LST rates are concentrated between 100 000 and 150 000 m³/y. The value corresponding to the 95th percentile of the resulting distribution is 50% higher than one correspondent to the 5th percentile. It is important to emphasize that these differences are caused only by the profiles.

Figure 3.10 shows the values of the profile features described in the last section plotted against the LST rates and respective linear regression results.

In Table 3.4 the r^2 values obtained for all the profile features are presented. The calculated LST rates show significant variability with the profiles used, considering that all profiles come from the same region. In this stretch of coast the average slope values are between 0.005 and 0.02. The best correlation was found for the root mean square downward slope, with r^2=0.77. The second best was the average downwards slope. The other parameters related to bed slope show lower r^2 values. The root mean square measures seem to be better indicators for the influence of profile features on LST rates calculated with UNIBEST-LT. The number of bars shows no correlation with the LST rates. Nevertheless, in Figure 3.10 it can be seen that high transport rates only occur for 0, 1 and 2 bars. For a number of bars higher than 2, LST rates are generally low. The fact that high numbers of bars usually happen with smaller slopes may explain this result.

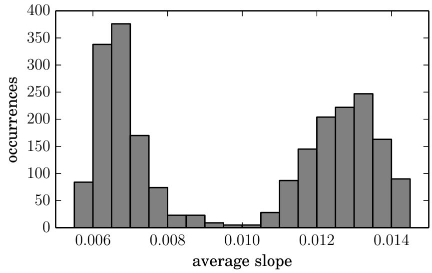

(a) average slope

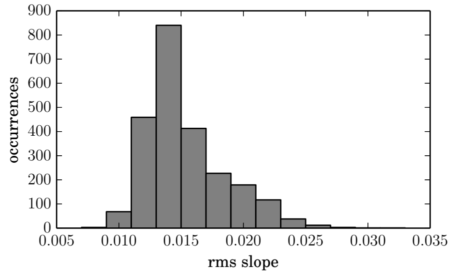

(b) root mean square slope

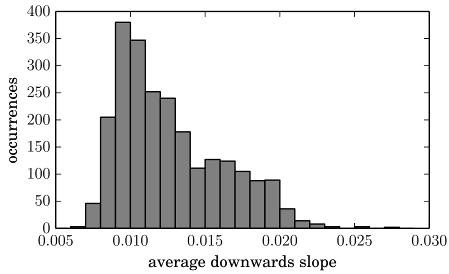

(c) average downwards slope

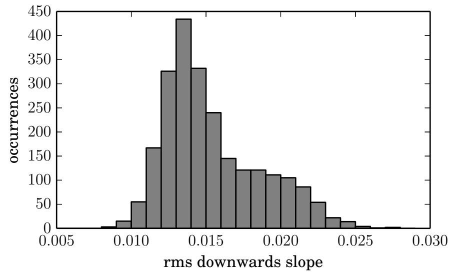

(d) rms downwards slope

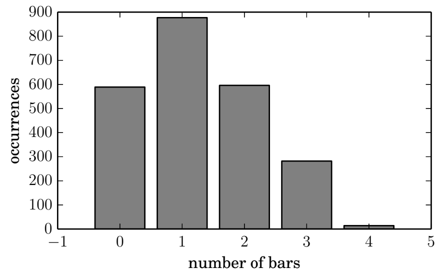

(e) number of bars

Figure 3.8: Histograms of profile features measures.

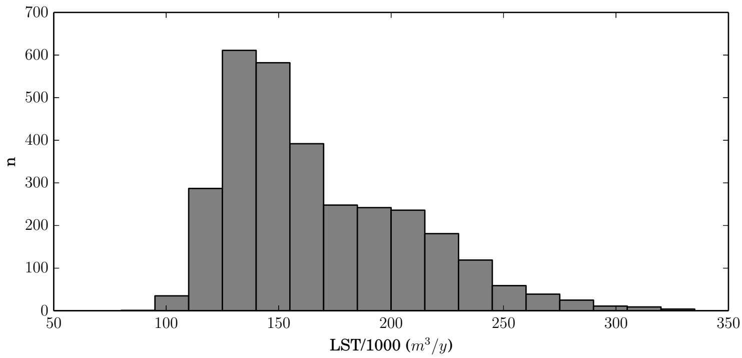

Figure 3.9: Distribution of the LST rates obtained.

3.7. CONCLUSIONS

LST rates calculated with the UNIBEST-LT model were tested for correlations with profile related parameters. The LST rates obtained with UNIBEST-LT vary significantly with the profile used ranging from less than 100 000 m^3/y to over 400 000 m^3/y. This is an indication that the model responds to differences in profile and that it accounts for the influence of profile features in LST rates. Still, the wave climate may also exert some influence and favour LST in some profiles. Further simulations with different years of wave measurements would help us to be more certain that these differences are not an effect of the wave climate used. The root mean square downward slope showed the best correlation (r^2) with the calculated LST rates and all parameters directly related with slope showed some correlation. The number of bars resulted in very small r^2 values. However, the number of bars was found to give an indication of the potential to have higher LST rates: the highest rates were obtained only for profiles with 2 or less bars.

It is unclear how the effects mentioned in section 3.2: wave breaking type and distribution of alongshore current, contribute to these differences in calculated rates due to profile features are generated. In the next chapter, I investigate whether UNIBEST-LT simulates these two phenomena well.

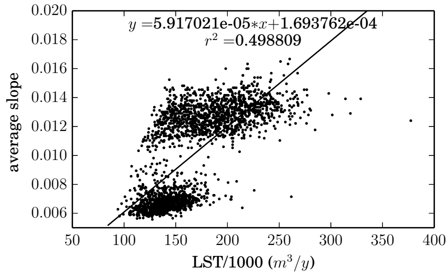

(a) mean slope

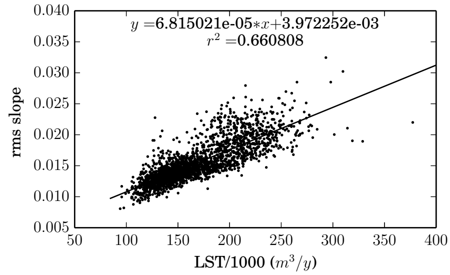

(b) root mean square slope

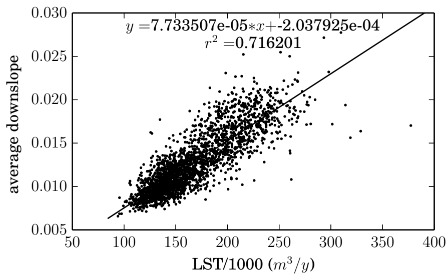

(c) average downwards slope

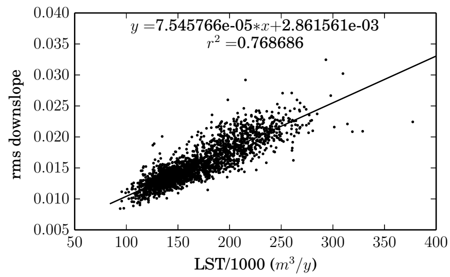

(d) rms downwards slope

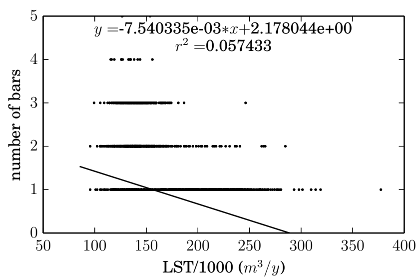

(e) number of bars

Figure 3.10: LST rates vs. profile features.

4

THE EFFECT OF TURBULENCE ON A LST MODEL

ABSTRACT

Wave breaking induced turbulence that reaches the bed, which varies according to the wave breaking type, plays an important part on sediment stirring and consequently is thought to be an important factor influencing LST rates. In this chapter an attempt is made to model this influence. For that effect a process based model is developed and implemented. This model includes a simple turbulence model and uses a novel parametrization for the vertical decay of the wave breaking generated turbulence. Laboratory data that includes test cases with different wave breaking types is used to calibrate the model.

The model was able to reproduce the differences in turbulence decay profiles between different wave breaking types and produced realistic cross-shore profiles of LST. Unfortunately no proper validation was possible due to lack of data.

4.1. INTRODUCTION

In chapter 3 the influence of profile features on LST rates calculated with UNIBEST-LT was investigated. The calculated LST rates varied significantly with the profile used but it was unclear which process was responsible for this variation. In this chapter I explore the effect of wave breaking type on LST rates. The wave breaking type is an indication to how strong is the effect of wave breaking induced turbulence.

The influence of wave breaking induced turbulence on longshore sediment transport (LST) is not explicitly represented in most existing models (e.g. UNIBEST-LT (van Rijn, 2007d,c), Bijker (1971)). However, field and laboratory observations indicate that this effect is important and an effort must be made to include wave breaking induced turbulence in LST models. For example, in a laboratory experiment, Cox and Kobayashi

(2000) identified intermittent episodes of strong turbulence at the bottom inside the surfzone and although those episodes were infrequent, the turbulence was of an order of magnitude larger than the one generated at the bed. Beach and Sternberg (1992) and Wang et al. (2002) also observed the same type of episodic events of high sediment concentration high in the water column under breaking waves. Field observations in Grasso et al. (2012) showed that wave breaking induced turbulence dissipation at the bed was at least two times larger than the current induced turbulence dissipation (generated by bed shear stresses), even in the presence of strong alongshore currents. In another laboratory experiment, Smith et al. (2009) measured significant differences on total LST rates between tests with different wave breaking types.

The wave breaking induced turbulent kinetic energy that reaches the bed has the potential to stir a significant amount of sediment and carry it higher in the water column. However, this happens intermittently in the surfzone (Beach and Sternberg, 1992) and has been observed to be related to the beginning of the breaking and to be more frequent with plunging breakers. Ting and Kirby (1995) observed differences in the turbulence dissipation between spilling and plunging wave breaking types. The former occurs violently over a short time and across the water column (turbulence is transported downwards by the jet) and the latter occurs smoothly and is confined to a region near the surface. In field experiments, Beach and Sternberg (1996) observed that plunging breakers are associated with suspended sediment concentrations roughly four to six times higher than the concentrations associated with bores and concluded that plunging waves are responsible for the greatest share of the suspended load. Grasso et al. (2012) also observed that the turbulent dissipation rate was almost depth uniform where waves were starting to break and that it decayed radically with depth where bores were predominant. Also based on field data, Aagaard and Hughes (2010) concluded that plunging breakers are significantly more efficient in stirring sediment than surf bores. These results are not surprising when one ponders about the mechanics of a plunging breaker where a jet of water is ejected from the crest and falls on the base of the wave face. This jet penetrates the surface and provokes a downward transfer of turbulence that may reach the bed and increase drastically the local instantaneous bed shear stress.

In this chapter I evaluate the effect of wave breaking induced turbulence on LST results from a laboratory experiment. The LST physical model data comes from the Longshore Sediment Transport Facility (LSTF) located at Vicksburg, USA (Hamilton et al., 2001).

This chapter is organized as follows: the data used to calibrate and validate the models is presented in Section 4.2. The UNIBEST-LT model's performance on this dataset is presented in Section 4.3. A wave propagation and longshore current model is presented in Section 4.4 In Section 4.5 I describe the sediment transport model and in Sections 4.6 and 4.7 the results and conclusions are presented and discussed.

4.2. DATA

The laboratory data used in this study were obtained at the LSTF physical model (Hamilton et al., 2001). The LSTF simulates nearshore hydrodynamic and sediment transport processes at a relatively large geometric scale, including situations where considerable sand is mobilized and transported in suspension. The LSTF consists of a 30-m wide,

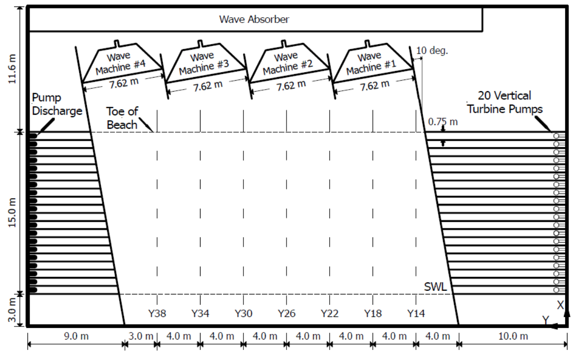

Figure 4.1: Layout of the LSTF (from Smith (2006))

Table 4.1: Incident wave conditions for each test (in front of the wave generator)

Test	Breaker type	$H_{s,o}$ (m)	T_p (s)	θ_o (degrees)
1	Spilling	0.25	1.5	10
3	Plunging	0.23	3.0	10
5	Spilling	0.16	1.5	10

50-m long, 1.4-m deep basin (figure 4.1), and includes wave generators, a sandy beach, a recirculation system (Visser, 1982), sand traps, and a movable instrumentation bridge where instruments can be mounted. These included wave gauges, Accoustic-Doppler Velocimeters (ADV), Fiber Optic Backscatter (FOBS) sensors and a beach profiler. The current data imposed by the recirculation system was also registered. Sediment traps were installed in the downdrift recirculation flow channels to collect sand transported through the downdrift boundary (Smith, 2006).

Four irregular wave conditions with a relatively broad spectral shape, representing typical sea conditions, were generated in the LSTF. The wave conditions were designed to obtain and compare LST rates for different breaker types by varying incident wave height and period. In this study data from tests 1, 3 and 5 is used. The wave conditions are shown in Table 4.1. The tests were performed on a movable bed with sediment with D_{50} = 0.15 mm. The profiles were the result of the wave action, and represent equilibrium situations.

Within each test, 3 measurement runs were carried out - cases 1, 2 and 3. The bathymetry varied slightly from case to case and these small variations may be significant to the model. For that reason I decided to use data from only one case per test: Case 3 from Test 1, Case 2 from Test 3 and Case 3 from Test 5. The cases were chosen taking into account a subjective appreciation of the quality of the data. The bathymetry profiles were smoothed to eliminate ripples and are shown in figure 4.2. More details on this experiment can be found in Smith (2006).

The longshore current velocity data points were obtained by depth averaging values measured by the ADVs at different depths, weighted by each measurement's corresponding water column fraction. The values of the current forced by the pumps were also

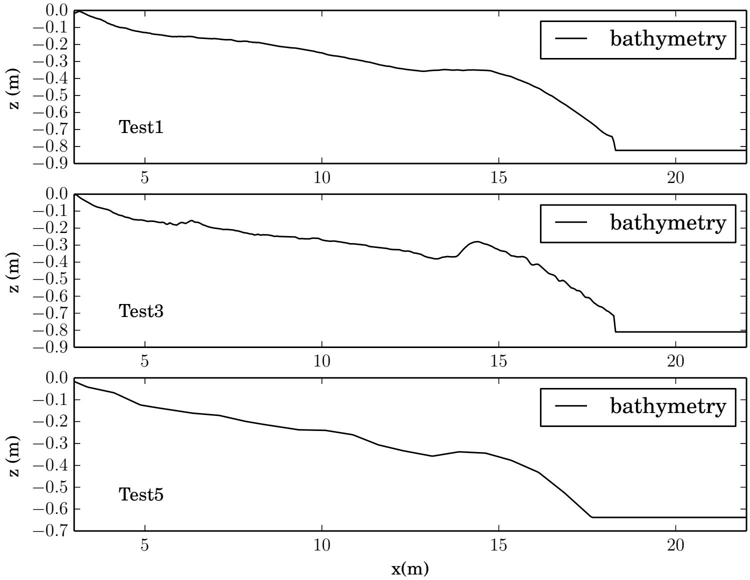

Figure 4.2: bathymetry on the 3 tests

measured and were usually higher than the depth averaged ones. This may be explained by the presence of a small recirculation current close to the wave generators. This small recirculation current may also have affected slightly the current values at the beginning of the surfzone.

The root mean square wave height and setup data were measured directly from the surface elevation time series recorded by the wave gauges.

All bathymetry, velocity and surface elevation measurements considered in this study were measured at a position slightly downdrift from the center of the basin, preferably at profile Y22 (see figure 4.1). When data were not available for this profile, the closest profile with valid data was used. The LST rates were measured by the sediment traps located at the downdrift boundary.

4.3. UNIBEST-LT: APPLICATION TO THE LSTF TEST

I applied the model UNIBEST-LT with the Van Rijn 2004 sediment transport formula to the laboratory tests at the Longshore Sediment Transport Facility. The input values for the Van Rijn 2004 formula are shown in Table 4.2.

One case from each test was used. The resulting LST rates are shown in figure 4.3. The LST rates along the profile follow the measured trend in test 3 and roughly on test 5. In test 1 UNIBEST-LT over-estimates LST at the beginning of the breaker zone and under-estimates values well inside the surfzone. In all tests, peaks of LST occurring very close to the shore were measured. These peaks are not present in the UNIBEST-LT results. I don't

Table 4.2: Values used for the Van Rijn (2004) formula

D_{10}	D_{50}	D_{90}	D_{ss}	ρ_{water}	$\rho_{sediment}$	Porosity	Temperature	Salinity
μm				kg/m³		-	°C	ppm
140	225	280	200	1025	2650	0.4	15	30

Table 4.3: LST values (m³/y) obtained for each case.

	Measured			UNIBEST-LT
Test-case	Swash-zone	rest of domain	Total	Total
1-1	581	2940	3521	1626
1-2	951	2818	3769	1633
1-3	965	2544	3509	1646
3-1	2240	7530	9770	5773
3-2	2064	6595	8659	5818
3-3	2545	7175	9720	5818
5-1	531	1079	1610	413
5-2	394	1018	1412	416
5-3	290	708	998	418

know exactly the cause of these peaks but they could be a result of transport in the swash zone, excessive longshore current forcing by the recirculation system or the combination of both. In any case, UNIBEST-LT is not expected to be accurate in very shallow water where the assumptions of the model lose validity.

I also looked at the longshore velocities (figure 4.4) along the profile. Here the model is less successful in replicating the measured velocities. The model results seem to overestimate longshore velocities at the start of the breaker zone in tests 1 and 3, and underestimate velocities close to the shore in all tests. It is important to notice that in the UNIBEST-LT results, the longshore velocity is the factor that has more influence on the predicted LST. This can be seen when comparing figures 4.3 and 4.4. The suspended sediment concentration seems to play a secondary role.

Even though the model has some difficulties replicating the longshore velocities, the results for the total load (LST integrated across the profile) shown in table 4.3 are good (within a factor of approximately 2), considering that no fine tuning of calibration parameters was necessary. The results improve if one excludes the high transport peaks in very shallow water (for simplicity I call this area the swash-zone). More importantly, figure 4.5 shows that there is an approximately linear relation between measured and calculated total loads when considering all tests together. This indicates that the model behaves consistently with different types of wave breaking.

Although the model predicts total loads with reasonable accuracy, it fails to give the correct distribution of LST across the profile. This seems to be caused by an incorrect longshore current generation due to the lack of a roller model. Reniers and Battjes (1997) have shown that a roller model is needed for an accurate longshore current prediction, especially on barred profiles. Nevertheless, this error is compensated by an underes-

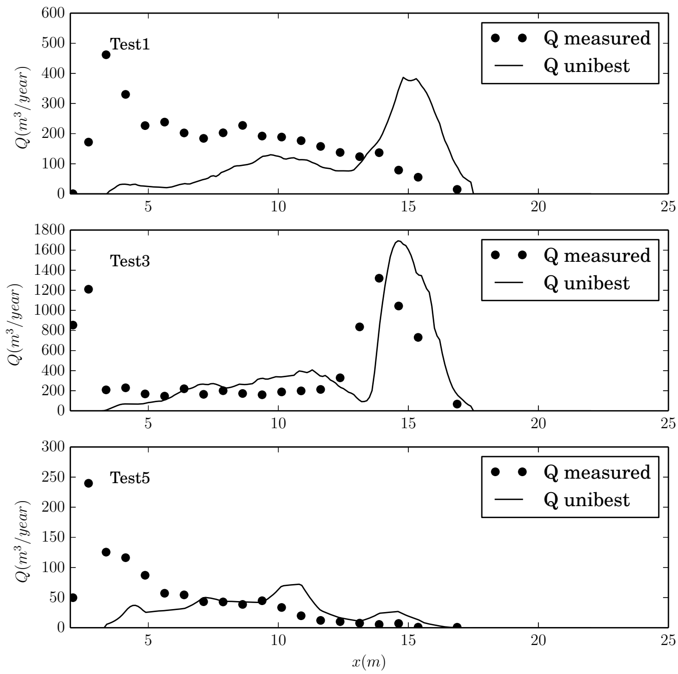

Figure 4.3: LST rates across the profile: measured and calculated with UNIBEST-LT

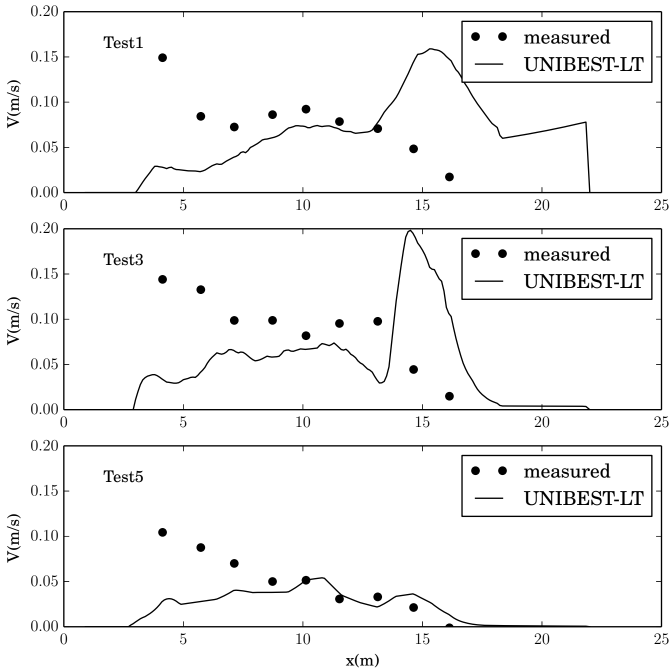

Figure 4.4: longshore velocities across the profile: measured and calculated with UNIBEST-LT

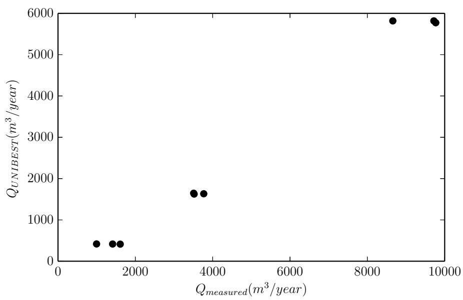

(a) with swash-zone transport

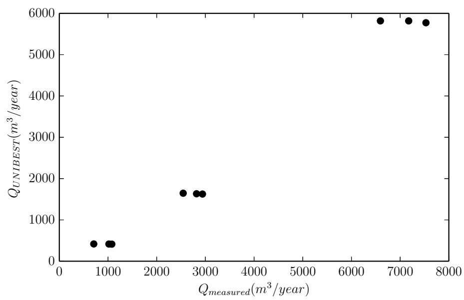

(b) without swash-zone transport

Figure 4.5: measured vs. calculated LST rates:

timation of the suspended sediment concentration at the start of the breaking area. These two shortcomings cancel each other effectively to give a reasonable total load estimation, especially in test 3. This suggests that UNIBEST-LT

However, for the purpose of studying the effect of wave breaking generated turbulence these are important problems that led us to conclude that UNIBEST-LT is not suited to be used in this chapter.

4.4. WAVE PROPAGATION MODEL

In order to simulate with accuracy the effect of wave breaking in LST, it is necessary to have a model that, drives an alongshore current in a realistic manner. The wave propagation model used in this study is a wave energy balance model (Battjes and Janssen, 1978), that includes a roller energy balance (Stive and Vriend, 1994, Reniers and Battjes, 1997).

$$\frac{\partial}{\partial x}\left(Ec_g cos\theta\right) + \frac{\partial}{\partial x}\left(E_r c\cos\theta\right) = -D_r \tag{4.1}$$

Eq.(4.1) can be separated in two (interdependent) equations for the wave energy (eq.4.2) and roller energy (eq.4.4):

$$\frac{\partial}{\partial x}\left(Ec_g\cos\theta\right) = -D_b \tag{4.2}$$

where E is the wave energy, θ is the wave angle, D_b is the energy dissipation due to wave breaking and c_g is the group velocity. The wave energy is related to the wave height through eq.4.3.

$$E = \frac{1}{8}\rho g H_{rms}^2 \tag{4.3}$$

where g is the gravitational acceleration, ρ is the water density and H_{rms} is the root mean squared wave height. The roller energy balance is given by:

$$\frac{\partial}{\partial x}\left(E_r c\cos\theta\right) = D_b - D_r \tag{4.4}$$

where E_r is the roller energy (Svendsen, 1984) given by

$$E_r = \frac{\rho A c^2}{2L} \tag{4.5}$$

where A is the roller area and L the wavelength corresponding to T_p. D_r is the roller dissipation given by eq.4.6.

$$D_r = 2\frac{gE_r\beta}{c} \tag{4.6}$$

where β represents the slope of the wave front which is assumed to be $\mathcal{O}(0.1)$, but no bigger than 0.1 (Walstra et al., 1996).

Other wave related quantities are determined using linear wave theory:

$$\omega^2 = gk \tanh(kh) \tag{4.7}$$

$$c = \frac{\omega}{k} \tag{4.8}$$

$$c_g = \frac{\partial \omega}{\partial k} = nc \tag{4.9}$$

$$n = \left(\frac{1}{2} + \frac{kh}{\sinh(2kh)}\right) \tag{4.10}$$

where h is the water depth, $\omega = 2\pi/T_p$ is the angular velocity and $k = 2\pi/L$ the wave number. T_p is the peak period and L the wavelength.

The radiation stresses are given by:

$$S_{xx} = E\left[n\left(1+\cos^2\theta\right) - \frac{1}{2}\right] + E_r \cos^2\theta \tag{4.11}$$

$$S_{xy} = (nE + E_r)\sin\theta\cos\theta \tag{4.12}$$

4.4.1. ENERGY DISSIPATION BY WAVE BREAKING

The energy dissipation due to wave breaking is the most important and at the same time the most difficult phenomenon to simulate. In this section I present four models for the energy dissipation by wave breaking.

The wave breaking dissipation in a wave energy balance model can be represented by the product of two factors: the wave breaking dissipation of a single breaking wave with a certain height (B) and the fraction of waves breaking at a given position of the profile (Q_b). The later can be understood also as the probability that a single wave in a wave train with a certain H_{rms} value is breaking.

$$D_b = Q_b B \tag{4.13}$$

Following the bore analogy suggested in Mehauté (1962), the formula for the dissipation in a single breaking wave with wave height H is:

$$B = \alpha \frac{\rho g}{8\pi} \omega \frac{H^3}{h} \tag{4.14}$$

with α being a calibration factor $O(1)$.

BATTJES AND JANSSEN (1978) (BJ78)

In a wave energy balance model, the incident wave heights at deep water are assumed to obey a Rayleigh distribution defined by the value of H_{rms} :

$$P(H) = \frac{2H}{H_{rms}^2} \exp\left[-\left(\frac{H}{H_{rms}}\right)^2\right] \tag{4.15}$$

When waves reach shallower areas they begin to break and the wave height distribution changes. Battjes and Janssen (1978) suggested that the probability function becomes truncated at the maximum wave height limited by depth H_b. The goal of this assumption is not to simulate in detail the wave height distribution, but to derive mean square values from a distribution which is truncated in the upper region by depth limited wave breaking. Using this assumption, the fraction of breaking waves can be calculated through the relation:

$$\frac{1-Q_b}{\ln Q_b} = -\left(\frac{H_{rms}}{H_b}\right)^2 \tag{4.16}$$

where H_b which is given by the "Miche criterion":

$$H_b = \frac{0.88}{k}\tanh\left(\frac{\gamma k h}{0.88}\right) \tag{4.17}$$

being γ the wave breaking height to depth ratio, that is usually used to calibrate the wave breaking dissipation. Battjes and Stive (1985) derived empirically an expression for γ using both laboratory and field data on it's calibration:

$$\gamma = 0.5 + 0.4\tanh\left(33\frac{H_{rms,0}}{L_0}\right) \tag{4.18}$$

where the subscript $_0$ ("nought") indicates the deep water value of the parameter.

For the calculation of B in eq.4.13, Battjes and Janssen (1978) assumed that all breaking waves had the depth limited maximum wave height (H_b) and considered that H_b/h was $\mathcal{O}(1)$:

$$B = \alpha\frac{\rho g}{8\pi}\omega H_b^2 \tag{4.19}$$

The final formula for the wave breaking dissipation is:

$$D_{b,BJ78} = \alpha\frac{\rho g}{8\pi}\omega H_b^2 Q_b \tag{4.20}$$

THORNTON AND GUZA (1983) (TG83)

In a field experiment, Thornton and Guza (1983) observed that even inside the surfzone, a Rayleigh distribution (that is not truncated) was still valid and its shape was determined by the local H_{rms}. Taking into account analytical and empirical arguments, Thornton and Guza (1983) characterized a distribution of breaking waves $P_b(H)$ that is a subset of the Rayleigh distribution $P(H)$ and that can be expressed as a weighting of the later:

$$P_b(H) = W(H)\,P(H) \tag{4.21}$$

with a weighting function (always ≤ 1) that was created in a way that more weight is given to higher waves:

$$W(H) = \left(\frac{H_{rms}}{\gamma h}\right)^n\left[1-\exp\left(\left(\frac{H}{\gamma h}\right)^2\right)\right] \tag{4.22}$$

being n and γ empirical coefficients with default values of 4 and 0.42 respectively. The fraction of breaking waves can be calculated integrating eq.4.22 over all values of wave height. Combining with eq.4.14 and assuming $n = 4$ the integration results in:

$$D_{b,TG83} = \alpha \frac{\rho g}{8\pi} \frac{\omega}{h} \int_0^{\infty} H^3 p_b(H)\, dH = \cdots$$
$$= \frac{3\sqrt{\pi}}{32} \rho g \alpha \omega \frac{H_{rms}^5}{\gamma^2 h^3} \left[1 - \frac{1}{\left(1 + (H_{rms}/\gamma h)^2\right)^{5/2}} \right] \quad (4.23)$$

ROELVINK (1993) (R93)

Roelvink (1993) presented a model the propagation of a wave group varying energy. This formulation is not supposed to be applied to stationary models. Nevertheless I attempt to use this simple implementation in our case using the following expression:

$$P_{b,R93} = 1 - \exp\left(\left(\frac{H_{rms}}{\gamma h}\right)^n\right) \quad (4.24)$$

where n is a calibration parameter that controls the spreading of the transition between breaking and non-breaking waves. n should have different values for different types of breakers. The calibration of γ resulted on a value of 0.55.

The dissipation by a single wave is also given by the bore analogy (eq.4.14) with $H = H_{rms}$ resulting in:

$$D_{b,R93} = \alpha \frac{\rho g}{8\pi} \omega \frac{H_{rms}^3}{h} P_{b,R93} \quad (4.25)$$

ALSINA AND BALDOCK (2007) AND JANSSEN AND BATTJES (2007) (AB07)

Following Thornton and Guza (1983), Baldock et al. (1998) derived an expression for the energy dissipation that is later improved by Alsina and Baldock (2007) and Janssen and Battjes (2007) who arrived independently at eq.4.26:

$$P_{b,A\&B07} = \left[\left(\frac{H_b}{H_{rms}}\right)^3 + \frac{3}{2} \frac{H_b}{H_{rms}} \right] \exp\left[-\left(\frac{H_b}{H_{rms}}\right)^2 \right] + \cdots$$
$$+ \frac{3}{4} \sqrt{\pi} \left[1 - \operatorname{erf}\left(\frac{H_b}{H_{rms}}\right) \right] \quad (4.26)$$

where H_b is obtained with eq.4.17 with γ given by eq.4.18.

The dissipation by a single wave is also given by eq.4.14, setting $H = H_{rms}$, yielding:

$$D_{b,AB07} = \alpha \frac{\rho g}{8\pi} \omega \frac{H_{rms}^3}{h} P_{b,AB07} \quad (4.27)$$

4.4.2. ALONGSHORE CURRENT AND SETUP

The wave energy dissipation forces alongshore currents and setup. An accurate prediction of these currents is fundamental to correctly estimate sediment transport. Following Longuet-Higgins (1970), the depth integrated forces acting in the water volume on a alongshore uniform situation are:

$$F_x = \frac{\partial S_{xx}}{\partial x} \tag{4.28}$$

$$F_y = \frac{\partial S_{xy}}{\partial x} \tag{4.29}$$

The cross-shore variation of set-up is given by:

$$\frac{d\bar{\eta}}{dx} = -\frac{F_x}{g} \tag{4.30}$$

The alongshore current forcing F_y is obtained combining eq.4.29, eq.4.2, eq.4.4 and eq.4.12:

$$F_y = \frac{dS_{xy}}{dx} = D_r \frac{\sin\theta}{c} \tag{4.31}$$

The alongshore current is determined by the balance of the forcing F_y and the alongshore component of the bed shear stress τ_y. Considering the alongshore momentum equation on an alongshore uniform case:

$$\frac{dV}{dt} = \frac{F_y}{\rho h} - \frac{\tau_y}{\rho h} - \frac{d}{dx}\left(D_h \frac{dV}{dx}\right) \tag{4.32}$$

where D_h is the depth averaged horizontal turbulence viscosity and V the alongshore current. eq.4.32 includes lateral mixing by the diffusion term. After a simple calibration procedure, a constant (across the domain) D_h value equal to $0.01 m^2/s$ was adopted. It was found that his value could change within this order of magnitude without a significant difference in the results. The D_h value is much smaller than the one suggested as "background viscosity" in Roelvink and Reniers (2011) for field conditions, $0.1 m^2/s$, and than the value used in Ruessink and Miles (2001), 0.5 m^2/s, also for field conditions. This may indicate that this factor is dependent on scale.

The time averaged bed shear stress was calculated using the expression of Feddersen et al. (2000), assuming that the mean component of the longshore current is much higher than the mean component of the cross-shore current:

$$\tau_y = \rho c_f V \sqrt{(1.16s)^2 + |V|^2} \tag{4.33}$$

where s is the standard deviation of the velocity and c_f is the drag coefficient. Assuming a linear velocity function (i.e. with mean equal to zero), the standard deviation of the velocity series is equal to u_{rms}.

$$u_{rms} = \frac{1}{2\sqrt{2}} \omega \frac{H_{rms}}{\sinh(kh)} \tag{4.34}$$

The drag coefficient c_f was considered to be constant along the domain and was adjusted to 0.014. With this value the calculated alongshore velocities showed reasonable agreement with the measured values. Reniers and Battjes (1997) also found a similar c_f value to provide good estimates of alongshore velocities on a laboratory test.

4.4.3. NUMERICAL IMPLEMENTATION

The equations were implemented using a Runge-Kutta of 4^{th} order scheme available on the Python module "Odespy" (Langtangen and Wang, 2013). This scheme is an explicit method for solving differential equations. The calculations were done using an irregular grid where the spacing varied from 0.2 m on the offshore boundary to 0.01 m close to the shoreline. To avoid numerical instabilities points with depths lower than 0.05 m were not considered.

For the alongshore current the adaptive solver on time VODE (Brown et al., 1989) was used, starting with zero current on all domain, until an equilibrium was reached between the forcing and the bed shear stress (eq.4.32).

4.4.4. CALIBRATION

The breaking dissipation models were used with the *default* values and only the alongshore current model needed calibration. For this model, the conjunction of β equal to 0.04 and the bottom friction equal to 0.014 was considered optimal, upon visual inspection of the results. I opted for not using error measures like the root mean square error or bias to evaluate the optimal coefficients for two reasons: 1) our goal was to have a model that was successful in predicting the trends in all tests and these error measures are less capable to evaluate trends and 2) it is not the goal of this study to fine tune these coefficients. Instead I carried out a small sensitivity analysis for the calibration coefficients of the longshore current model, using the AB07 dissipation formulation.

4.4.5. RESULTS WITH DIFFERENT WAVE BREAKING DISSIPATION FORMULATIONS

All four breaking dissipation formulations were tested. All methods, given the right calibration factors are capable of predicting reasonably well the evolution of wave height along the domain (figure 4.7). However, without calibrating the coefficients of the dissipation formulation, wave heights calculated with TG83 seem to be consistently underpredicted. The other formulations are more successful in predicting wave heights, with R93's results appearing to be the best. BJ78 and AB07 result in very similar wave height predictions for all tests.

Concerning the longshore current velocities (figure 4.8) it can be seen that: TG83's results are too high at the beginning of the breaker zone in tests 1 and 3, R93's results are too low for tests 1 and 5 and results with BJ78 and AB07 are generally between the results of the other two formulas. The only important distinction between the results of BJ78 and AB07 occurs in test 3 at the bar, where the later results in predictions that are nearer to the measured values. This confirms the results obtained in Alsina and Baldock (2007). This area is of crucial importance for our study because the plunging breakers occur only there. Considering these reasons, the AB07 formulation for wave breaking dissipation was used herein.

4.4.6. DISCUSSION

A few aspects are important to emphasize when trying to build a longshore current model: 1) the inclusion of a roller model is very important, especially if one wants to estimate

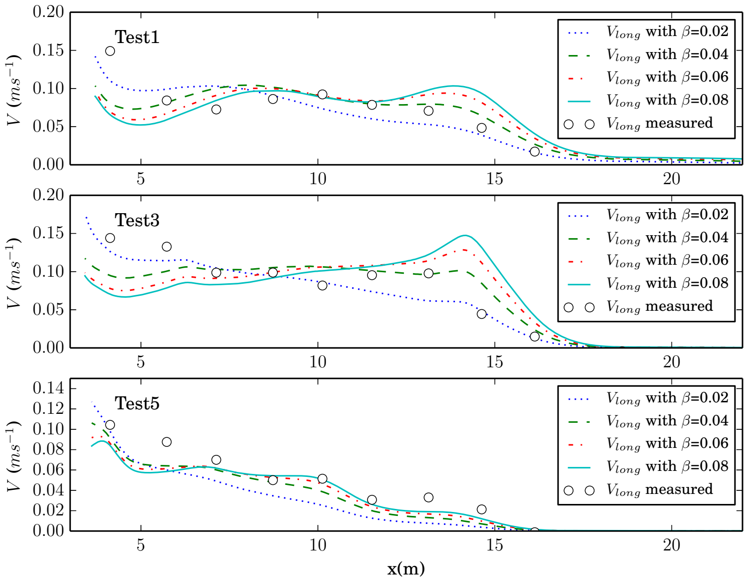

(a) β coefficient (assuming $c_f = 0.014$)

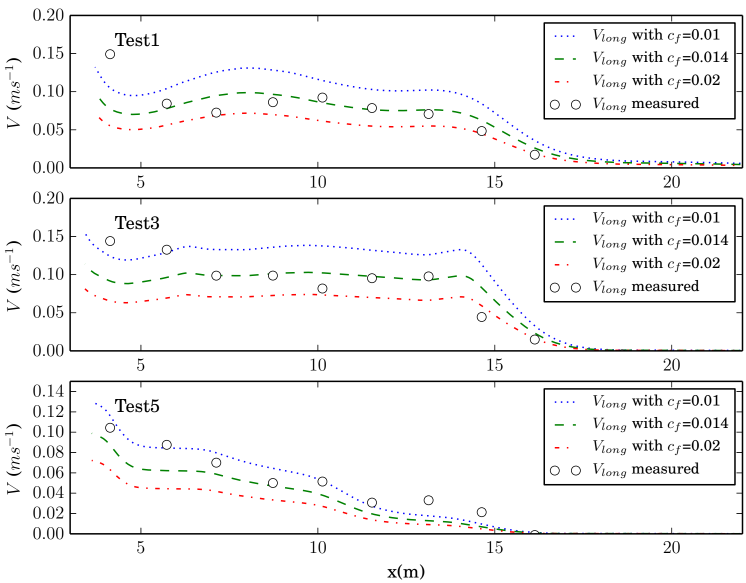

(b) drag coefficient c_f (assuming $\beta = 0.04$)

Figure 4.6: sensitivity analysis for the coefficients β and c_f using AB07

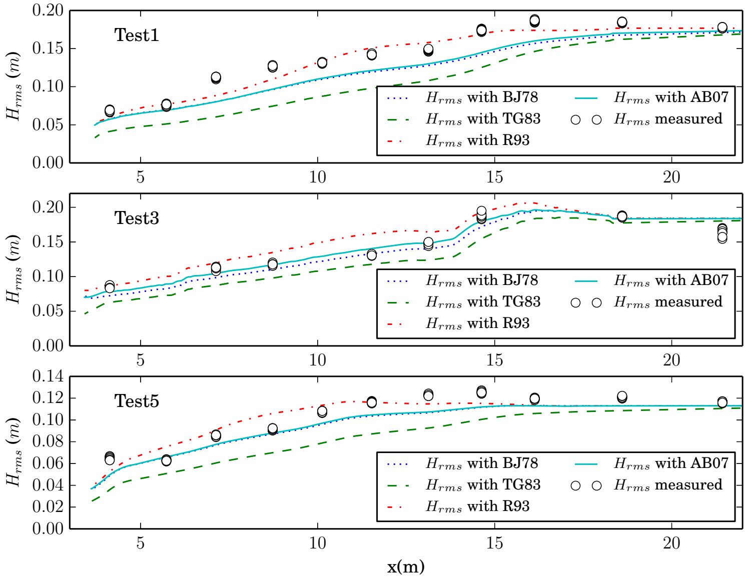

Figure 4.7: H_{rms} results with different formulas for breaking induced dissipation and measured values.

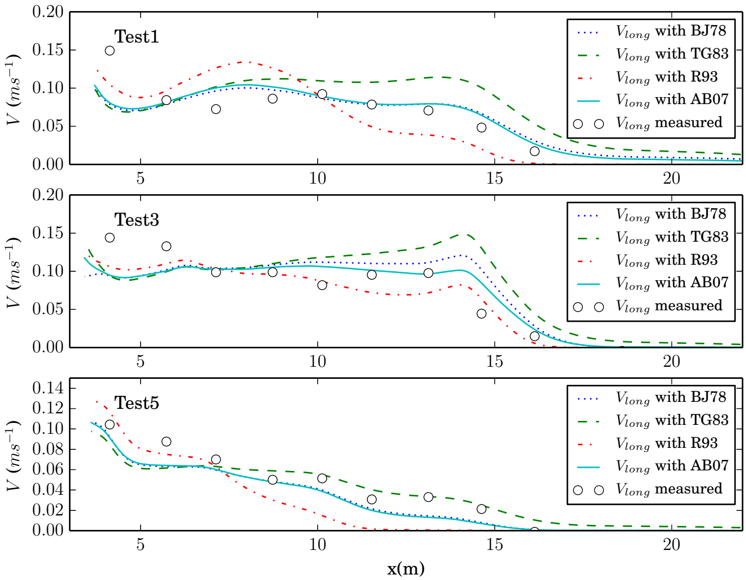

Figure 4.8: Longshore current results with different formulas for breaking induced dissipation and measured values.

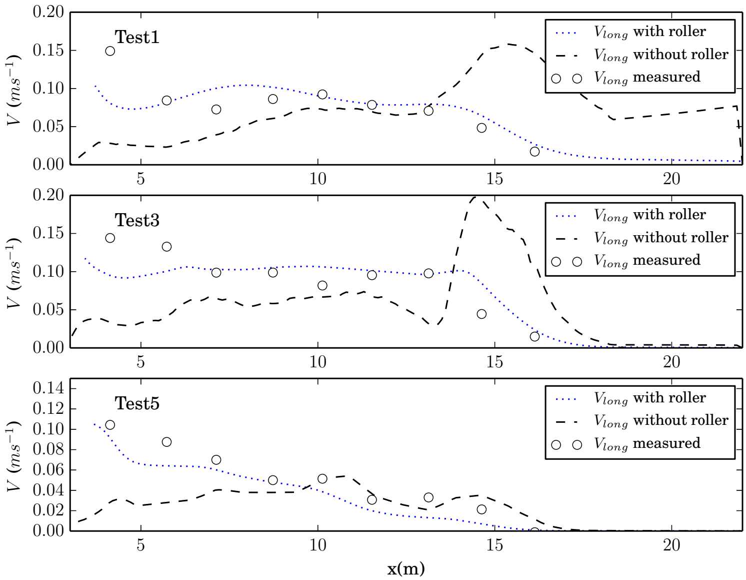

Figure 4.9: Differences between a model with roller (the model presented in this chapter) and a model without a roller (UNIBEST-LT)

the cross-shore profile of velocities on barred profiles. The difference between results with and without a roller (UNIBEST-LT in this case) is presented in figure 4.9. The differences are important, especially on test 3 where the bar is more prominent. The roller distributes the longshore forcing across the surfzone resulting in a much more realistic prediction. 2) Within the roller model, the β coefficient can influence significantly the trend of the velocities across the profile. This coefficient is understood as being the representation of the wave front angle. However, it is used as a free parameter in this study. In Walstra et al. (1996) this parameter was found to be a function of the depth and wave height and is expected to vary across the profile having a maximum value of 0.1. In our case the expression derived in Walstra et al. (1996) did not give better results than a constant value. Figure 4.6(a) shows the influence of the value of beta in the results. The value found to better simulate the behavior in test 3 was 0.04. 3) The bottom friction coefficient is also a very important calibration parameter. It controls the magnitude of the velocity which is very sensitive to this parameter as can be seen in figure 4.6(b). For the sake of simplicity I opted to consider the bottom friction constant along the profile. The value that appears to result in a better estimation of the longshore velocities was 0.014.

As noted above, the results using the formulations BJ78 and AB07 are very similar except for the zone at the bar crest in test 3. This happens because the AB07 formulation dissipates more energy where the wave breaking becomes more of the plunging type. This appears to be done by increasing the factor that can be interpreted as the fraction

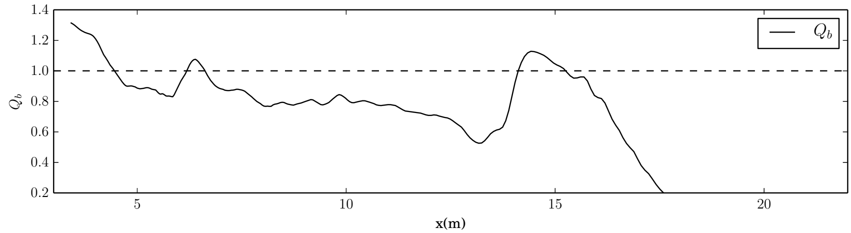

Figure 4.10: fraction of breaking waves with AB07

or probability of breaking waves (eq.4.13) to a value above 1 as can be seen in figure 4.10. This appears to compensate the deficiency in energy dissipation obtained with the bore analogy when simulating plunging breakers.

4.5. SEDIMENT TRANSPORT MODEL

For the sediment transport I use a Bagnold/Bailard/Bowen (BBB) (Bagnold, 1966, Bailard, 1981, Bowen, 1980) model. Such a model has been previously used in a cross-shore sediment transport model (Roelvink and Stive, 1989) to include the effects of wave breaking induced turbulence. Turbulence effects have been also incorporated in different types of models, e.g., Feddersen and Trowbridge (2005). I adopt the approach of Roelvink and Stive (1989) to model the effect of turbulence in our model. All inputs of the model are obtained from the 1D wave model presented on this Chapter.

In Bailard (1981) a general formula for sediment transport (in terms of immersed weight, I_t) was derived:

$$\langle \vec{I_t} \rangle = \rho c_f \frac{\epsilon_B}{\tan\phi}\left[\langle |\vec{u}_t|^2\,\vec{u}_t\rangle - \frac{\tan\beta}{\tan\phi}\langle |\vec{u}_t|^3\rangle\,\hat{i}\right] + \cdots$$
$$\rho c_f \frac{\epsilon_S}{W}\left[\langle |\vec{u}_t|^3\,\vec{u}_t\rangle + \frac{\epsilon_S}{W}\tan\beta\langle |\vec{u}_t|^5\rangle\,\hat{i}\right] \quad (4.35)$$

where ρ is the water density, c_f the drag coefficient, subscript t denotes a time-varying quantity, ϕ is the angle of internal friction of the sediment, β is the angle of the bed slope, ϵ_B and ϵ_S are the efficiency factors for sediment transport in the bed layer and in suspension, respectively, W is the sediment fall velocity, $\vec{u}$ is the horizontal near-bottom velocity, $\hat{i}$ and $\hat{j}$ are the cross-shore and longshore directions respectively. The angled brackets represent the time average over a wave period. Velocity can be expressed as x an y components:

$$\vec{u}_t = (\tilde{u}\cos\alpha + u)\hat{i} + (\tilde{u}\sin\alpha + v)\hat{j} \quad (4.36)$$

where α is the wave angle, u and v are the steady velocity components on axes x and y, and

$$\tilde{u} \cong \vec{u_{m1}}\cos\omega t + \vec{u_{m2}}\cos(2\omega t + \sigma_{12}) + \ldots \quad (4.37)$$

where u_{mn} is the amplitude of the n^{th} harmonic and σ_{12} the phase difference between harmonics 1 and 2. All $\vec{u_{mn}}$ have the same direction.

This formula was derived considering that immersed mass sediment transport is a function of time varying vectors associated with bed and suspended load ($\vec{k_s}$ and $\vec{k_b}$) times the local rate of energy dissipation ω_t.

$$\vec{I_t} = \left(\vec{k_s} + \vec{k_b}\right)\omega_t \tag{4.38}$$

$$\omega_t = \rho c_f \, |\vec{u}_t|^3 \tag{4.39}$$

From field and lab data, the efficiency constants values were set at: $\epsilon_s = 0.10$ and $\epsilon_b = 0.020$ (Nairn and Southgate, 1993).

The immersed mass transport (I) expressed in kg/s, is related to the volume rate L[1] in m^3/s by:

$$L = \frac{I}{g(\rho_s - \rho)(1-p)} \tag{4.40}$$

4.5.1. LONGSHORE COMPONENT

For the calculation of LST all cross-shore terms in eq.4.35 can be crossed out. The bed load transport term is also considered to be of an order of magnitude smaller than the suspended load and is therefore neglected (Nairn and Southgate, 1993). The sediment transport expression is thus reduced to eq.4.41.

$$\left\langle \vec{I_t} \right\rangle = \rho c_f \frac{\epsilon_S}{W} \left[\left\langle |\vec{u}_t|^3 \, \vec{u}_t \right\rangle\right] \tag{4.41}$$

I assume that:

$$\vec{u}(t) = \vec{u}_0 + \tilde{\vec{u}}(t) \tag{4.42}$$

being u_0 the constant alongshore current.

To calculate the 4$^{\text{th}}$ odd moment $\left\langle |\vec{u}_t|^3 \, \vec{u}_t \right\rangle$ I use a Taylor series expansion, as in Bowen (1980). The resulting expression (eq.4.43) can be simplified to eq.4.46 using the previously adopted notation and considering the first harmonic only (linear theory):

$$\left\langle |\vec{u}_t|^3 \, \vec{u}_t \right\rangle = 4\bar{u}\left\langle |\tilde{u}|^3 \right\rangle + 6\bar{u}^2 \left\langle \tilde{u}\,|\tilde{u}| \right\rangle + 4\bar{u}^3 \left\langle |\tilde{u}| \right\rangle + \cdots \tag{4.43}$$

$$\left\langle |\tilde{u}|^3 \right\rangle = \frac{1}{T}\int_0^T \left(u_{m1}\left|\sin\left(\frac{2\pi}{T}t\right)\right|\right)^3 dt = \frac{4u_{m1}^3}{3\pi} \tag{4.44}$$

$$\left\langle |\tilde{u}| \right\rangle = \frac{1}{T}\int_0^T u_{m1}\left|\sin\left(\frac{2\pi}{T}t\right)\right| dt = \frac{u_{m1}}{\pi} \tag{4.45}$$

$$\left\langle |\vec{u}_t|^3 \, \vec{u}_t \right\rangle = 16u_0\frac{u_{m1}^3}{3\pi} + 8u_0^3\frac{u_{m1}}{\pi} + \cdots \tag{4.46}$$

[1] The letter L was chosen to represent the volume transport rate instead of the commonly used letter Q to avoid confusion with the fraction of breaking waves Q_b.

For the case of irregular waves, u_{m1} is a representative value for the whole distribution of orbital velocities and its derivation is presented in APPENDIX B1.

4.5.2. TURBULENCE MODEL

Roelvink and Stive (1989) presented a cross-shore sediment transport model that includes turbulence effects. In that model a term is added to the suspended immersed weight to account for sediment suspension due to turbulence generated by wave breaking (eq.4.47). This equation can be separated in two terms representing the immersed weight suspended sediment transport by the effect of the orbital velocities at the bottom $I_{ss} = K_s \epsilon_S \omega_s$ and the transport due to wave breaking induced turbulence $I_{st} = K_s \epsilon_T \omega_t$. Here I adopt a similar model but accounting for different efficiency factors for suspended transport caused by shear stresses due to orbital velocities at the bed (ϵ_S) and turbulence generated by wave breaking at the surface (ϵ_T).

$$I_s(t) = K_s(\epsilon_S \omega_s + \epsilon_T \omega_t) \tag{4.47}$$

where:

$$K_s = \frac{u(t)}{w} \tag{4.48}$$

$$\omega_s = \rho c_f |u(t)|^3 \tag{4.49}$$

$$\omega_t = \rho \beta_d k_b^{\frac{3}{2}} \tag{4.50}$$

where ω_s is the term referring to the work done by the shear stress, ω_t refers to the local rate of energy dissipation due to turbulence near the bed generated by wave breaking and β_b a coefficient expected to be close to 1. k_b is the near bottom magnitude of the time averaged turbulent kinetic energy (TKE) and it's estimated assuming that it's value decreases exponentially with the depth (Roelvink and Stive, 1989). The exponential decay rate is set by a vertical scale length scale λ (eq.4.51) and a calibration factor A:

$$k(z) = \overline{k} \frac{A\lambda}{1 - \exp(-A\lambda h)} \exp(-A\lambda z) \tag{4.51}$$

where $\overline{k}$ is the time and depth averaged TKE and $k(z)$ is the time averaged TKE. The depth integration of the right-hand side of eq.4.51 results in $\overline{k}$. At the bed:

$$\overline{k_b} = \overline{k} \frac{A\lambda \exp(-A\lambda h)}{1 - \exp(-A\lambda h)} = \overline{k} \frac{A\lambda}{\exp(A\lambda h) - 1} \tag{4.52}$$

The TKE can be related to the dissipation of turbulent energy via the expression (Launder and Spalding, 1974):

$$\varepsilon = c_d \frac{k^{\frac{3}{2}}}{l} \tag{4.53}$$

where c_d is an empirical constant equal to 0.09 (Svendsen, 1987) and l is a turbulence length scale assumed to be a fraction (b_1) of H_{rms} (depth constant). b_1 is used as a calibration factor. Integrating eq.4.53 over depth yields:

$$\overline{\epsilon} = c_d \frac{h}{b_1 H_{rms}} \overline{k}^{\frac{3}{2}} \tag{4.54}$$

where $\overline{\epsilon}$ is the depth and time averaged dissipation of TKE. In Roelvink and Stive (1989) this variable is related with the wave breaking dissipation through a time averaged turbulent energy flux model which has the function of generating a delay between production of turbulent kinetic energy and dissipation. In the model described in this chapter the roller model already plays that role, hence I relate $\overline{\epsilon}$ directly to the roller dissipation D_r. However, it can reasonably assumed that only a fraction b_2 of the energy dissipated at the roller acts as a source of turbulence in the water column. Feddersen and Trowbridge (2005) estimated the fraction to be 25%. This estimation was based on previous estimations that around 50% of the roller energy dissipation is used pushing air bubbles in the water column (Lamarre and Melville, 1991) and 25% in turbulent dissipation above the trough level, i.e., in the roller itself. This estimation is somewhat simplistic and I preferred to use b_2 as a calibration factor.

$$\overline{\epsilon} = b_2 \frac{D_r}{\rho} \tag{4.55}$$

The depth averaged TKE value becomes:

$$\overline{k} = \left(B \frac{D_r}{\rho} \frac{H_{rms}}{c_d h} \right)^{2/3} \tag{4.56}$$

where the calibration factors are grouped as $B = b_1 b_2$.

CALIBRATION OF THE TURBULENCE MODEL

The model was calibrated with TKE estimated from the velocity data measured with the ADVs. Assuming that the velocity can be decomposed on three components: a mean component $\overline{u}$, a wave component $\tilde{u}$ and a turbulent component u', TKE is defined by:

$$k = \frac{1}{2} \left(\widehat{u'^2} + \widehat{v'^2} + \widehat{w'^2} \right) \tag{4.57}$$

where u', v' and w' represent the turbulent components of the three directions: cross-shore, alongshore and vertical. The "hat" denotes time averaging. The turbulent components were estimated using a frequency filtering method. A high-pass filter (Nadaoka et al., 1989) was applied with a cut-off frequency determined by the start of the turbulent saturation regime characterized by a $f^{-\frac{5}{3}}$ dependency in the spectrum (Kolmogorov, 1991, Frisch and Kolmogorov, 1995) (figure 4.11). The start of this region is not clearly defined so a degree of subjectivity is present in the definition of this cut-off frequency. Although velocities were measured at ten vertical positions, the velocity time series measured close to the surface appeared corrupted, possibly due to the presence of air bubbles. Turbulence estimations close to the bed also presented suspicious values and were also disregarded. I only considered points where all three velocity directions (u, v and w) were measured. The results are shown in figure 4.12 where it can be seen that TKE over the bar is significantly higher than in the other parts of the domain. There are more

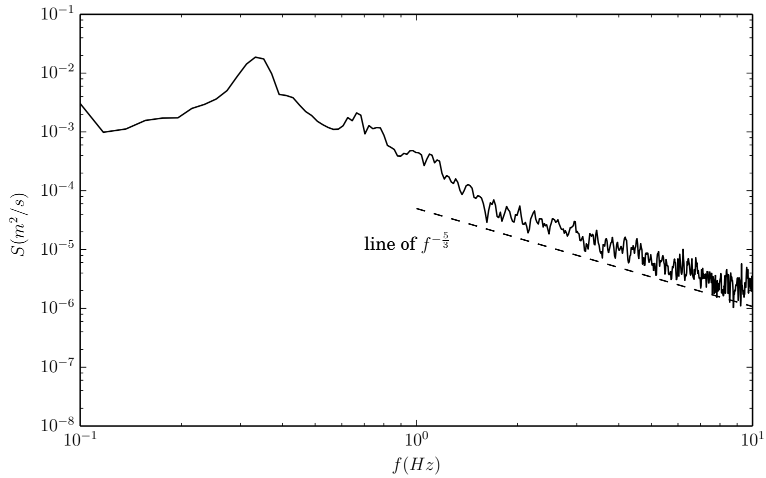

Figure 4.11: Spectrum of u measured over the bar (x=13.3m) showing the signature slope of the turbulent regime ($f^{-3/5}$)

efficient techniques to isolate the turbulent components, e.g., Trowbridge (1998) and Shaw and Trowbridge (2001) but those require that measurements are made with pairs of sensors separated by a distance much smaller than a wavelength, which is not the case in this data-set.

4.5.3. SEDIMENT SUSPENSION UNDER BREAKING WAVES

The increased sediment concentration induced by plunging breakers can be clearly seen in the data collected with the FOBS (figure 4.13). In Test 3 the FOBS positioned just offshore of the bar crest measured high concentrations higher in the water column where the plunging breakers were more likely to occur. The other tests appear to show mostly sediment suspended very close to the bed, most probably due to bed shear stresses generated by the wave orbital velocity alone. The importance of wave breaking induced turbulence is also visible in the values for LST measured by the sediment traps (figure 4.14) when compared to LST rates calculated without wave breaking induced turbulence (a pure Bagnold/Bailard/Bowen model, using only the first term in eq.4.47).

The length scale of the turbulence decay in eq.4.51 (λ) is the parameter that controls the amount of turbulent energy dissipation that reaches the bottom. For the reasons explained above, I want this factor to be an indication of the initiation of breaking and of the presence of plunging breakers. The value used in Roelvink and Stive (1989) is H_{rms}^{-1} and thus the amount of turbulence reaching the bed ($\bar{k_b}$) is ultimately dependent on the parameter H_{rms}/h that has been accepted as a good indication to whether waves are breaking or propagating as bores (Ting and Kirby, 1995). Yet, if this parameter is computed for Test 3, it is clear that it assumes values that are too high well inside the surfzone when compared to the values at the bar (figure 4.15) whereas it would be expected that values closer to the shore, where most waves already broke, to be smaller. In figures

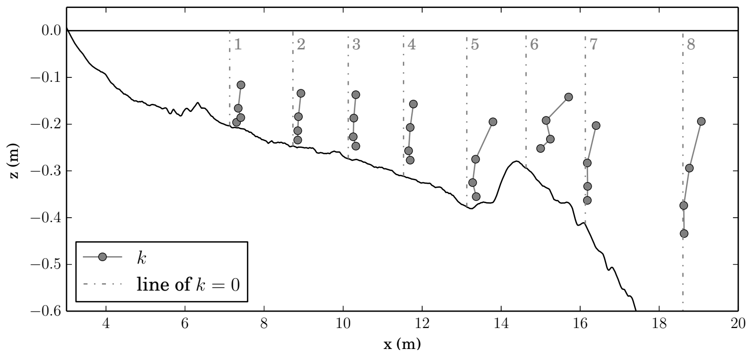

Figure 4.12: measured TKE values (Test 3)

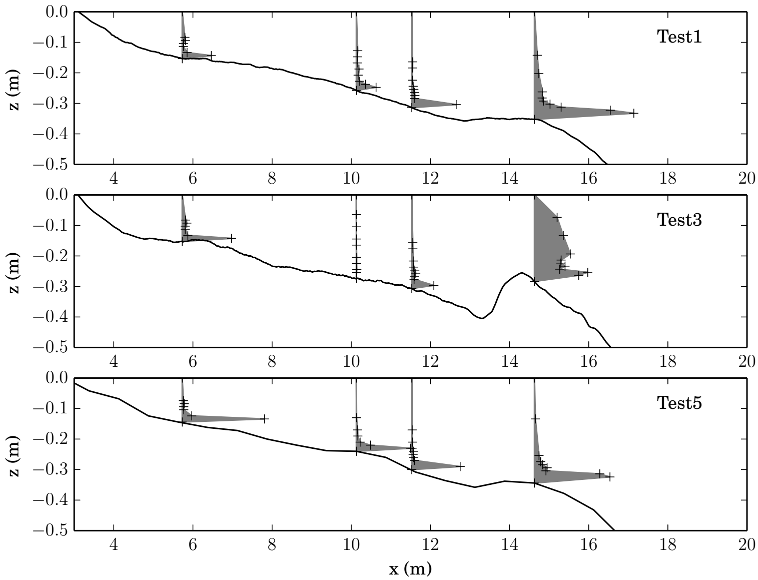

Figure 4.13: Sediment concentrations on the water column measured with the FOBS for the 3 tests at 4 positions. Data points are represented with cross hairs and the concentration is proportional to the displacement in the horizontal in relation to the point where the FOBS array is positioned. All concentration data points use the same scale.

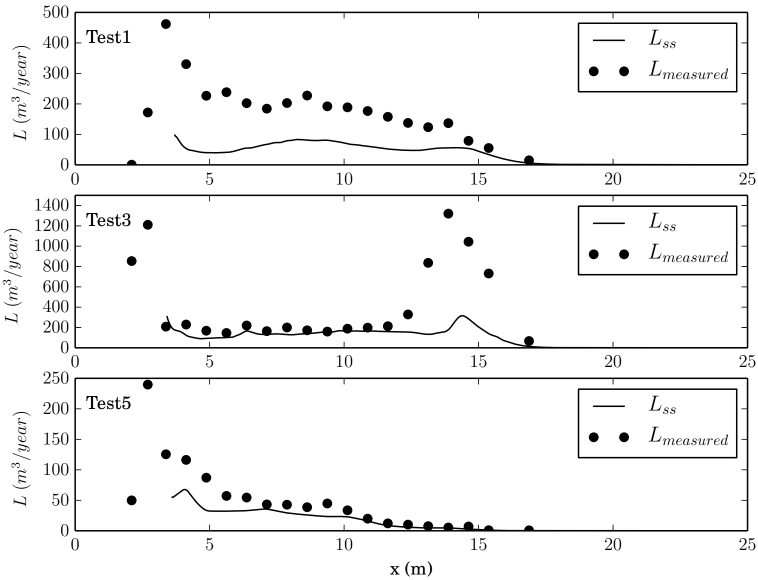

Figure 4.14: Volume transport rates measured (dots) and calculated without breaking induced turbulence (line)

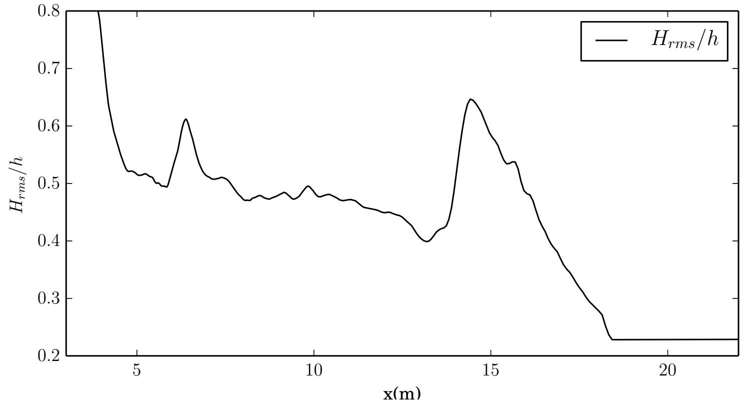

Figure 4.15: H_{rms}/h values across the domain for Test 3

4.13 and 4.14 it can be observed that for Test 3 there is a significant increase of sediment concentration and LST over the bar (almost one order of magnitude), where the plunging breakers occur. The rest of the domain, with the exception of the swash area is more or less constant and well simulated by the LST model without breaking induced turbulence. There is a need for a better indicator that accounts for the two factors: beginning of wave breaking and predominant type of breaker. In the following paragraph three parameters are defined.

The most used parameter to indicate the type of breaker is the Iribarren number (Battjes, 1974) (also known as the surf similarity parameter). I used a local version of the parameter, i.e., an Iribarren number value ξ_n was calculated for every grid point n in the domain (with local bed slope and breaking wave height). Because ξ_n can be high in places where waves don't break, the length scale was obtained multiplying ξ_n by the fraction of breaking waves at each location. To keep dimensions correct I introduced a dependence on H_{rms}. Waves start breaking only on positive slopes (decreasing depth when moving towards the shore) so I consider only positive m_n values.

$$\lambda_\xi = [\xi_n Q_b H_{rms}]^{-1} = \left[\frac{\max(0, m_n)}{\sqrt{H_b/L_0}} Q_b H_{rms} \right]^{-1} \tag{4.58}$$

where m_n is the bed slope at each grid point.

The Iribarren based parameter gives no indication to where most waves begin to break. One way to express the beginning of breaking is with the cross-shore gradient of Q_b. To relate this gradient with a wave related horizontal length scale and the wave height, and to give it the right dimensions I multiply the parameter by L_0 and H_{rms}. The parameter may also indicate indirectly the type of breaker. The area where there is a strong increase in Q_b must have a higher steepness because waves with different heights are breaking on a shorter space. As in the Iribarren number, higher profile steepness values cause breakers to be more of the plunging type. I am only interested in zones where Q_b increases so I consider only the positive gradients of this parameter.

$$\lambda_Q = \left[\max\left(0, \frac{\partial Q_b}{\partial x}\right) L_0 H_{rms}\right]^{-1} \tag{4.59}$$

Both parameters described above have a problem: they are both calculated with local values of wave height and depth, and thus have no memory of what happened with the wave before. When a wave breaks it keeps propagating as a bore until all the energy in the roller is dissipated. When a significant fraction of the waves is propagating as a bore, even if there is a high value of λ_Q or λ_ξ, there is no new initiation of breaking and less turbulence is dissipated close to the bed. To overcome this problem I use a variable that has "memory": the gradient of the roller energy E_r (eq.4.1). The roller energy increases were waves start breaking and then decreases slowly as the roller energy is dissipated. To keep the length scale with the right units a simple dimensional analysis was performed taking into account parameters that are expected to influence the decay of turbulence: L_0, H_{rms}, T_p and the (dynamic) water viscosity μ=0.00108 kg m^{-1}s^{-1}(salt water at 20^{o}C). Only areas where E_r increases are considered.

$$\lambda_{E_r} = \left[\max\left(0, \frac{\partial E_r}{\partial x}\right) \frac{L_0 T_p}{\mu}\right]^{-1} \tag{4.60}$$

Figure 4.16 shows the values of these scale lengths along the domain for the 3 tests. It can be observed that the parameters λ_{E_r}, λ_Q and λ_ξ are significantly higher where most waves start breaking than inside the surfzone in Test 3 where the plunging breakers were observed. However the parameter λ_{E_r} shows the highest ratio between magnitudes at the bar and inside the surfzone. Therefore λ_{E_r} was chosen as an indicator for beginning of breaking and occurrence of plunging breakers.

The coefficients A and B in eqs. 4.56 and 4.51 were calibrated with the TKE values calculated in the previous section. A crude calibration was done and the best results were obtained with $A = 0.0012$ and $B = 2 \times 10^6$. The resulting functions, using λ_{E_r} as a length scale, are shown in figure 4.17. In this figure it can be seen that only the cross-shore positions 6 and 7 have significant values of breaking induced TKE deep in the water column while TKE decays very quickly in the other cross-shore positions. It is important to stress that this is a simplistic model and that its main goal is to estimate the amount of TKE injected by plunging breakers in the water column and its decay with depth. Ultimately, the model provides the needed breaking induced TKE value close to the bed. Figure 4.17 shows non-zero TKE in the water column in the inner surfzone (cross-shore positions from 1 to 5). However, these TKE values appear not to contribute to longshore transport and thus are unimportant to our model.

The TKE profiles shown in figure 4.17 are very sensitive to small variations of the calibration coefficients (figure 4.18). As said before, this calibration is very crude because only two profiles are used (the profiles where the model gives some TKE close to the bed). It is expected that these values will not fit a different dataset. Only with a much larger dataset, a more robust calibration of the model could be possible.

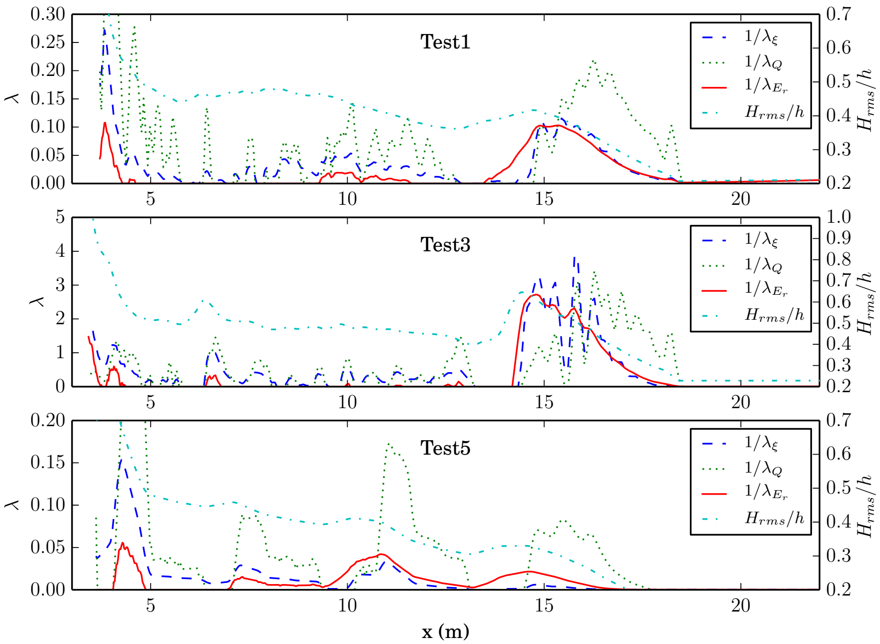

Figure 4.16: Suggested scale lengths for eq.4.51 (values multiplied by a constant to fit the same scale)

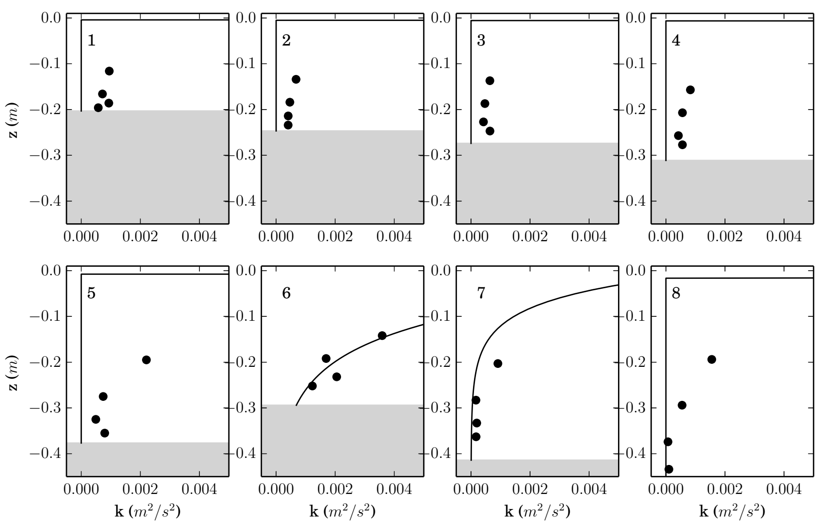

Figure 4.17: test 3: measured TKE and calculated with eq.4.51 at the positions pictured in figure 4.12

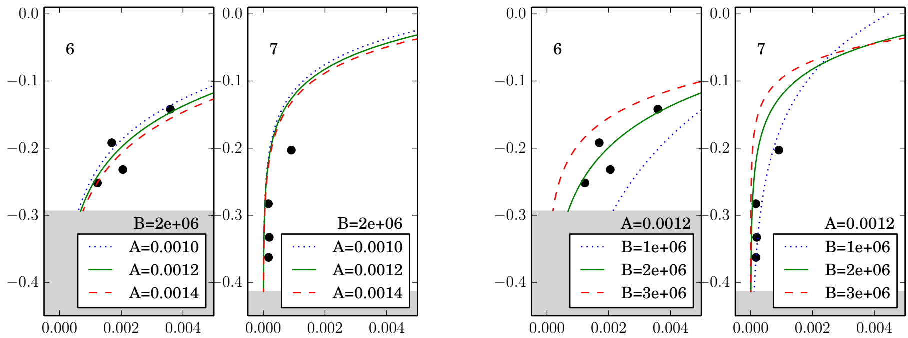

(a) coefficient A

(b) Coefficient B

Figure 4.18: Sensitivity of the TKE profiles to the calibration coefficients A and B for positions 6 and 7

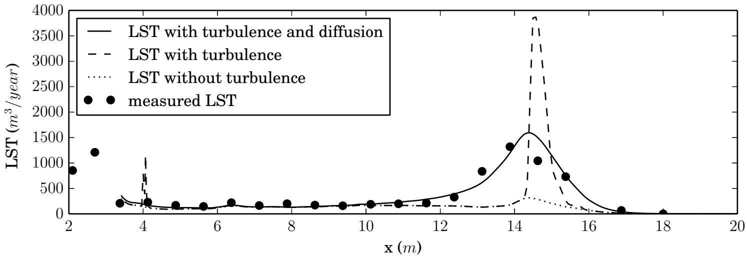

Figure 4.19: LST values for Test 3

4.6. RESULTS

Having in the previous section calculated an estimation for the value of TKE close to the bed $\overline{k_b}$, eq.4.47 can be applied to calculate LST. The value of the efficiency of wave breaking induced turbulence ε_T was calibrated with measured LST values. Because the LST values calculated with eq.4.47 are concentrated over a very short area while measured values are more spread (figure 4.19), the calibration of ε_T was done comparing integrated values over the bar, more precisely between cross-shore positions x=12 m and x=18 m. The best agreement with measured LST values was found for $\varepsilon_T = 9.5$. The discrepancy in concentration of transport can have two reasons: a) there is some lateral (cross-shore) advection/diffusion of the sediment in suspension due to turbulence and cross-shore net velocities (e.g. undertow) that are not taken into account in the model and b) the possible presence of infra-gravity waves may change slightly the water level and make waves break at slightly different positions spreading the area where transport occurs. A simple approximation to the evolution of the depth-averaged sediment concentration cross-shore profile can be calculated with a conservation equation.

$$\frac{\partial C}{\partial t}+\frac{\partial \bar{u}C}{\partial x}=\frac{\partial}{\partial x}\left(A\frac{\partial C}{\partial x}\right) \tag{4.61}$$

where $C = L/V$ is the sediment concentration (depth-averaged), $\bar{u}$ is the residual cross-shore velocity and A is a diffusion coefficient. Because our model is depth integrated and the cross-shore velocity under breaking waves has a complex residual velocity vertical profile (typically offshore directed near the bottom and onshore near the surface) I did not make an attempt to estimate the advection term in eq.4.61. Instead, the effect of the complex vertical profile of cross-shore velocities must be somehow included in the diffusion coefficient. This coefficient must also account for the possible influence of infra-gravity waves on the water level and the spatial spreading of the breaking zone and the effect of infra-gravity flows that can also transport (advect) sediment in both onshore and offshore directions of the cross-shore transect. To simplify the numerical implementation, and taking advantage of the fact that the results of the model tend to be composed of individual peaks of transport[2], one can apply eq.4.61 to each LST peak n and consider a constant diffusion value A_n for each peak.

$$\frac{\partial C}{\partial t}=A_n\frac{\partial^2 C}{\partial x^2} \tag{4.62}$$

Eq.4.62 can be easily (and computational efficiently) solved using a convolution of L and a Green's function Φ. The diffusion coefficient A_n is a crucial parameter in this calculation, which is assumed to be a function of the orbital horizontal velocity (u_{rms}) and orbital excursion (a_{orb}) calculated at the location of the n$^{\text{th}}$ peak of L. In this case of the diffusion will take place while the sediment is suspended so the time scale used (t_d) is assumed to be proportional to the settling time of sediment falling from the top of the water column. The Green's function, here presented on a discrete form with the maximum at the middle of the series, is:

$$\Phi_n=\frac{1}{\sqrt{4\pi A_n t_d}}\exp\left(-\frac{\left(n-\frac{N}{2}\right)^2}{4A_n t_d}\right) \tag{4.63}$$

with N being the total number of points in the domain, $t_d=\frac{h_n}{W}$ where the depth h_n is taken at the location of each peak, $A_n=\frac{u_{rms,n}a_{orb,n}}{\Delta x_n^2}$ where Δx_n is the grid spacing and $a_{orb,n}=\frac{H_{rms,n}}{2k_n h_n}$, all values taken at the n$^{\text{th}}$ peak. The discrete convolution takes the form:

$$C_n=\sum_{m=0}^{N}\Phi_{n-m}C_m(0) \tag{4.64}$$

The transport L is recovered by multiplying the depth and time averaged concentration C by the depth and time averaged longshore current V. Only the result for test 3 is shown in figure 4.19. In the other tests there is no significant TKE reaching the bed and thus the LST results show no difference from the ones shown in figure 4.14.

[2]If the wave breaking is spread over a larger cross-shore section the contribution of surface generated turbulence will be zero.

Table 4.4: Test 3 - LST values (m^3/y) obtained for each case (transport at the bar was matched through calibration)

	Area	LST (m^3/y)
measured	bar	4059
	rest of profile	1626
	total	5686
calculated with no turbulence	bar	1420
	rest of profile	2327
	total	3748
calculated with turbulence	bar	4059
	rest of profile	2370
	total	6430

4.6.1. COMPARISON OF RESULTS WITH AND WITHOUT TURBULENCE EFFECT

The total loads calculated with and without the turbulence effect and the measured values are presented in table 4.4. The peaks of transport that were measured close to the shore visible in figure 4.14 are not considered. The profile was divided in two areas: the bar area between x=12 m to x=18 m and the rest of the profile, from x=3 m to x=12 m. Without turbulence, the transport at the bar is considerably lower than the transport in the rest of the profile. With turbulence the results follow the trend of the measured values, but with slightly higher values in the rest of the profile.

4.7. DISCUSSION

In this chapter I analyzed the effect wave breaking induced turbulence on LST and made an attempt to produce a predictive model. I was able to confirm the importance of the effect on laboratory data. The laboratory data set includes three tests, two with mostly spilling breakers and one where plunging breakers were predominant. The differences between cross-shore profiles of LST were significant (figure 4.14), with up to an order of magnitude higher values of LST over the bar where the plunging breakers were observed. This behavior can be caused by: higher velocities, higher sediment concentrations or the combination of both effects. Figures 4.8 and 4.13 indicate that higher concentrations are the main cause as they are significantly higher in Test 3 over the bar, while velocities are similar in the three tests. Another important fact visible in figure 4.13 is that Test 3 is the only case where significant concentrations were observed higher in the water column. These high concentrations are most likely caused by wave breaking induced turbulence resulting from the plunging breakers observed by the experimenters. Besides that, a sequence of waves that start breaking approximately at the same point of the domain can also generate high sediment concentrations higher in the water column. In this case sediment stirring is done in steps, where the sediment does not settle totally between waves and is pushed higher in the water column by successive breaking waves. This generates higher concentrations on steeper bars where waves with different heights start breaking at locations that are close to each other, over a short cross-shore stretch.

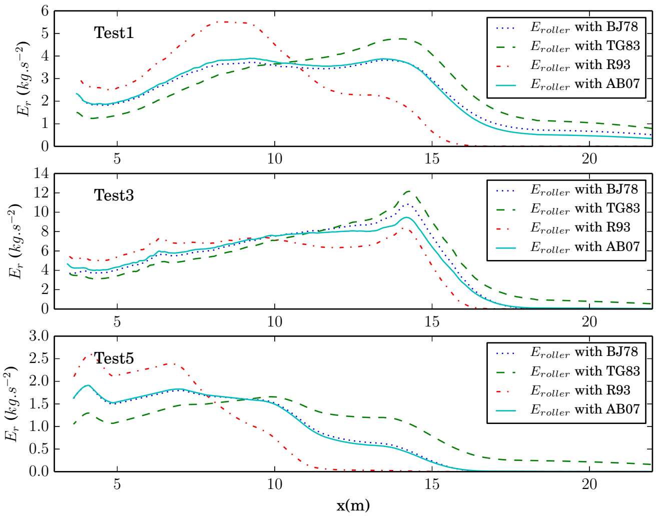

Figure 4.20: E_r with the different wave breaking formulations.

These two effects, i.e., plunging breakers and narrow profile stretch where waves start breaking may cause the higher suspended sediment concentrations observed in test 3.

I attempted to model numerically the phenomena described in the previous paragraph. For that I chose a Bagnold/Bailard/Bowen model coupled with a simple turbulence model. The main challenge was to find a factor that accounts for the effects of plunging breakers and initiation of breaking. The generally accepted parameters that account for these effects (H_s/h and Iribarren number) depend only on local conditions and have no "memory" of what happened to the waves before. Our solution uses the cross-shore gradient of the roller energy (E_r) as a parameter. The increase of roller energy denotes the initiation of breaking and the higher the gradient is, the more likely plunging breakers are. The dependency on E_r has the disadvantages: a) has a different value in the different breaking dissipation formulations, b) depends heavily on the empirical factor β (eq.4.6) and c) is quite sensitive to a bathymetry that has not been smoothed to eliminate ripples. Concerning a) all formulations showed identical behavior with clearly higher gradients for the plunging breaker case (figure 4.20).

The only test with significant turbulence higher in the water column was Test 3 and was therefore used to calibrate the turbulence model. Obviously this calibration is poor (I could only use the two points over the bar) but I was unable to find another dataset to perform further validation. However, the model does simulate the turbulence and longshore transport reasonably well in test 3 and is based on sound physical reasoning. With these facts in mind it can be argued that the cross-shore gradient of the roller energy is a good proxy to sediment concentration in the water column and could be included in more sophisticated sediment transport models.

For tests 1 and 2, i.e., the cases without plunging breakers, the Bagnold/Bailard/Bowen sediment transport model was reasonably accurate at predicting LST across the profiles as can be seen in figure 4.14.

It is important to note that transport that occurs very close to the shore (I will refer to this area as the swash zone for simplicity, although I have no way to confirm that this transport is a result of swash-zone related phenomena) seems important in all the 3 tests (figure 4.14). In fact it accounts for a significant part of the transport in Test 5 and a non negligible part in tests 1 and 3. The transport in the swash zone cannot be calculated with the kind of model used in this study as its assumptions lose validity on very shallow water. Users of such models should be aware that a significant part of the transport is not being (directly) estimated.

One must also have in mind that this type of models make a number of assumptions and simplifications that introduce errors in the predictions,e.g, depth averaged velocities and concentrations, longshore uniformity, exponential decay of turbulence. These uncertainties are dealt with in an empirical way by the tuning of the calibration parameters of the model. This fact stresses the need for a proper calibration and validation.

5

LST MODEL EVALUATION

ABSTRACT

In this chapter the results of a LST process based model are examined. A parameter space exploration is performed using constant slope ("flat") and real profiles. Results are in the same order of magnitude as the results of bulk formulas and in agreement to what is expected.

The model is applied to field data gathered in a survey in Vluchtenburg. The survey comprises measurements that detail the evolution of a large scale nourishment. The results of the model follow a trend that is similar to the observed data, showing higher volume losses in the period immediately after the conclusion of the nourishment.

5.1. INTRODUCTION

In this Chapter the results of the model described in Chapter 4 are examined. In section 5.2 "flat" profiles with varied wave conditions are used to evaluate the effect of the inclusion of wave breaking induced turbulence. In section 5.3 the measurements used to further examine the model (in section 5.4) are described.

5.2. PARAMETER SPACE EXPLORATION WITH FLAT PROFILES

In this section the influence of the turbulence effect on the model's results for different input conditions is examined. I varied the inputs of the model, i.e., H_s, T_p, deep water wave angle and bed slope and plotted the resulting cross-shore profiles and bulk values of LST, with and without turbulence effects. The different bed slope values were inspected using profiles with constant bed slope. The results are shown in figures 5.1 and 5.2. For the bulk LST values, the results were compared with the updated Kamphuis bulk LST formula presented on chapter 2 (eq.2.26). This formula requires wave parameters taken at the breaking point. The breaking point was defined as the point of the maximum wave height. Several combinations of the parameters were used.

Figure 5.1 shows that with identical wave conditions the turbulence generated component of the transport increases as the slope steepens. The peak of the transport is slightly shifted offshore. In figure 5.2 the comparison between results of the model and of the Kamphuis formula is shown. The results are in general of a similar magnitude order. For lower slopes (up to 0.02) the turbulence generated component is very small, regardless of the conditions, and the Kamphuis formula predictions are very similar to the results of the model. It is only for higher slopes (from 0.025) that transport increases due to the turbulence related transport component. The magnitude of this increase is higher for lower wave steepness, i.e., longer periods associated to lower wave heights, and higher wave angles.

5.3. VLUCHTENBURG CASE STUDY

In 2008 a large scale nourishment was performed at Vluchtenburg, in the Dutch coast (Hoogheemraadschap van Delfland, 2007). This area suffered from structural erosion and was subjected to regular (almost biennially) small scale nourishments which amounted to an average of $1x10^6$ m^3 per year. During the large nourishment initiated in 2008, almost 12×10^6 m^3 of sand was deposited in the shoreface, beach and dune, moving the shoreline up to 300 m offshore with relation to its original position. Accomplishing this shoreline displacement implied a significant steepening of the profile as can be seen in Figure 5.3. Immediately after the nourishment, profiles presented steepnesses around 1:40, while the original steepness was 1:73. The average steepness decreased with the passing of time, returning almost to the original steepness.

After the conclusion of the intervention the bathymetry of the area was surveyed almost on a monthly basis (De Schipper et al., 2014). In each survey 22 profiles were obtained, representing an alongshore distance of 1745 m. It was observed that after the conclusion of the nourishment the evolution of the sediment volume was not linear in time. In the 3 years of the survey, a grand total of circa 103 m^3/m were lost in the measured area. From this volume, around 74% was lost in the first year alone (in reality this volume loss happened almost entirely in the first 5 months). In De Schipper et al. (2014) and De Schipper et al. (2015) it was hypothesized that this significantly higher loss in the first year was due to the steepening of the profile, which yielded higher LST rates when compared to the neighboring areas that conserved the original steepness. The hypotheses that profile steepness can influence LST rates is also argued in this thesis.

5.4. PARAMETER SPACE EXPLORATION WITH REALISTIC PROFILES

The model was tested with realistic bathymetric profiles. The inputs to the model: tidal level, wave height, period and direction were varied between runs. Two profiles taken from the survey described in the previous section were chosen for this study: a profile measured in 19/07/2011 that can be classified as a "summer" profile (it was measured in the summer after a period of low energy wave conditions) and profile measured in

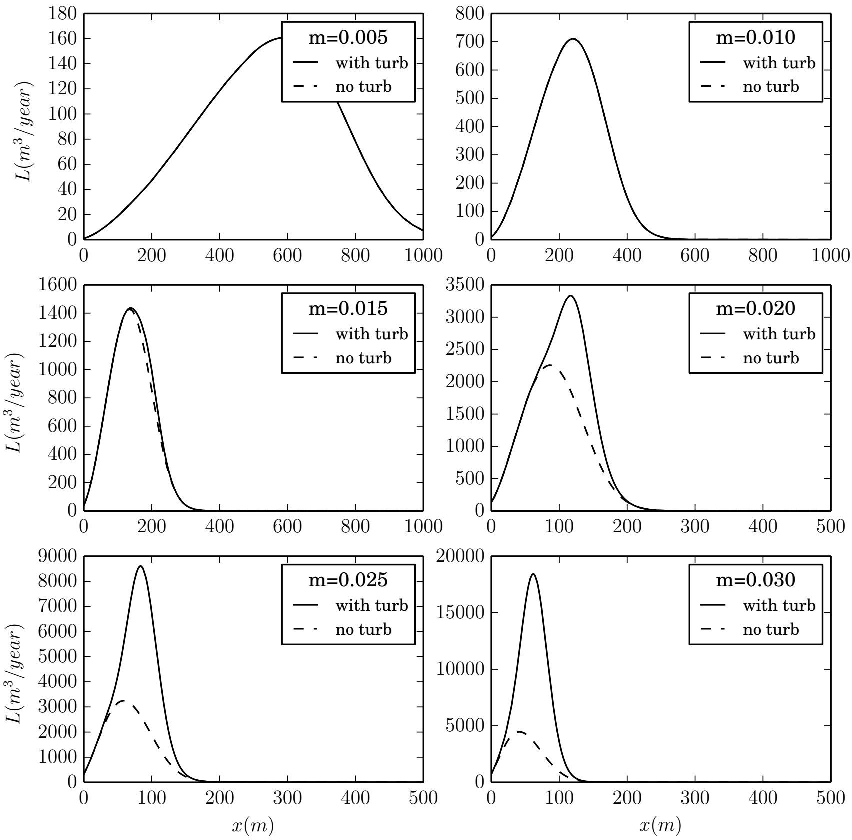

Figure 5.1: Influence of turbulence effects on LST cross-shore profiles for bathymetric profiles with different slopes (H_{rms} = 1 m, α = 10° and T_p = 10 s)

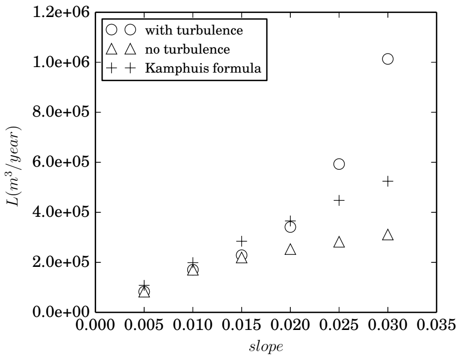

(a) $H_{rms} = 1$ m, $\alpha = 10°$ and $T_p = 10$ s

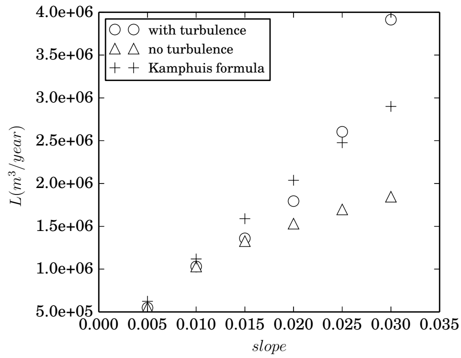

(b) $H_{rms} = 2$ m, $\alpha = 10°$ and $T_p = 10$ s

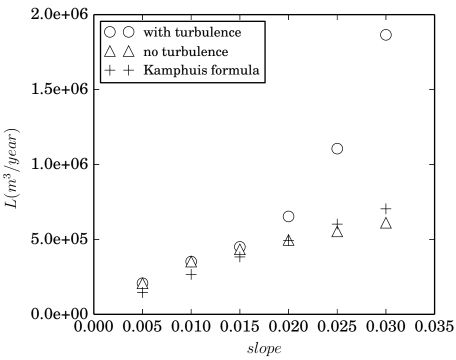

(c) $H_{rms} = 1$ m, $\alpha = 20°$ and $T_p = 10$ s

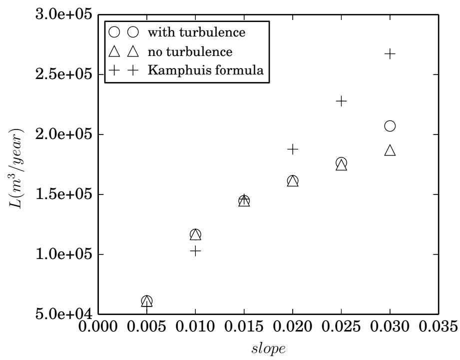

(d) $H_{rms} = 1$ m, $\alpha = 10°$ and $T_p = 6$ s

Figure 5.2: Influence of turbulence effects on bulk LST values for profiles with different slopes and wave conditions.

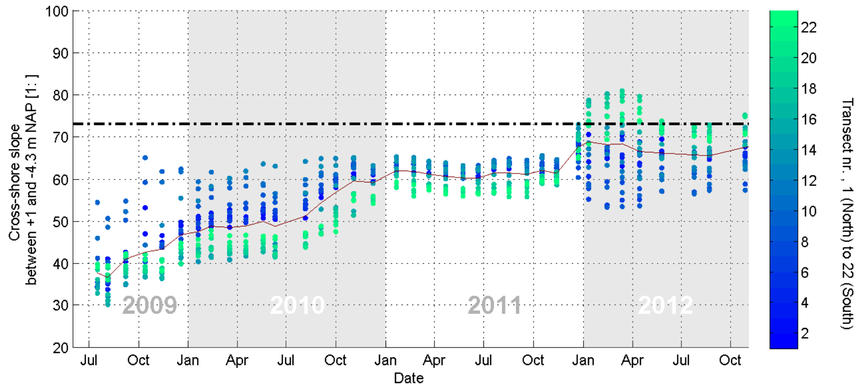

Figure 5.3: Profile slope measured between +1 and -4.3m NAP during the survey (from De Schipper et al. (2014)). The solid line represents the average slope across all profiles. The color mapping refers to the position of each profile. The dashed horizontal line represents the mean slope for the period 1965-2007.

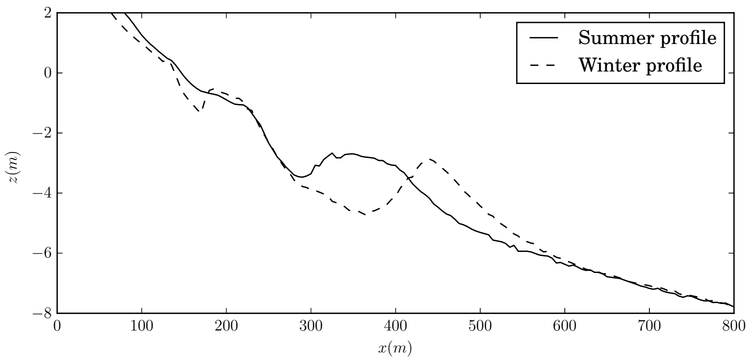

Figure 5.4: Real profiles used for the parameter space exploration

10/01/2012, a "winter" profile, measured after a period of high energy waves (Figure 5.4). Both profiles were measured at the location identified as 10 in the Vluchtenburg survey. The winter profile has a very steep berm between the cross-shore locations x=100 and x=150 m. In this area, the summer profile is much smoother.

The results show that the results of the model can vary significantly with the profile, water level and wave conditions. As expected from the results of section 5.2, an especially important factor appears to be the slope in the area where energy is dissipated. This can be observed clearly in Figures 5.5, 5.6, 5.7 and 5.8. The bulk LST rates, i.e., the values integrated in the cross-shore direction, are also compared to the results obtained with the CERC formula (eq.2.1). The computation of the CERC formula is not trivial in this case. This formula asks for wave height at the breaking point and multiple breaking points may exist (Figure 5.5). I chose to use the location of the highest transport maximum as the breaking point.

The model predicts higher transports for the winter profile, especially when the breaking zone falls in a part of the profile that is very steep like the berm area (water levels between -1 m and 1 m) when compared to less steep areas (water levels 1.5 m and 2 m). For the summer profile lower transport values are predicted. The difference between results with and without wave breaking generated turbulence effects is also higher for the winter profile (Figure 5.6) than for the summer profile (5.8).

For the other input parameters, the model results follow more or less expected trends with transport increasing with increasing incident wave height and period. The wave angle transport increases up to around 40° and 50°. The differences between the Summer and Winter profiles are also significant both in magnitude and relative importance of the turbulence effect (Figure 5.9).

5.5. SIMULATIONS WITH VLUCHTENBURG DATA

I applied the model described in chapter 4 to the data obtained with the Vluchtenburg survey. The goal of this exercise was to investigate if a model with these assumptions could reproduce the behavior observed, i.e., a volume loss that is high in the period immediately after the nourishment and that eases towards the end of the survey period.

Assuming that sediment transport in the cross-shore direction is not significant at this time scale, the observed volume losses must be a result of gradients in the rate of sediment transported alongshore. A volume loss happens when the LST rate a stretch of coast is higher than in its surroundings, i.e., there is more volume leaving this particular stretch in a downstream direction, than volume entering from upstream. To investigate if there is such a gradient I needed to compare LST rates in and outside of the surveyed area (Vluchtenburg). Outside the surveyed area I used JARKUS profiles measured in 2009, the year of the start of the survey. Unfortunately the information about the month of the JARKUS survey is not available. The area from where the profiles were taken is located to the North of the Vluchtenburg (Figure 5.11). The neighboring stretch of coast just South of Vluchtenburg is significantly affected by the harbor moles of the port of Rotterdam, which shadow the area from southerly waves. This fact makes it impossible to use that area to compare with the survey area using a 1D model. Furthermore, the profiles in that area vary significantly alongshore, violating the assumption of alongshore uniformity of the bathymetry used in the model. Because of these limitations, I could only compare the survey area with the neighboring area to the North. Nevertheless, this comparison may show important differences in LST rates that may explain the volume losses observed, especially if one examines their evolution in time. It is expected greater differences to be observed in the first 5 months and that these differences tamper down to a more or less steady value. Differences are still expected in the end because the survey area was not in equilibrium at the start, which was the reason for the intervention in the first place.

Simulations were done using the first 10 surveys, which cover a period between July 2009 to May 2010. The simulations were carried out for a period starting on the date of the correspondent survey and ending at the date of the next. For each simulation the profiles considered were the ones measured at the beginning of the period. The model was run for each time step (1 hour) in the wave time series with the correspondent water level. The results were summed to give the total volume transported in that period. Both

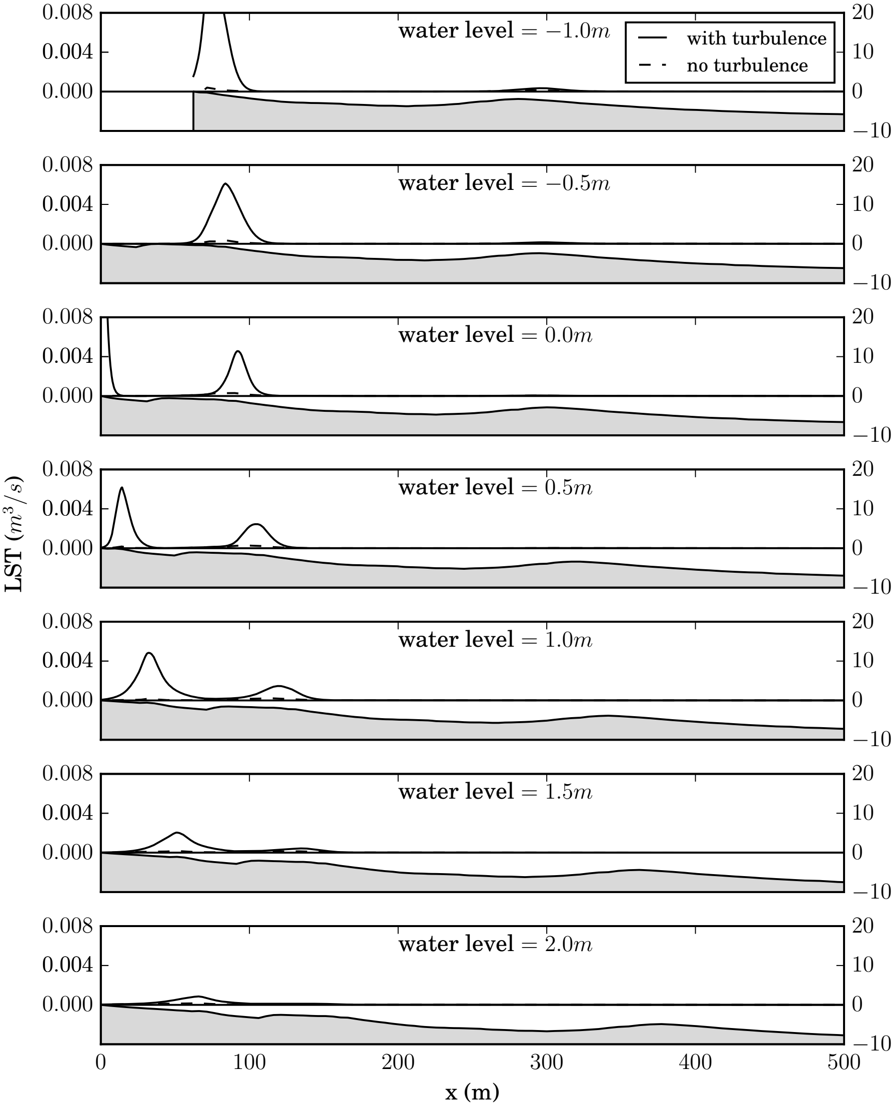

Figure 5.5: Variation of the LST cross-shore profile with different water levels for the Winter profile (wave conditions: $H_{rms} = 1$ m, $\alpha = 10°$ and $T_p = 10$ s)

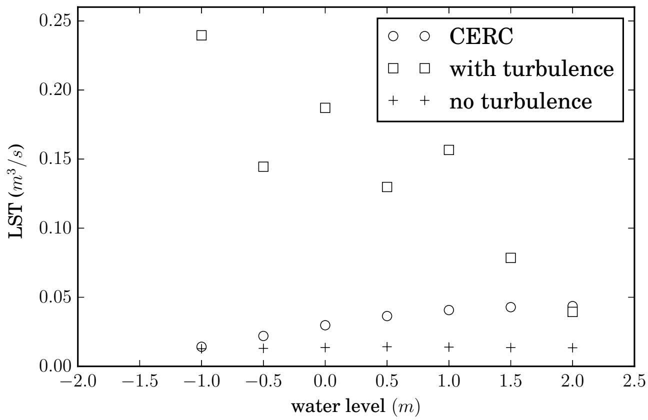

Figure 5.6: Total LST calculated with the model with and without turbulence, and calculated with the CERC formula (winter profile, wave conditions: $H_{rms} = 1$ m, $\alpha = 10°$ and $T_p = 10$ s)

net and gross transport volumes were calculated. These calculations were done for each of the 22 profiles measured, covering the entire area of the survey.

There was considerable variation between gross LST volumes calculated with different profiles as can be seen in Figure 5.10. The representative value of LST rate of the survey area was considered to be the average of all profiles.

The same procedure described in the previous section was repeated using the JARKUS profiles measured in 2009 on a neighboring stretch of coast that I considered being far enough not to be affected by the intervention in Vluchtenburg (the intervention started in 2008). This area was chosen by visually inspecting the evolution of JARKUS profiles in 2008 and 2009. In this manner one could assume that the intervened area was compared to an area that is unaffected by the intervention (this area will be herein referred to as "control area"). For this unaffected area, 43 profiles were used covering an alongshore distance of 5690 m.

This methodology has some caveats: 1) possible wave height gradients that result from the shadowing effect of the proximity of the Rotterdam harbor moles are ignored. These may shadow some of the waves with the most southern angles. 2) it is assumed that the control area maintains the same profile throughout the year. This may introduce higher transport differences either in the winter because if the profiles in the control area were measured in the summer or vice-versa. 3) I used the profile measured at the one survey to calculate the transport for the whole period until the next survey, disregarding changes (of which I don't have any information) that may occur during considered period. This may lead to errors if the profile measurement was done at a time when exceptionally steep sections were present. These sections are probably smoothed within days but the whole period will be calculated using the measured profile. Also, a high energy event that occurs between surveys has the potential to change the profile significantly.

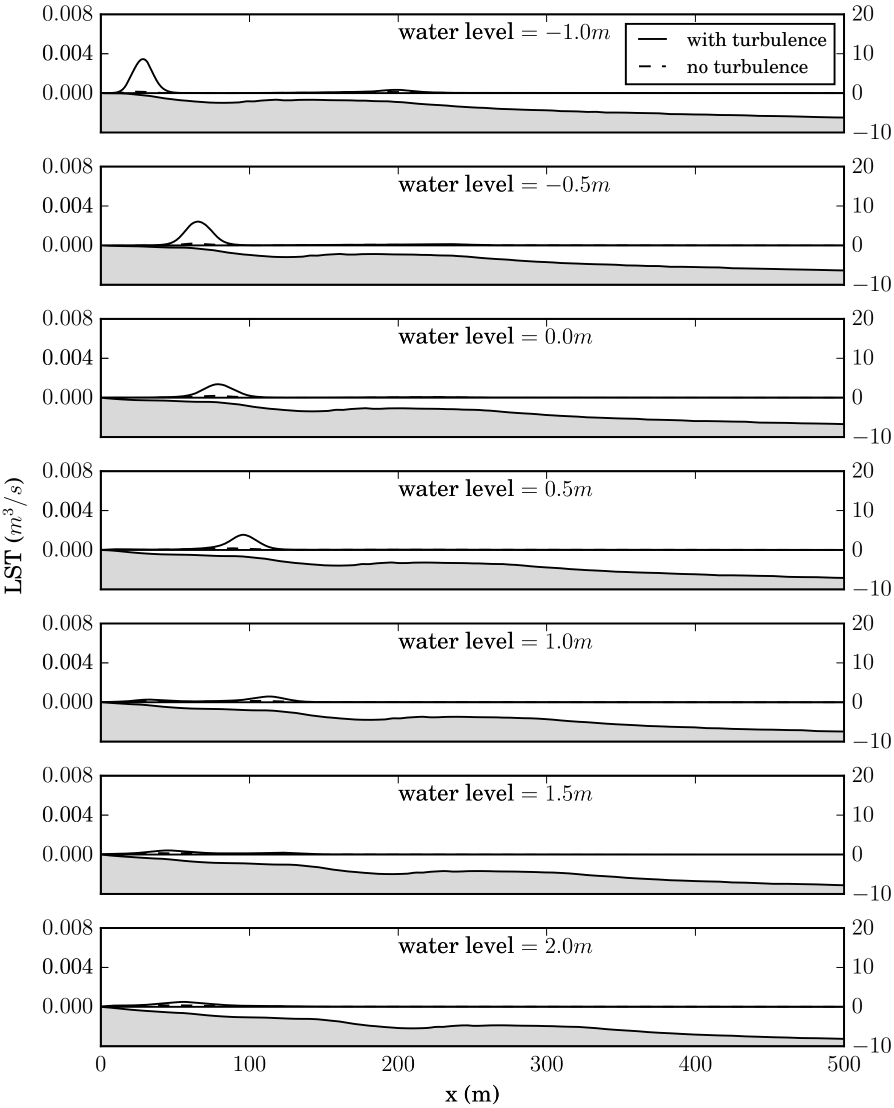

Figure 5.7: Variation of the LST cross-shore profile with different water levels for the Summer profile (wave conditions: H_{rms} = 1 m, α = 10° and T_p = 10 s)

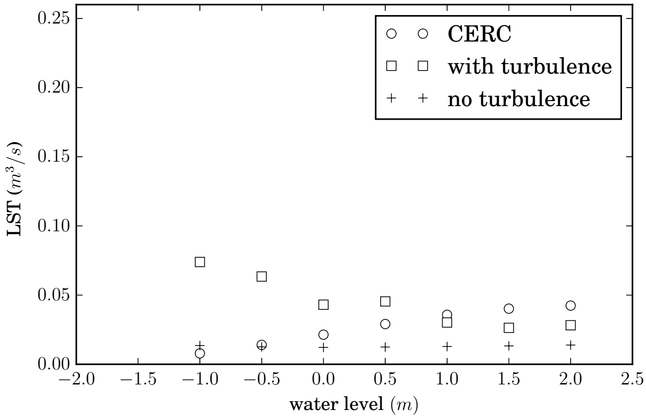

Figure 5.8: Total LST calculated with the model with and without turbulence, and calculated with the CERC formula (Summer profile, wave conditions: H_{rms} = 1 m, α = 10° and T_p = 10 s)

5.5.1. HYDRODYNAMIC CONDITIONS

As inputs to the model I used the wave conditions measured by Rijkswaterstaat at the "Europlatform" station, located approximately 40 km offshore at a water depth of 32 m. The dataset is composed by hourly measurements of significant wave height, mean zero-crossing period[1] (T_{m02}) and wave direction. The tidal levels were measured at the Hoek van Holland tidal gauge. The time series of wave conditions was propagated from the 32 m depth until a 8 m depth (where the measured profiles start), assuming parallel contours with a constant slope of 0.0006 (24:40000). Due to limitations of the model, wave angles higher than 75 degrees with relation to the orientation of the normal to the coast were not considered. The resulting time series (at 8 m depth) served as input to the model.

5.5.2. RESULTS

The results obtained are displayed in Figure 5.12. The control area average values are an indication of the wave power available, as they were calculated with the same 2009 JARKUS profiles. The October survey profile measurement was deemed unreliable and for that reason the profile measured at the September survey was also used for the October-November period. Also for that reason, I opted to represent together the calculated volumes that refer to the period between September and November (3rd bar in figures 5.12, 5.13 and 5.14).

The net transport values (Figure 5.13) show that a high gross LST value do not always correspond to high net LST values. For example, when comparing the August and November results it can be observed that whereas the gross transport values are identical in November and August, the net transport value is considerably smaller in November. In December the net transport was almost zero but the gross transport was

[1]The conversion to T_p was done in the same way as in Chapter 3

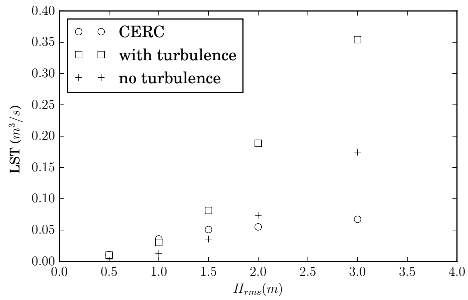

(a) Summer profile - H_{rms}

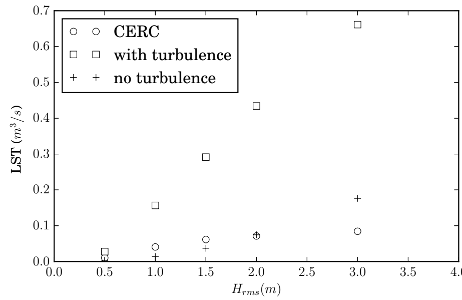

(b) Winter profile - H_{rms}

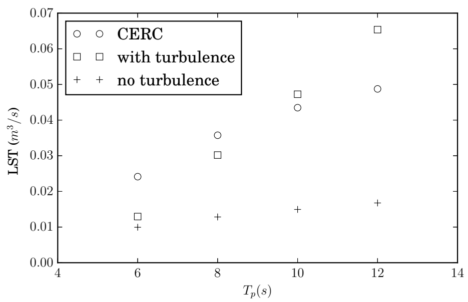

(c) Summer profile - T_{p}

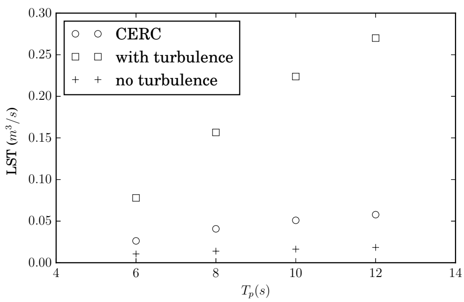

(d) Winter profile - T_p

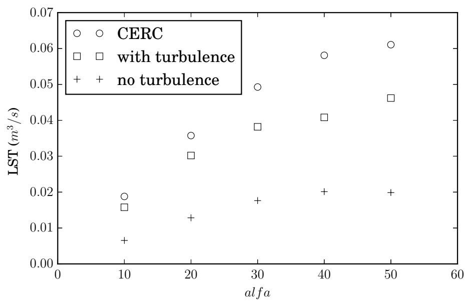

(e) Summer profile - α

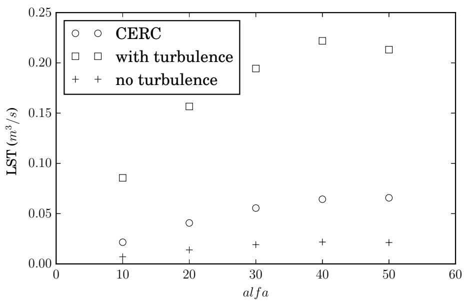

(f) Winter profile - α

Figure 5.9: Bulk LST values for the Summer and Winter profiles with different wave conditions

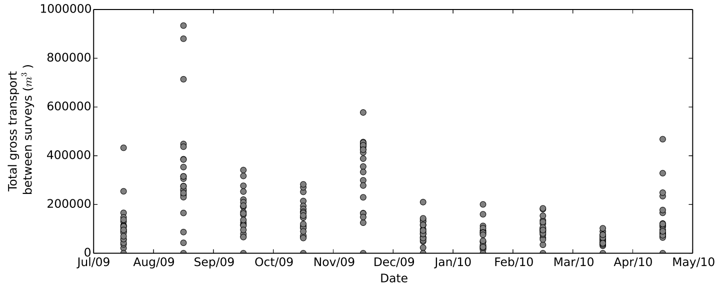

Figure 5.10: Variation of gross LST within the profiles measured on each survey. Each point represents LST calculated on each of the 22 profiles.

Figure 5.11: Areas used in the comparison. Surveyed area in red and control area in blue.

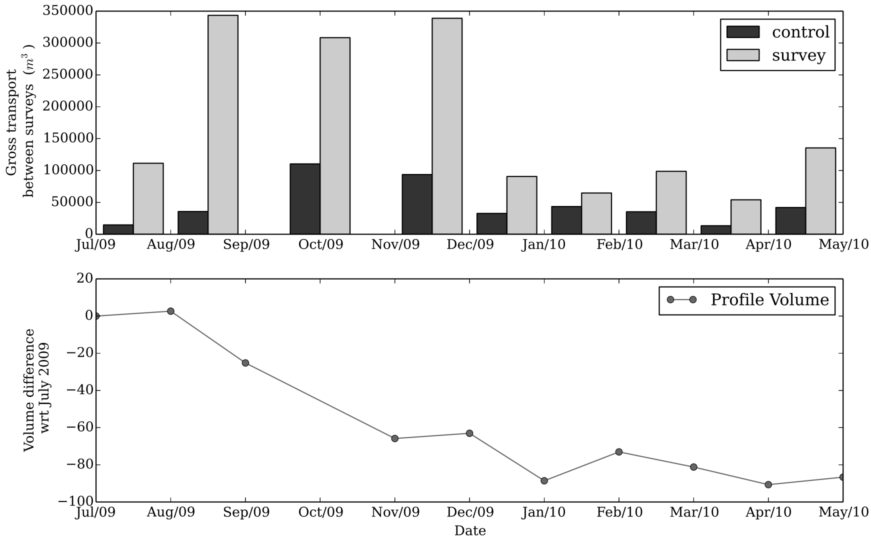

Figure 5.12: LST gross values calculated with the model in the surveyed area and in the control area. In the lower panel, the total volume of sediment (with relation to the volume measured in the first survey) is shown.

around 100 000 m³ which means that approximately the same amount of sediment was transported in each direction North and South.

In figure 5.12 it can be observed that the in the first 5 months, and especially in the second month (between the August and September surveys), the transport in the surveyed area is much higher than the transport in the control area. It is apparent that most of the volume is lost in the same 5 months period where the transport calculated in the survey area is noticeably higher. These differences between transport in these areas would generate a gradient in longshore transport that could explain the observed volume losses. There are however some results that appear not to follow the measured trend. The model predicts an high gradient between the survey and control areas between November and December whereas the measured volume increases slightly. For this discrepancy I have no explanation.

5.6. DISCUSSION

The results presented in this chapter indicate that this kind of model can possibly explain the volume losses observed at Vluchtenburg.

Although the evidence is not strong enough to represent a validation of the model, these results are encouraging and may indicate that this approach to the turbulence inclusion, is valid. It is also, in our opinion, evidence enough to warrant further data collection, especially detailed data from the surf zone so that the model can be properly validated.

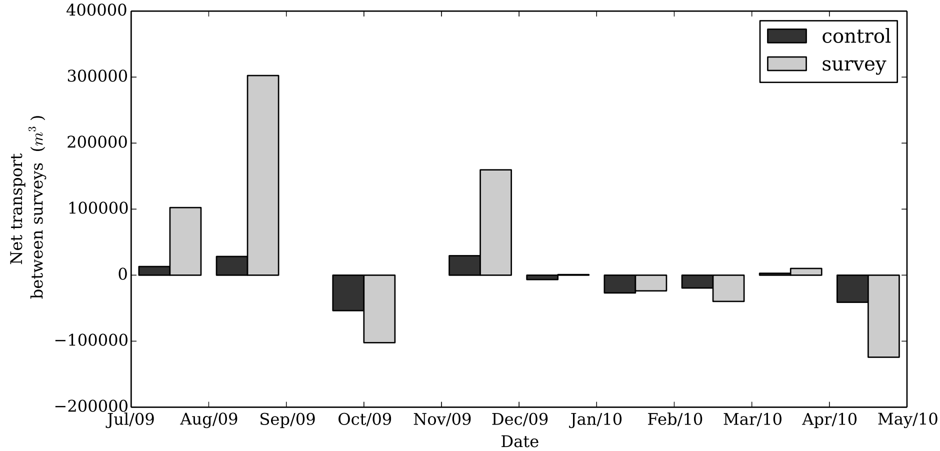

Figure 5.13: LST net values calculated with the model in the surveyed area and in the control area. Transport in the North direction is assumed to be positive.

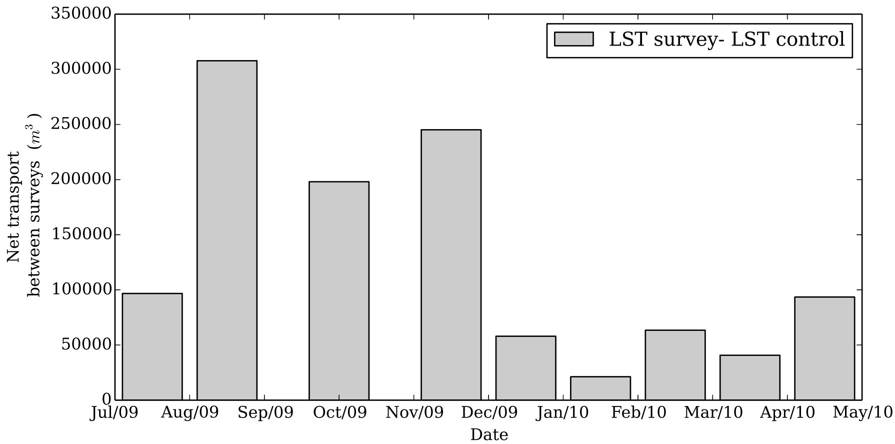

Figure 5.14: Difference between LST gross values calculated with the model in the surveyed area and on the control area.

Somewhat remarkable was the fact that results are in the same magnitude order as values calculated with Kamphuis or CERC formulas, even though the model was calibrated using only laboratory data.

6

GENERAL CONCLUSIONS AND DISCUSSION

6.1. SYNTHESES

This study concerns Longshore Sediment Transport, more specifically with the methods to predict it. In this chapter I present summaries of the conclusions of each chapter and an overall discussion. I finish with some recommendations for future research and for the potential application of the knowledge here presented.

The so-called bulk formulas were studied on Chapter 2. In that chapter I analyzed the results of the most used formulas (CERC and Kamphuis) and a more recent one (Bayram) with an extensive data set and improved or updated the calibration coefficients. I used a "moving window" technique to produce a density measure of what I called *deltas*, i.e., the logarithm of the difference between results of the original LST formulas and measurements, which allowed us to inspect the respective distributions. An Anderson-Darling test was used to check whether these *deltas* samples were likely to come from a normal distribution. I found that that was more likely if the *deltas* were plotted as a function of H_{sb}/L_o. A Levenberg-Marquardt optimizing algorithm was then used to find the best function and coefficients for the LST formulas.

The predictive skill of all three improved formulas (RMSE between 0.4 and 0.41, negligible *bias* and percentage within a factor of 2 between 53% and 56%) was significantly better than their previous versions (RMSE between 0.52 and 0.56, *bias* between -0.4 and 0.5 and percentage within a factor of 2 between 32% and 48%). The generality of the improved formulas was examined by applying the *bootstrapping* and *cross-validation* statistical methods, both of which returned similar results and confirmed the generality of the formulations.

In Chapter 3 the influence of profile features was studied. I tested LST rates calculated with the UNIBEST-LT (using the Van Rijn 2004 sediment transport formula) model for correlations with profile related parameters. The LST rates obtained with UNIBEST-LT varied significantly with the profile used ranging from less than 100 000 m^3/y to over

400 000 m^3/y. The root mean square downward slope showed the best correlation with the calculated LST rates and all parameters directly related with slope showed some correlation. It is important to notice that these results were obtained with a model and can not be considered a proper dataset. However, the sediment transport formulation has been calibrated with an extensive laboratory dataset. It is also important to notice that our UNIBEST-LT simulations didn't account for tide or wind generated currents and obviously also for 3D effects (longshore variability).

In Chapter 4 I examined the effect of wave breaking induced turbulence on LST rates and attempted to implement a model that takes that effect into account. The effect was clearly observed on laboratory data measured at the LSTF basin in Vicksburg. The dataset included tests with (Test 3) and without (Tests 1 and 5) plunging wave breaking. LST rates in Test 3 were significantly higher than in Test 1, even though the incident wave energy was similar. This difference could be caused by either higher longshore velocities, higher sediment concentrations or the combination of both effects. Sediment concentration and velocity measurements indicate that higher concentrations were the main cause as they were significantly higher in Test 3 over the bar, while velocities were similar in the three tests. One could safely conclude that these high concentrations were most likely caused by wave breaking induced turbulence resulting from the plunging breakers. Moreover, a sequence of waves that start breaking approximately at the same point of the domain could also have contributed to the higher sediment concentrations higher in the water column. In this case sediment stirring is done in steps, where the sediment does not settle totally between waves and is pushed higher in the water column by successive breaking waves. This mechanism potentially generates higher concentrations on steeper bars where waves with different heights start breaking at locations that are close to each other, over a short cross-shore stretch. These two effects: plunging breakers and narrow profile stretch where waves start breaking may have caused the higher suspended sediment concentrations observed in test 3.

In order to estimate LST rates accurately, a reliable wave propagation and longshore current generation model is necessary. I implemented a wave energy balance model and tested four different formulations for wave breaking dissipation. The results obtained with different formulations didn't vary notably but the formulation by (Alsina and Baldock, 2007) compared slightly better with the measurements and was chosen for that reason. From the implementation process I found the following aspects to be very important: 1) the difference between results with and without a roller were significant, especially on test 3 where the bar is more prominent. The roller distributes the longshore forcing across the surfzone resulting in a much more realistic prediction. 2) within the roller model, the β coefficient can influence significantly the trend of the velocities across the profile. This coefficient is understood as being the representation of the wave front angle. However, it was used as a free parameter in this study. 3) The bottom friction coefficient is also a very important calibration parameter. It controls the magnitude of the velocity which is very sensitive to this parameter.

I attempted to model numerically the influence of wave breaking induced turbulence on LST. For that a Bagnold/Bailard/Bowen model coupled with a simple turbulence model was chosen. The main challenge was to find a factor that accounts for the effects of plunging breakers and initiation of breaking that could be used to control the rate of turbulence decay in the vertical profile. The generally accepted parameters that account for these effects (H_s/h and Iribarren number) depend only on local conditions and have no "memory" of what happened to the waves before. Our solution uses the cross-shore gradient of the roller energy (E_r) as a parameter. The only test with significant turbulence higher in the water column was Test 3 and was therefore used to calibrate the turbulence model. Obviously this calibration is poor (I could only use the two points over the bar) but I was unable to find another dataset to perform further validation. However, the model simulated the turbulence and longshore transport reasonably well in test 3 and is based on sound physical reasoning. For tests 1 and 5, i.e., the cases without plunging breakers, the Bagnold/Bailard/Bowen sediment transport model was quite accurate at predicting LST across the profiles. It is important to note that a significant parcel of the transport occurs very close to the shore (referred in the text as the swash zone). It accounts for a significant part of the transport in Test 5 and a non negligible part in tests 1 and 3. The transport in the swash zone cannot be calculated with the kind of model used in this study as its assumptions lose validity on very shallow water.

In Chapter 5 I investigated the validity of the model. On a first step I studied the model results on a parameter space exploration using flat profiles (profiles with a constant slope) and different wave inputs. It was observed that the results that include the turbulence effects start differing from the results without this turbulence effect in slopes steeper than 0.025, increasing almost exponentially in steeper slopes. The effect is stronger for conditions with lower wave steepness, suggesting a Iribarren number type of dependency. The results with turbulence effects were also compared to the results of the Kamphuis formula (eq.2.26) presented in Chapter 2 as this formula also includes a slope factor. Results were of the same magnitude order, but the dependency on slope was stronger with our model, while the Kamphuis results showed an almost linear dependency.

Next, the same analysis was performed on real profiles, measured at the Dutch coast. I chose two profiles from the same location, one measured in the summer and one measured in the winter. The profiles, that had similar average slope values, differed in the smoothness: the summer profile was much smoother while the winter profile had higher slope variability as expected. The calculated transport was significantly higher for the winter profile. Especially important for these results was the steep berm present in the winter profile. The LST values calculated are much higher when the breaking zone falls in that area.

In the end I used the Vluchtenburg case study to find how the model performs when applied to a real case. Having in mind that the model could not be properly calibrated and validated I tried to assess the competence of the model in predicting the evolution of volume loss observed at the large-scale nourishment in Vluchtenburg in the first 10 months. The results indicate that the model could, although not perfectly, predict the trend of volume losses in the initial period. This result does not constitute proper validation but it is evidence that this way to include turbulence effects may be valid.

6.2. DISCUSSION

In this study I covered different approaches to estimate LST. I started analyzing the so called bulk formulas. As expected from their simplicity their accuracy is low. In this dataset and using the improved coefficients, almost 50% of the predicted points were more than a factor of two different from the measurements. Perhaps this variability can be further reduced with the inclusion of other coefficients that account for phenomena that are not included in the formulas. One such coefficient could be a representation of the effect of the slope on the breaking type which introduces differences on sediment stirring and consequently leads to higher LST. Currently only the Kamphuis formula includes a slope factor. Because this factor, slope at the breaker point, is hard to define, many times the average slope of the profile is introduced in the formula instead. This happens for two reasons: 1) rarely there is detailed information about the bathymetry and 2) even with that information one must decide which slope to use, which can be difficult when there are multiple breaking zones.

In Chapter 3 I attempted to find a slope related parameter that correlated well with LST results calculated with the model UNIBEST-LT on a high number of profiles measured on the Dutch coast. The best parameter was the "root-mean-square downwards slope". Intuitively, the use of this parameter makes sense because waves break only in downward slopes (going down in the offshore direction) and because the root-mean-square measure penalizes profiles with higher variability, i.e., profiles with steeper sections. Although the UNIBEST-LT model results vary proportionally with the slope (figure 3.1), later in the study, when comparing with laboratory data, I found that it was not representing wave breaking accurately. For that reason I developed a new model that aimed to represent more accurately the processes involved in wave breaking. Unfortunately I did not have the data to properly validate this model and then repeat the exercise using it. Nevertheless, UNIBEST-LT seemed to produce reliable bulk load predictions in the laboratory case and that is a reason to trust these results. This is evidence that one should consider the use of profile related parameters as factors in bulk formulas. Unfortunately, the data set used in Chapter 2 does not have detailed profile information that could be used to test this hypothesis.

The process-based model implemented in Chapter 4 presents a novel parametrization for the vertical decay of wave breaking generated turbulence. The ruling parameter is proportional to the cross-shore gradient of the energy of the roller. I showed that this parameter captured the initiation of breaking and the breaking type effects present in the laboratory data. This parametrization also has the advantage of having a memory, i.e., it does not depend only on local factors but also on what happened before the wave reached a given position. It was this fact the led me to choose this parameter instead of a more traditional parameter such as the Iribarren number (eq.2.2) that also looked like a good candidate (figure 4.16).

As I explored the parameter space of the model results in Chapter 5 I could see that as intended the model produces more transport on steeper slopes. Also remarkable is the fact that the results were of the same magnitude order as the bulk formulas results, despite being calibrated with only three data points that refer to a completely different (much smaller) scale. What needs attention in a further calibration/validation study are the very high transport values registered close to the shore (figure 5.5), which happen when a maximum of transport occurs close to the end of the calculation domain. I did not find a numerical reason for this somewhat unexpected result but I do not rule out that there is a numerical problem. These very high values close to the shore may result in a overestimation of the bulk predictions that may have introduced more uncertainty in the modeling exercise with field data. As for our case study application, it is important to notice that the measured volume losses could also be influenced by factors that are not taken into account in the model such as: currents generated by tide or wind and the alongshore variability of the profiles. The tide generated currents may play some special role when one considers figure 5.5. In this situation, more sediment is transported during low tide than in high tide. On the Dutch coast the horizontal and vertical tides are in phase which means that during low tide there is a southwards directed alongshore current which could generate a net southwards transport component that is independent of the wave generated alongshore current.

The knowledge of the dependency between the slope at the breaking point and LST has the potential be useful to control the volume loss rate of sediment nourishments in the coast. Depending on the goal of the nourishment, the slope at the breaking zone can be differently engineered: milder slope if the goal is that the sediment stays in the nourished area and steeper slope if the goal is that sediment spreads quickly to the adjacent areas. Another potential use of this knowledge is of a real time vulnerability warning system, when used in conjunction with coastal video monitoring systems like Argus (Lippmann and Holman, 1989) and wave forecast. The monitoring can give an estimation of the bathymetry, e.g., with the cBathy (Holman et al., 2013) algorithm, or using time-stacked images of the breaking waves to have a measure of the width of the transition zone between no-breaking and breaking waves. This measurement is directly related to the cross-shore gradient of roller energy. This way it would be possible to forecast potentially threatening LST gradients with a few days in advance.

6.3. RECOMMENDATIONS

The most obvious recommendation is that much more LST data is needed if we want to improve the accuracy of the predictions. This is also stressed in (Van Rijn et al., 2013). Even the most sophisticated model uses simplifications as it is impossible to simulate all processes up to the molecular level. Therefore there will always be a need for data to calibrate and validate the models. More specifically for our model, detailed concentration data in the surfzone is highly needed along with longshore current measurements. Also, turbulence measurements in the surfzone would be very useful for a calibration of the turbulence model. Once the model presented in chapter 4 is properly validated, the methodology presented in chapter 3 could be repeated using it. It would be then interesting to compare its results with UNIBEST-LT's and verify if the correlations between the calculated LST and the parameters considered still hold. With more data is also possible to improve the model and test, for example, a more sophisticated turbulence model.

When measurements are carried out, it would be interesting to measure also the transport that occurs in the swash zone. Although this kind of transport does not concern the model presented in this study, it is important to know how important is its contribution.

In terms of general scientific research I emphasize the importance of a good validation (using the bootstrapping or cross-validation techniques) for scientific repeatability. If the data set is to be divided into calibration and validation sets, it is desirable that this division is made available so the results can be replicated. Also very important for scientific progress is the availability of the data sets so results can be easily replicated.

6.4. ACKNOWLEDGEMENTS

I would like to thank specially Rosh Ranasinghe for supervising my first three years of the PhD. I would also like to thank Jaap van Thiel de Vries for the great help in that same period of time.

I would like to acknowledge the USACE and Ernest R. Smith for allowing public use of the laboratory dataset used in chapter 4. I also wish to express our gratitude to Dr. Atilla Bayram (Halcrow, Inc.) and Prof. Magnus Larson (Lund University, Sweden) for kindly providing the data set used in chapter 2. The authors also acknowledge the contribution of Pieter van Gelder for his help and insights in the statistical analysis.

This research was funded by "Fundação para a Ciência e a Tecnologia" and the European Union, to which I am deeply grateful.

A

DATA SET CHARACTERIZATION

In this study the same data set used in Bayram et al. (2007) is used. The data set consists on a compilation of several smaller data sets, that span in time from 1953 to as recently as 2004. There is a big variety of methods used in the data collection, from visual observation of wave heights, to the more sophisticated backscattering methods of measuring suspended sediment concentration. There are also measurements with different time frames, ranging from the space of a few minutes to months.

A.1. DATA SETS

The data sets are enumerated in the following paragraphs. Each description consists of a summary of the methods used, and the score given is an evaluation of the quality of the data set performed in Schoonees and Theron (1993) (when available).

South Lake Worth Inlet, Florida, USA (Watts, 1953) The longshore transport was estimated from the pumping rate of a sand bypass system located at the referred inlet. The experiment went on from February to June 1952. The wave data was measured at the tip of the Palm Beach Pier (5.5m depth), located 15km north of the place of the experiment. The wave angle was determined by visual observation, from the rooftop of a nearby building. The current in the surf zone were measured with a fluorescent dye.

The data consists in 3 points of long term measurements. The wave measurements were averaged during the period of observation. The averaging of results, and the poor accuracy of the wave angle measurements, makes this data set somehow unreliable.

In Schoonees and Theron (1993) this data set had a score of 42.

Anaheim Bay, California, USA (Caldwell, 1956) Dredged material from the entrance to Anaheim Bay was placed on the downdrift (southeast) shore, and repeated surveys of this area were conducted as the material was transported in a southerly direction. Changes in volume were interpreted as longshore transport rates. Estimates of longshore component of wave energy flux were based on: wave staff measurements from the

Huntington Beach pier about 9 kilometers to the south, and wave directions based on hindcasts and recognition of the sheltering by the offshore islands for waves originating from certain directions. This study provided five data points.

In Schoonees and Theron (1993) this data set had a score of 46.

Miyazu, Japan (Ishihara et al., 1958) Longshore transport was measured by means of long term accretion at temporary groyne. The data set contains 10 points. The reference to this data set could not be found. In Schoonees and Theron (1993) this data set had a score of 37.

Cape Thompson, Alaska, USA (Moore and Cole, 1960) The growth of a spit and associated waves were observed over a 3-hour period. Spit volumes were measured by plane table survey, and wave characteristics were based on visual estimates. Only one data point was obtained.

In Schoonees and Theron (1993) this data set had a score of 60.

Cototnou, Benim (Sireyjol, 1964) One data point obtained by measured accretion. In Schoonees and Theron (1993) the score was 51.

Aveiro, Portugal and Lobito, Angola (Castanho, 1966) Longshore transport was measured by means of long term accretion at breakwater (Aveiro) and growth of a sand spit (Lobito). The data set contains 2 points. The reference to this data set could not be found. In Schoonees and Theron (1993) this data set had a score of 52.

Ivory Coast (Bijker, 1968) Publication not available.

In Schoonees and Theron (1993) this data set had a score of 17.

El Moreno and Silver Strand, California, USA and Mexico (Komar and Inman, 1970) The two different locations were chosen in order to collect data under a variety of wave conditions. The two locations differ significantly in beach configuration and in the magnitude of the waves causing the sand transport. The direction and flux of wave energy were measured by an array of digital wave sensors placed in the nearshore zone. Longshore currents were measured using a dye patch injected into the surf zone and or floats of near neutral buoyancy. Grain diameter and beach slope were also measured. In this data set, the sediment transport was measured with tracers. Two to four hours after the injection of the dyed sediment, samples were collected at points a grid.

In Schoonees and Theron (1993) this data set had a score of 62.

Lake Michigan, Wisconsin, USA (Lee, 1975) In this study, the bed-load transport was measured with box-type samplers. The suspended load was also measured with mechanical samplers. The sampling time was kept at 20 min.

The wave characteristics were measured mostly with visual methods: wave height was measured from visual observation of a graduated pole standing at the breaker zone, the wave period with a stop watch and wave angle from pictures taken from a bluff.

The longshore current at the breaker was estimated with a water filled balloon or with a fluorescent dye. The movements of the balloons and dye were tracked and timed from shore during intervals of 5 to 10 min. All this measurements were averaged during the sampling time.

Beach profiles were also measured, using transit and rods. The beach slope was plotted for every sampling interval.

In Schoonees and Theron (1993) this data set had a score of 57.

Price Inlet, South Carolina, USA ((Kana, 1977) Sampler measurements were made with a portable device that could sample several heights in the water column at the same time. Wave heights were measured with a staff placed in the breaker zone. Longshore current velocities were measured with floats. There are 4 data points from this experiment in the data set.

The method used in this experiment seems to be incapable of estimating the whole cross-shore section transport. The wave characteristics were not very reliably measured.

In Schoonees and Theron (1993) this data set had a score of 48.

Ventnor and Nags Head, East Coast, USA (Fairchild, 1977) A pump-sampler was used to measure sediment concentration along the piers at the two locations. Wave data was obtained from a wave gage system (Ventnor) or a staff gage on the pier (Nags Head).

In Schoonees and Theron (1993) this data set had a score of 36 (Ventnor) and 37 (Nags Head).

Torrey Pines, USA(Inman et al., 1980) Two data points obtained with tracers and samplers. In Schoonees and Theron (1993) the score was 60.

Point Mugu(Duane and James, 1980) Tracers were used to measure sediment transport. Wave data was measured by an array of pressure gages at a depth of -9m. The experiment produced only one data point.

In Schoonees and Theron (1993) this data set had a score of 56.

Channel Islands, California, USA (Bruno et al., 1981) An offshore breakwater and twin jetties at the Channel Islands Harbor form a unique sand trap, and was therefore an ideal case for measuring longshore sand transport. This setup is considered to be nearly a total littoral barrier to longshore sand transport.

The data collection program consisted of periodic bathymetric and topographic surveys, routine wave data from which longshore transport and the wave energy flux could be calculated, and sediment samples taken during the study period to obtain quantitative information on the sand size at the site. This study lasted three years and was divided in two phases, yielding 18 data points.

In Schoonees and Theron (1993) this data set had scores of 55 (phase I) and 67 (phase II).

West Africa (Delorme, 1981) In Schoonees and Theron (1993) this data set had a score of 49.

Leadbetter Beach, California, USA (Gable, 1981) The LST rates were measured from observed accretion at a break-water. Every 6-8 weeks, bathymetry surveys were performed, extending from dry beach to a depth of about 10 m. Wave climate was measured by two arrays located at a depth of approximately 7 m. The wave climate was averaged during the period of observation. The measurements yielded 8 LST data points.

In Schoonees and Theron (1993) this data set had a score of 68.

Pointe Sapin, Canada (Kooistra and Kamphuis, 1984) Couldn't find original paper.

In Schoonees and Theron (1993) this data set had a score of 71.

University of Florida Coastal and Oceanographic Engineering Laboratory, Florida, USA (Bodge and Dean, 1987) A set of experiments were performed in the University of Florida Coastal and Oceanographic Engineering Laboratory's basin. The basin is approximately 28 m x 28 m, and is equipped on one end with an 88 paddle directional "snake" wavemaker capable of producing regular waves with a single desired direction. The main method used to measure sediment transport was impoundment on a sheet-metal barrier. Tracers were also used to estimate cross shore distribution of transport and to access possible groyne bypass.

In Schoonees and Theron (1993) there was no mention of this data.

Black Sea coast, Ukraine (Voitsekhovich, 1986) The measurements were done using samplers. The data set contains 32 points. The reference to this data set could not be found. In Schoonees and Theron (1993) this data set had a score of 57.

Shoreham, UK (Chadwick, 1989) The measurements were done using gravel traps. The data set contains 7 points. The reference to this data set could not be found. In Schoonees and Theron (1993) this data set had a score of 60.

Southeast and Gulf coast, USA (Wang et al., 1998) The LST measurements were carried out with streamer traps. In two of the data points, at the Indian Rocks beach, short-term impoundment was also used. The field sites were chosen so wide ranges of morphodynamic and hydrodynamic conditions were included. Sediment size and beach slope were also measured. The traps were mounted on a rack. The number of traps on each rack varied from four to eight, depending on the water depth and breaker height. Depending on the with of the surf zone, three to six racks were mounted along a cross-shore section.

The wave height and period were measured by video recording of scaled photo poles. At least 20 waves were measured to determine H_{rms} and T_p. Five to fifteen wave angles were also measured with an hand-held compass and averaged.

For the impoundment measurements, a 10 m long temporary barrier was used. The bathymetry surveys were conducted before and at two times after the barrier was deployed. Streamer traps were used at the same time.

This data set appears to be quite reliable.

Duck, North Carolina, USA A number of experiments were carried out in the Coastal Engineering Research Center's (CERC) Field Research Facility (FRF), near Duck, North Carolina, USA:

Bodge (Bodge and Dean, 1987) This data set was collected using impoundment of longshore sediment transport against a shore-perpendicular barrier rapidly deployed across an initially undisturbed beach. For each impoundment experiment, a shore-perpendicular sand-bag groyne was constructed approximately 150 meters south of the FRF pier, during the low tide period. Usually two beach profile surveys were possible before the surf zone migrated offshore of the groyne tip, one during the rising tide, and one during the falling tide.

Current was measured with impeller-type current meters (aligned shore parallel), mounted close to the bed on jetted steel pipes. Directional and spectral wave data was collected by gauges located close to the FRF pier. Wave height at the breaker was visually recorded, and wave angle was measured by HF radar imagery. Sediment samples were also analyzed.

In general, impoundment data is considered to be less reliable because of the long term character. In this case, however, the measurement time is short enough to have constant wave characteristics during the experiment. There are six points in the data set.

In Schoonees and Theron (1993) this data set had scores of 56 (groyne 2), 58 (groyne 3) and 61 (groyne 4).

DUCK85(Kraus et al., 1989) The LST was measured with portable streamer traps in the surf zone (depths of about 1 m). Six or seven arrays of traps were deployed simultaneously along a line crossing the surf zone. The wave heights were measured by filming poles that were positioned along a cross shore section in the surf zone. Longshore currents were also measured with electromagnetic current meters.

The main problem with this data set is that the wave angle at the breaker zone was not recorded.

In Schoonees and Theron (1993) this data set had a score of 55.

SANDYDUCK (Miller, 1999) This experiment made use of optical backscattering sensors. The optical backscatter sensor (OBS) allows for a measurement of the sediment concentration within the water column in great detail at time scales of fractions of a second. Measurements were made at at least nine positions across a barred profile. The sensors (OBS, electromagnetic current meters, wave gauges, amongst others) were mounted in an array fixed to a track-mounted crane that could move along the research pier (the Sensor Insertion System, SIS). The measurements were made in the most possible stable hydrodynamic conditions (within 1.5 hours of high or low tide). During this three hour period, several measurements were made along the profile. Each measurement took 512 seconds, which allowed for the SIS to measure at least nine locations on the profile.

Wave data was obtained from a directional pressure gauge array, located at -8 m depth, slightly offshore and north of the research pier.

Most of the measurements were taken in storm conditions, in opposition to most of the other data sets. The methods used in this experiment make this data set very reliable.

LSTF (Smith et al., 2003) This data set was collected at the Large-scale Sediment Transport Facility (LSTF) of the US Army Engineer Research and Development Center's Coastal and Hydraulics Laboratory. The LSTF is a large-scale laboratory facility, 30-m wide, 50-m long, 1.4-m deep, and is capable of simulating conditions comparable to low-energy coasts.

Sediment transport was measured with traps located at the downdrift boundary, which covered the entire surf zone. Wave data was measured by ten single-wire capacitance-type wave gauges, mounted in the instrumentation bridge that was placed in a cross shore transect.

From the methods used, the measurements in this data set seem to be very reliable.

Karwar, India (Kumar and Anand, 2003) In this study, the cross-shore distribution of LST was estimated daily, using simultaneous measurements at 6 points across the surf zone during February to May. At each point, vertical distributions of the LSTR were obtained by placing a number of traps in an array. Mesh traps having circular openings were used for measuring the suspended load transport and the streamer traps for measuring bed load transport.

The wave data used was collected by India's National Institute of Oceanography using wave buoy at 16-m water depth off Arge Beach. Significant wave height (H_s), mean wave period (T_m), and wave direction with respect to north corresponding to the peak of the wave spectrum (maximum spectral energy) data were used. Surf zone width and longshore current were also measured.

One problem with the data set is that only "wet weight" is given as a result. The author mentions dry mass values, but doesn't specify how he converted those values. A conversion assuming that the porosity of the collected sediment was still $p = 0.4$, and the pores were filled with salt water. The density values used were:$\rho_s = 2650\ kg/m^3$ and $\rho = 1025\ kg/m^3$.

There are 80 points in this data set but in 22 wave data was collected only by visual observation.

publication	location	method	number of points	score (Schoonees and Theron, 1993)
Watts (1953)	South Lake Worth	sand bypass	3	42
Caldwell (1956)	Anaheim Bay	erosion	5	46

Table A.1: Data set summary

publication	location	method	number of points	score (Schoonees and Theron, 1993)
Ishihara et al. (1958)	Miyazu	accretion	6	37
Moore and Cole (1960)	Cape Thompson	spit-growth	1	60
Sireyjol (1964)	Cotonou	accretion	1	51
Castanho (1966)	Aveiro	accretion	1	52
Castanho (1966)	Lobito	spit-growth	1	52
Bijker (1968)	Ivory Coast	unknown	1	17
Komar and Inman (1970)	El Moreno/ Silver Strand	tracer	11	62
Lee (1975)	Lake Michigan	samplers	8	57
Kana (1977)	Price Inlet	samplers	4	48
Fairchild (1977)	Ventnor and Nags Head	samplers	2	36/37
Inman et al., 1980	Torrey Pines	tracers	2	60
Duane and James (1980)	Point Mugu	tracers	1	56
Bruno et al. (1981)	Channel Islands	accretion	18 (6)	55 (phase I) 67 (phase II)
Delorme (1981)	West Africa	unknown	5	49
Gable (1981)	Leadbetter Beach	accretion	8	68

Table A.1: Data set summary

publication	location	method	number of points	score (Schoonees and Theron, 1993)
Kooistra and Kamphuis (1984)	Pointe Sapin	accretion	2	71
Bodge and Dean (1987)	University of Florida	impoundment	0	-
Voitsekhovich (1986)	Black Sea Coast	samplers	32	57
Chadwick (1989)	Shoreham	traps	7	60
Wang et al. (1998)	Southeast/ Gulf Coast	traps	27	-
		impoundment	2	-
Bodge and Dean (1987)	Duck	impoundment	6	56/58/61
Kraus et al. (1989)		samplers	8	55
Miller (1999)		OBS	10	-
Smith et al. (2003)	LSTF	traps	4	-
Kumar and Anand (2003)	Karwar	traps	80	-

B

REPRESENTATIVE VALUE OF ORBITAL VELOCITY

For the sediment transport formulation (eq.4.43) it is necessary to know the value of near bottom orbital velocity. With irregular waves this value is a representative value of the whole distribution of orbital velocities. This distribution of orbital velocities can be derived from the Rayleigh distribution of wave heights characterized by H_{rms} (eq.B.1).

$$P(H) = \frac{2H}{H_{rms}^2} \exp\left(-\left(\frac{H}{H_{rms}}\right)^2\right) \tag{B.1}$$

To estimate the representative value of a given power n of H one must calculate the following integral:

$$repr(H^n) = \int_0^\infty P(H) H^n dH \tag{B.2}$$

From linear theory and for monochromatic waves, H can be related to the orbital velocity U through eq.B.3.

$$U = \frac{1}{2}\omega \frac{H}{\sinh(kh)} \tag{B.3}$$

Performing a variable change, the distribution of orbital velocities $P(U)$ as a function of H_{rms} becomes:

$$P(U) = \frac{\frac{4U}{A}}{H_{rms}^2} \exp\left(-\left(\frac{\frac{2U}{A}}{H_{rms}}\right)^2\right) \tag{B.4}$$

with $A = \frac{\omega}{\sinh(kh)}$. The representative value of U^n is found integrating the probability function times U^n, as in eq.B.2. To complete the variable change the integration variable must be:

$$dH = \frac{2dU}{A} \tag{B.5}$$

From the distribution $P(U)$ it is possible to determine the representative values for different powers of u (representative value of U).

$$u_{repr}^{n} = \int_{0}^{\infty} U^{n} P(U) \frac{2}{A} dU \tag{B.6}$$

The resulting representative values for the orbital velocities are:

$$u_{repr}^{1} = \frac{\sqrt{\pi}}{4} H_{rms} \left(\frac{\omega}{\sinh(kh)} \right) \tag{B.7}$$

$$u_{repr}^{2} = \frac{H_{rms}^{2}}{4} \left(\frac{\omega}{\sinh(kh)} \right)^{2} \tag{B.8}$$

$$u_{repr}^{3} = \frac{3\sqrt{\pi}}{32} H_{rms}^{3} \left(\frac{\omega}{\sinh(kh)} \right)^{3} \tag{B.9}$$

BIBLIOGRAPHY

T. Aagaard and M.G. Hughes. Breaker turbulence and sediment suspension in the surf zone. *Marine Geology*, 271(3-4):250–259, 2010.

Peter Ackers and WR White. Sediment transport: new approach and analysis. *Journal of the Hydraulics Division*, 99(11):2041–2060, November 1973.

J.M. Alsina and T.E. Baldock. Improved representation of breaking wave energy dissipation in parametric wave transformation models. *Coastal Engineering*, 54(10):765–769, October 2007. ISSN 0378-3839. doi: 10.1016/j.coastaleng.2007.05.005.

TW Anderson and D.A. Darling. Asymptotic theory of certain" goodness of fit" criteria based on stochastic processes. *The annals of mathematical statistics*, 23(2):193–212, June 1952. ISSN 0003-4851. doi: 10.1214/aoms/1177729437.

Ralph A. Bagnold. An approach to the sediment transport problem from general physics. Technical report, United States Geological Survey, 1966.

James A. Bailard. An Energetics Total Load Sediment Transport Model For a Plane Sloping Beach. *Journal of Geophysical Research: Oceans (1978–2012)*, 86(C11):954, 1981.

James A Bailard. A simplified model for longshore sediment transport. In *Proceedings of the 19th International Conference on Coastal Engineering*, number 1, pages 1454–1470. ASCE, 1984.

T.E. Baldock, P. Holmes, S. Bunker, and P Van Weert. Cross-shore hydrodynamics within an unsaturated surf zone. *Coastal Engineering*, 34(3-4):173–196, September 1998. ISSN 0378-3839. doi: 10.1016/S0378-3839(98)00017-9.

J. A. Battjes and M. J. F. Stive. Calibration and verification of a dissipation model for random breaking waves. *Journal of Geophysical Research: Oceans*, 90(C5):9159–9167, 1985. ISSN 2156-2202. doi: 10.1029/JC090iC05p09159.

J.A. Battjes. Surf similarity. *Coastal Engineering Proceedings*, 1:466–480, 1974. ISSN 2156-1028.

JA Battjes and J Janssen. Energy loss and set-up due to breaking of random waves. *Coastal Engineering Proceedings*, 1(16), January 1978. ISSN 2156-1028. doi: 10.9753/icce.v16.

Atilla Bayram, Magnus Larson, and Hans Hanson. A new formula for the total longshore sediment transport rate. *Coastal Engineering*, 54(9):700–710, 2007. ISSN 0378-3839. doi: 10.1016/j.coastaleng.2007.04.001.

RA Beach and RW Sternberg. Suspended sediment transport in the surf zone: Response to incident wave and longshore current interaction. *Marine Geology*, 108(3–4):275–294, November 1992. ISSN 0025-3227. doi: 10.1016/0025-3227(92)90201-R.

Reginald A. Beach and Richard W. Sternberg. Suspended-sediment transport in the surf zone: response to breaking waves. *Continental Shelf Research*, 16(15):1989–2003, 1996. ISSN 0278-4343. doi: 10.1016/0278-4343(96)00029-5.

E.W. Bijker. Some considerations about scales for coastal models with movable bed. 1967.

EW Bijker. Littoral drift as function of waves and current. *Coastal Engineering Proceedings*, 1:415–435, 1968.

E.W. Bijker. Longshore transport computations. *Journal of the Waterways, Harbors and Coast Engineering Division*, (97):687–701, 1971.

KR Bodge and RG Dean. Short-Term Impoundment of Longshore Sediment Transport. 1987.

AJ Bowen. Simple models of nearshore sedimentation; beach profiles and longshore bars. *The coastline of Canada*, 1980.

P. Brown, G. Byrne, and A. Hindmarsh. VODE: A Variable-Coefficient ODE Solver. *SIAM Journal on Scientific and Statistical Computing*, 10(5):1038–1051, September 1989. ISSN 0196-5204. doi: 10.1137/0910062.

R.O. Bruno, Robert G. Dean, C.G Gable, and T. Walton. *Longshore sand transport study at Channel Islands Harbor, California*. Fort Belvoir, Va. :National Technical Information Service, distributor, 1981.

Per Bruun. *Sea-level Rise as a Cause of Shore Erosion*. Florida Engineering and Industrial Experiment Station, 1962.

JM Caldwell. Wave action and sand movement near Anaheim Bay, California. 1956.

J. Castanho. Rebentação das ondas e transporte litoral. Technical report, Laboratorio Nacional de Engenharia Civil, Lisboa, 1966.

CERC. *Shore protection manual*. Dept. of the Army, Waterways Experiment Station, Corps of Engineers, Coastal Engineering Research Center, For sale by the Supt. of Docs., U.S. G.P.O., (Vicksburg, Miss, Washington, DC), 4th ed. edition, 1984a.

CERC. *Shore Protection Manual*, volume I. Dept. of the Army, Waterways Experiment Station, Corps of Engineers, Coastal Engineering Research Center, For sale by the Supt. of Docs., U.S. G.P.O., Vicksburg, 4th ed. edition, 1984b.

A.J. Chadwick. Field measurements and numerical model verification of coastal shingle transport. *Advances in Water Modelling and Measurement*, pages 381–402, 1989.

J.a. Church, P.U. Clark, A. Cazenave, J. M. Gregory, S. Jevrejeva, A. Levermann, M. a. Merrifield, G.a. Milne, R.S. Nerem, P.D. Nunn, A.J. Payne, W.T. Pfeffer, D. Stammer, and a. S. Unnikrishnan. Sea Level Change. In *Climate Change 2013: The Physical Science Basis. Contribution of Working Group I to the Fifth Assessment Report of the Intergovernmental Panel on Climate Change.* Cambridge University Press, Cambridge, United Kingdom and New York, NY, USA., 2013. ISBN ISBN 978-1-107-66182-0. doi: 10.1017/CBO9781107415324.026.

Carlos Coelho, Raquel Silva, Fernando Veloso-Gomes, and Francisco Taveira-Pinto. Potential effects of climate change on northwest portuguese coastal zones. *ICES Journal of Marine Science*, 66(7):1497–1507, August 2009. ISSN 10543139. doi: 10.1093/icesjms/fsp132.

P.J. Cowell, M.J.F. Stive, A.W. Niedoroda, H.J. de Vriend, D.J.P. Swift, G.M. Kaminsky, and M. Capobianco. The coastal-tract (part 1): a conceptual approach to aggregated modeling of low-order coastal change. *Journal of Coastal Research*, pages 812–827, 2003a.

P.J. Cowell, M.J.F. Stive, A.W. Niedoroda, H.J. de Vriend, D.J.P. Swift, G.M. Kaminsky, M. Capobianco, M.C. Buijsman, R.J. Nicholls, P.S. Roy, J. Cleveringa, C.W. Reed, and P.L. de Boer. The coastal-tract (part 2): A conceptual approach to aggregated modeling of low-order coastal change. *Journal of Coastal Research*, 19:828–848, 2003b.

Daniel T. Cox and Nobuhisa Kobayashi. Identification of intense, intermittent coherent motions under shoaling and breaking waves. *Journal of Geophysical Research: Oceans*, 105(C6):14223–14236, 2000. ISSN 2156-2202. doi: 10.1029/2000JC900048.

RA Dalrymple. *Coastal processes with engineering applications.* Cambridge University Press, March 2004. ISBN 9780521602754.

M.A De Schipper, M.J.F. Stive, and A.J.H.M. Reniers. *Alongshore Variability of Nourished and Natural Beaches.* PhD thesis, TUDelft, 2014.

M.A De Schipper, Sierd De Vries, J Mil-Homens, A. J. H. M. Reniers, R. Ranasinghe, and M. Stive. Initial volume losses at nourished beaches and the effect of surfzone slope. In *Coastal Sediments 2015, San Diego*, 2015.

R. Deigaard, J Fredsø e, and IB Hedegaard. Mathematical model for littoral drift. *Journal of Waterway, Port, Coastal, and Ocean Engineering*, 112(3):351–369, May 1986. ISSN 0733-950X.

R del Valle, Raul Medina, and MA Losada. Dependence of coefficient K on grain size. *Journal of Waterway, Port, Coastal and Ocean engineering*, 119(5):568–574, 1993. doi: 10.1061/(ASCE)0733-950X(1993)119:5(568).

L. Delorme. Erosion des cotes due a des travaux portuaires et mesures visant a y remedier. volume 5, pages 771–797, Edinburgh, 1981. Pergamon Press, Oxford.

DB Duane and WR James. Littoral transport in the surf zone elucidated by an Eulerian sediment tracer experiment. *Journal of Sedimentary Research*, 50(3):929–942, September 1980. doi: 10.1306/212F7B26-2B24-11D7-8648000102C1865D.

J. H. Duncan. An Experimental Investigation of Breaking Waves Produced by a Towed Hydrofoil. *Proceedings of the Royal Society of London. Series A, Mathematical and Physical Sciences*, 377(1770):331–348, July 1981. ISSN 0080-4630.

EEA. The changing faces of Europe's coastal areas. Technical report, European Environment Agency, 2006.

F Engelund and Eggert Hansen. A monograph on sediment transport in alluvial streams. page 72, 1972.

JC Fairchild. Suspended Sediment in the Littoral Zone at Ventnor, New Jersey, and Nags Head, North Carolina. 1977.

Falk Feddersen and JH Trowbridge. The Effect of Wave Breaking on Surf-Zone Turbulence and Alongshore Currents: A Modeling Study. *Journal of Physical Oceanography*, 35(11):2187–2203, November 2005. ISSN 0022-3670, 1520-0485. doi: 10.1175/JPO2800.1.

Falk Feddersen, RT Guza, Steve Elgar, and T. H. C. Herbers. Velocity moments in alongshore bottom stress parameterizations. *Journal of Geophysical Research*, 105:8673–8686, 2000.

DM FitzGerald. Shoreline erosional-depositional processes associated with tidal inlets. *Hydrodynamics and sediment dynamics of tidal inlets*, 29:186–225, 1988. doi: 10.1029/LN029p0186.

Uriel Frisch and Andrei Nikolaevich Kolmogorov. *Turbulence: The Legacy of A. N. Kolmogorov*. Cambridge University Press, November 1995. ISBN 9780521457132.

C.G. Gable. Report on data from the nearshore sediment transport study experiment at Leadbetter Beach, Santa Barbara, California, Jan-Feb, 1980. Technical report, Institute of Marine Resources, University of California, 1981.

F. Grasso, B. Castelle, and B.G. Ruessink. Turbulence dissipation under breaking waves and bores in a natural surf zone. *Continental Shelf Research*, 43:133–141, 2012.

DG Hamilton, BA Ebersole, ER Smith, and P Wang. Development of a large-scale laboratory facility for sediment transport research. (September), 2001.

H. Hanson. GENESIS: a generalized shoreline change numerical model. *Journal of Coastal Research*, 5(1):1–27, 1989.

MD Harley, IL Turner, AD Short, and Roshanka Ranasinghe. Assessment and integration of conventional, RTK-GPS and image-derived beach survey methods for daily to decadal coastal monitoring. *Coastal Engineering*, 58(2):194–205, February 2011. ISSN 0378-3839. doi: 10.1016/j.coastaleng.2010.09.006.

Carling C. Hay, Eric Morrow, Robert E. Kopp, and Jerry X. Mitrovica. Probabilistic reanalysis of twentieth-century sea-level rise. *Nature*, 517(7535):481–484, January 2015. ISSN 0028-0836. doi: 10.1038/nature14093.

Claire Hinton and RJ Nicholls. Spatial and temporalbehaviour of depth of closure along the Holland coast. *Coastal Engineering Proceedings*, pages 2913–2925, 1998.

Rob Holman, Nathaniel Plant, and Todd Holland. cBathy: A robust algorithm for estimating nearshore bathymetry. *Journal of Geophysical Research: Oceans*, 118(5): 2595–2609, May 2013. ISSN 2169-9291. doi: 10.1002/jgrc.20199.

Hoogheemraadschap van Delfland. Verbeteringsplan versterking delflandse kust (in dutch). Technical Report W3487-02.001/WG-SE20060877, 2007.

DL Inman, JA Zampol, and T.E White. Field measurements of sand motion in the surf zone. *Coastal Engineering Proceedings*, 1980.

T Ishihara, Y Iwagaki, and M Murakami. On the investigation of beach erosion along the north coast of Akashi Strait. *Coastal Eng. in Japan*, I:97–109, 1958.

TT Janssen and JA Battjes. A note on wave energy dissipation over steep beaches. *Coastal Engineering*, 54(9):711–716, September 2007. ISSN 0378-3839. doi: 10.1016/j.coastaleng.2007.05.006.

Pavel Kabat, Louise O. Fresco, Marcel J. F. Stive, Cees P. Veerman, Jos S. L. J. van Alphen, Bart W. A. H. Parmet, Wilco Hazeleger, and Caroline A. Katsman. Dutch coasts in transition, July 2009. ISSN 1752-0894.

J.W. Kamphuis. Alongshore sediment transport rate. *Journal of Waterway, Port, Coastal, and Ocean Engineering*, 117(6):624, 1991. ISSN 0733950X. doi: 10.1061/(ASCE)0733-950X(1991)117:6(624).

J.W. Kamphuis and J.S. Readshaw. A model study of alongshore sediment transport rates. *Coastal Engineering Proceedings*, pages 1656–1674, 1978.

J.W. Kamphuis, M.H. Davies, R.B. Nairn, and O.J. Sayao. Calculation of littoral sand transport rate. *Coastal Engineering*, 10(1):1–21, May 1986. ISSN 0378-3839. doi: 10.1016/0378-3839(86)90036-0.

TW Kana. Suspended Sediment Transport at Price Inlet, South Carolina. *Proceedings of the American Society of Civil Engineers*, November 1977.

A. N. Kolmogorov. The Local Structure of Turbulence in Incompressible Viscous Fluid for Very Large Reynolds Numbers. *Proceedings: Mathematical and Physical Sciences*, 434(1890):9–13, July 1991. ISSN 0962-8444.

Paul D. Komar. *Beach Processes and Sedimentation*. Prentice Hall, 1998. ISBN 9780137549382.

PD Komar. Environmental controls on littoral sand transport. *Coastal Engineering Proceedings*, 1988.

PD Komar and DL Inman. Longshore sand transport on beaches. *Journal of geophysical research*, 1970.

J. Kooistra and JW Kamphuis. Scale effects in alongshore sediment transport rates. 1984.

NC Kraus, KJ Gingerich, and JD Rosati. DUCK85 surf zone sand transport experiment. June 1989.

V Sanil Kumar and NM Anand. Longshore sediment transport rate—measurement and estimation, central west coast of India. *Coastal Engineering*, 48(2):95–109, April 2003. ISSN 0378-3839. doi: 10.1016/S0378-3839(02)00172-2.

Eric Lamarre and WK Melville. Air entrainment and dissipation in breaking waves. *Nature*, 351(6326):469–472, June 1991. doi: 10.1038/351469a0.

H. P. Langtangen and L. Wang. The Odespy package, 2013.

Magnus Larson and NC Kraus. Numerical model of longshore current for bar and trough beaches. *Journal of Waterway, Port, Coastal, and Ocean Engineering*, 117(4):326–347, July 1991. doi: 10.1061/(ASCE)0733-950X(1991)117:4(326).

Magnus Larson and NC Kraus. Prediction of cross-shore sediment transport at different spatial and temporal scales. *Marine Geology*, 126(1–4):111–127, August 1995. ISSN 0025-3227. doi: 10.1016/0025-3227(95)00068-A.

B.E. Launder and D.B. Spalding. The numerical computation of turbulent flows. *Computer Methods in Applied Mechanics and Engineering*, 3(2):269–289, March 1974. ISSN 0045-7825. doi: 10.1016/0045-7825(74)90029-2.

KK Lee. Longshore currents and sediment transport in west shore of Lake Michigan. *Water Resources Research*, 11(6):PP. 1029 —- 1032, 1975. doi: 197510.1029/WR011i006p01029.

K. Levenberg. A method for the solution of certain non-linear problems in least squares. *Quarterly Journal of Applied Mathmatics*, II(2):164–168, 1944.

T. C. Lippmann and R. A. Holman. Quantification of sand bar morphology: A video technique based on wave dissipation. *Journal of Geophysical Research: Oceans*, 94 (C1):995–1011, January 1989. ISSN 2156-2202. doi: 10.1029/JC094iC01p00995.

M. S. Longuet-Higgins. Longshore Currents Generated by Obliquely Incident Sea Waves, 1. *Journal of Geophysical Research*, 75(33):PP. 6778–6789, 1970. doi: 197010.1029/JC075i033p06778.

Bernard Le Mehauté. On non-saturated breakers and the wave run-up. *Coastal Engineering Proceedings*, (Figure 1):77–92, 1962.

WK Melville, Fabrice Veron, and CJ White. The velocity field under breaking waves: coherent structures and turbulence. *Journal of Fluid Mechanics*, 454:203–233, 2002. doi: 10.1017/S0022112001007078.

J Mil-Homens. Re-evaluation and improvement of three commonly used bulk longshore sediment transport formulas. *Coastal Engineering*, (March 2013), 2013.

João Mil-Homens, Roshanka Ranasinghe, J.S.M. van Thiel de Vries, and M.J.F. Stive. Re-evaluation and improvement of three commonly used bulk longshore sediment transport formulas. *Coastal Engineering*, 75:29–39, May 2013a. ISSN 0378-3839. doi: 10.1016/j.coastaleng.2013.01.004.

João Mil-Homens, Roshanka Ranasinghe, J.S.M. van Thiel de Vries, M.J.F. Stive, Jaap Van Thiel, and De Vries. Influence of profile features on longshore sediment transport. In *Coastal Dynamics 2013: 7th International Conference on Coastal Dynamics, Arcachon, France, 24-28 June 2013*. Bordeaux University, 2013b.

Herman C. Miller. Field measurements of longshore sediment transport during storms. *Coastal Engineering*, 36(4):301–321, May 1999. ISSN 0378-3839. doi: 10.1016/S0378-3839(99)00010-1.

G.W. Moore and J.Y Cole. Coastal processes in the vicinity of Cape Thompson, Alaska. Technical report, 1960.

JJ More, BS Garbow, and KE Hillstrom. User guide for MINPACK-1. 1980.

K Nadaoka, M Hino, and Y Koyano. Structure of the turbulent flow field under breaking waves in the surf zone. *Journal of Fluid Mechanics*, 204:359 – 387, 1989. ISSN 1469-7645. doi: 10.1017/S0022112089001783.

RB Nairn and HN Southgate. Deterministic profile modelling of nearshore processes. Part 2. Sediment transport and beach profile development. *Coastal Engineering*, 19 (1–2):57–96, February 1993. ISSN 0378-3839. doi: 10.1016/0378-3839(93)90019-5.

GF Oertel. Sediment transport of estuary entrance shoals and the formation of swash platforms. *Journal of Sedimentary Research*, 42(4):858–863, December 1972. ISSN 1527-1404,. doi: 10.1306/74D72658-2B21-11D7-8648000102C1865D.

MD Orzech, EB Thornton, and JH MacMahan. Alongshore rip channel migration and sediment transport. *Marine Geology*, 271(3–4):278–291, June 2010. ISSN 0025-3227. doi: 10.1016/j.margeo.2010.02.022.

Roshanka Ranasinghe, Charitha Pattiaratchi, and Gerhard Masselink. A morphodynamic model to simulate the seasonal closure of tidal inlets. *Coastal Engineering*, 37(1):1–36, June 1999. ISSN 0378-3839. doi: 10.1016/S0378-3839(99)00008-3.

Roshanka Ranasinghe, Rodney McLoughlin, Andrew Short, and Graham Symonds. The Southern Oscillation Index, wave climate, and beach rotation. *Marine Geology*, 204 (3–4):273–287, March 2004. ISSN 0025-3227. doi: 10.1016/S0025-3227(04)00002-7.

A.J.H.M. Reniers and J.A. Battjes. A laboratory study of longshore currents over barred and non-barred beaches. *Coastal Engineering*, 30(1–2):1–21, March 1997. ISSN 0378-3839. doi: 10.1016/S0378-3839(96)00033-6.

Dano Roelvink and Ad Reniers. *A Guide to Modeling Coastal Morphology*, volume 12 of *Advances in Coastal and Ocean Engineering*. WORLD SCIENTIFIC, October 2011. ISBN 978-981-4304-25-2, 978-981-4304-26-9.

J. A. Roelvink. Dissipation in random wave groups incident on a beach. *Coastal Engineering*, 19(1–2):127–150, February 1993. ISSN 0378-3839. doi: 10.1016/0378-3839(93)90021-Y.

JA Roelvink and MJF Stive. Bar-generating cross-shore flow mechanisms on a beach. *Journal of Geophysical Research*, 94(C4):4785–4800, 1989. ISSN 2156-2202. doi: 10.1029/JC094iC04p04785.

Julie D. Rosati, L. Walton Todd, and Kevin Bodge. Longshore Sediment Transport. In *Coastal Engineering Manual*. U.S. Army Corps of engineers, Washington, DC., engineer m edition, 2002.

BG Ruessink and JR Miles. Modeling the alongshore current on barred beaches. *Journal of Geophysical Research: Oceans (1978–2012)*, 106(C10):22451–22463, 2001.

R.P. Savage. Laboratory determination of littoral transport rates. *Journal of Waterways and Harbours Division*, pages 69–92, 1962.

J.S. Schoonees and A.K. Theron. Review of the field-data base for longshore sediment transport. *Coastal Engineering*, 19(1-2):1–25, 1993. ISSN 0378-3839. doi: 10.1016/0378-3839(93)90017-3.

JS Schoonees and AK Theron. Accuracy and applicability of the SPM longshore transport formula. *Coastal Engineering Proceedings*, pages 2595–2609, 1994.

J.S. S Schoonees and A.K. K Theron. Improvement of the Most Accurate Longshore Transport Formula. In *International Conference on Coastal Engineering*, volume 1, pages 3652–3665, 1996.

W. J. Shaw and J. H. Trowbridge. The Direct Estimation of Near-Bottom Turbulent Fluxes in the Presence of Energetic Wave Motions. *Journal of Atmospheric and Oceanic Technology*, 18(9):1540–1557, September 2001. ISSN 0739-0572. doi: 10.1175/1520-0426(2001)018<1540:TDEONB>2.0.CO;2.

Andrew D. Short. *Handbook of beach and shoreface morphodynamics*. John Wiley, January 2000. ISBN 9780471965701.

P. Sireyjol. Communication sur la construction du port de Cotonou (Dahomey). *Coastal Engineering Proceedings*, pages 580–595, 1964.

ER Smith. Longshore sediment transport rate calculated incorporating wave orbital velocity fluctuations. Technical report, USACE, 2006.

ER Smith, P. Wang, and J. Zhang. Evaluation of the CERC formula using large-scale model data. 3, 2003.

Ernest R. Smith, Ping Wang, Bruce A. Ebersole, and Jun Zhang. Dependence of Total Longshore Sediment Transport Rates on Incident Wave Parameters and Breaker Type. *Journal of Coastal Research*, 25(3):675–683, May 2009. ISSN 0749-0208. doi: 10.2112/07-0919.1.

Marcel J. F. Stive. How Important is Global Warming for Coastal Erosion? *Climatic Change*, 64(1-2):27–39, May 2004. ISSN 0165-0009, 1573-1480. doi: 10.1023/B:CLIM.0000024785.91858.1d.

MJF Stive and JA Battjes. A model for offshore sediment transport. *Coastal Engineering Proceedings*, 1984.

MJF Stive and HJ De Vriend. Shear stresses and mean flow in shoaling and breaking waves. *Coastal Engineering Proceedings*, 1(24):594–608, January 1994. ISSN 2156-1028. doi: 10.9753/icce.v24.

I. A. Svendsen. Wave heights and set-up in a surf zone. *Coastal Engineering*, 8(4):303–329, November 1984. ISSN 0378-3839. doi: 10.1016/0378-3839(84)90028-0.

IA Svendsen. Analysis of surf zone turbulence. *Journal of Geophysical Research: Oceans*, 92(C5):5115–5124, 1987. ISSN 2156-2202. doi: 10.1029/JC092iC05p05115.

Edward B. Thornton and R. T. Guza. Transformation of Wave Height Distribution. *Journal of Geophysical Research*, 88(C10):PP. 5925–5938, 1983. doi: 198310.1029/JC088iC10p05925.

FCK Ting. Laboratory study of wave and turbulence velocities in a broad-banded irregular wave surf zone. *Coastal Engineering*, 43(3–4):183–208, August 2001. ISSN 0378-3839. doi: 10.1016/S0378-3839(01)00013-8.

FCK Ting and JT Kirby. Dynamics of surf-zone turbulence in a strong plunging breaker. *Coastal Engineering*, 24(3–4):177–204, March 1995. ISSN 0378-3839. doi: 10.1016/0378-3839(94)00036-W.

C. G. Du Toit and J. F. a. Sleath. Velocity measurements close to rippled beds in oscillatory flow. *Journal of Fluid Mechanics*, 112:71, 1981. ISSN 0022-1120. doi: 10.1017/S002211208100030X.

J. H. Trowbridge. On a Technique for Measurement of Turbulent Shear Stress in the Presence of Surface Waves. *Journal of Atmospheric and Oceanic Technology*, 15(1):290–298, February 1998. ISSN 0739-0572. doi: 10.1175/1520-0426(1998)015<0290:OATFMO>2.0.CO;2.

L. van Rijn. Unified View of Sediment Transport by Currents and Waves. III: Graded Beds. *Journal of Hydraulic Engineering*, 133(7):761–775, 2007a. ISSN 0733-9429. doi: 10.1061/(ASCE)0733-9429(2007)133:7(761).

L. van Rijn. Unified View of Sediment Transport by Currents and Waves. II: Suspended Transport. *Journal of Hydraulic Engineering*, 133(6):668–689, 2007b. ISSN 0733-9429. doi: 10.1061/(ASCE)0733-9429(2007)133:6(668).

L. C. van Rijn. *Principles of sediment transport in rivers, estuaries and coastal seas.* Aqua Publications, 1993. ISBN 90-800356-2-9.

L. C. van Rijn, D. Walstra, and M. van Ormondt. Unified View of Sediment Transport by Currents and Waves. IV: Application of Morphodynamic Model. *Journal of Hydraulic Engineering*, 133(7):776–793, 2007. ISSN 0733-9429. doi: 10.1061/(ASCE) 0733-9429(2007)133:7(776).

LC van Rijn. Unified view of sediment transport by currents and waves. II: Suspended transport. *Journal of Hydraulic Engineering*, 133(6):668–689, 2007c. ISSN 0733-9429. doi: 10.1061/(ASCE)0733-9429(2007)133:6(668).

Leo C. van Rijn. Unified View of Sediment Transport by Currents and Waves. I: Initiation of Motion, Bed Roughness, and Bed-Load Transport. *Journal of Hydraulic Engineering*, 133(6):649–667, June 2007d. ISSN 0733-9429, 1943-7900. doi: 10.1061/(ASCE) 0733-9429(2007)133:6(649).

Leo C. Van Rijn, Jan S. Ribberink, Jebbe Van Der Werf, and Dirk J.R. Walstra. Coastal sediment dynamics: recent advances and future research needs. *Journal of Hydraulic Research*, 51(5):475–493, 2013. ISSN 0022-1686. doi: 10.1080/00221686.2013.849297.

P. J. Visser. The proper longshore current in a wave basin. Technical report, TU Delft: Civil Engineering and Geosciences: Hydraulic Engineering, January 1982.

Philip Vitale. Movable-bed laboratory experiments comparing radiation stress and energy flux factor as predictors of longshore transport rate. page 106, 1981.

O.V. Voitsekhovich. Longshore sediment transport –generalized relations and observation data. Technical report, Ukrainian State Planning, Surveying, and Scientific Research Institute of Water- Management Construction., 1986.

DJR Walstra, GP Mocke, and F. Smit. Roller contributions as inferred from inverse modelling techniques. *Coastal Engineering Proceedings*, 1(25), January 1996. ISSN 2156-1028. doi: 10.9753/icce.v25.

P. Wang, NC Kraus, and RA Davis Jr. Total longshore sediment transport rate in the surf zone: field measurements and empirical predictions. *Journal of Coastal Research*, 14 (1):269–282, 1998. ISSN 0749-0208.

Ping Wang, BA Ebersole, ER Smith, and BD Johnson. Temporal and spatial variations of surf-zone currents and suspended sediment concentration. *Coastal Engineering*, 46 (3):175–211, August 2002. ISSN 0378-3839. doi: 10.1016/S0378-3839(02)00091-1.

Akira Watanabe, Takuzo Shimizu, and Kosuke Kondo. Field application of a numerical model of beach topography change. *Coastal Sediments (1991)*, pages 1814–1828, 1991.

GM Watts. A Study of Sand Movement at South Lake Worth Inlet Florida. 1953.

E Van Wellen, AJ Chadwick, and T. Mason. A review and assessment of longshore sediment transport equations for coarse-grained beaches. *Coastal Engineering*, 40(3): 243–275, June 2000. ISSN 0378-3839. doi: 10.1016/S0378-3839(00)00031-4.

WL|Delft Hydraulics. UNIBEST, A software suite for simulation of sediment transport processes and related morphodynamics of beach profiles and coastline evolution. Model description and validation. Technical report, 1992.

L.D Wright and A.D Short. Morphodynamic variability of surf zones and beaches: a synthesis. *Marine geology*, 56(1–4):93–118, April 1984. ISSN 0025-3227. doi: 10.1016/0025-3227(84)90008-2.

Curriculum Vitæ

João Mil-Homens

05-06-1976	Born in Caldas da Rainha, Portugal.

Education

1987–1994	High School - Escola Secundária do Bombarral, Bombarral
1994–2001	Bachelor in Physics Engineering Instituto Superior Técnico, Lisboa
2003–2005	MSc. Hydraulics and Water Resources Instituto Superior Técnico, Lisboa *Thesis:* Numerical Modelling of Wave Propagation with a Phase Resolving Model *Promotors:* Prof. A. Pires-Silva and Dr. Conceição Juana Fortes *Institution:* LNEC, Lisbon

Professional experience

2006–2010	WW – Consultores de Hidráulica e Obras Marítimas S.A. (Hydraulycs Consultancy), Lisbon

List of Publications

- Matthieu de Schipper, Sierd de Vries, J Mil-Homens, Ad Reniers, R Ranasinghe, MJF Stive,“Initial volume losses at nourished beaches and the effect of surfzone slope”, Coastal Sediments 2015: 8th International Symposium on Coastal Engineering and Science of Coastal Sediment Processes, San Diego, USA

- J Mil-Homens, R Ranasinghe, JSM van Thiel de Vries, MJF Stive,“Influence of profile features on longshore sediment transport”, Coastal Dynamics 2013: 7th International Conference on Coastal Dynamics, Arcachon, France

- J Mil-Homens, R Ranasinghe, JSM van Thiel de Vries, MJF Stive,“Re-evaluation and improvement of three commonly used bulk longshore sediment transport formulas”, Coastal Engineering 75, 29–39

- J Mil-Homens, R Ranasinghe, JT de Vries, M Stive, “Re-assessment and update of bulk longshore sediment transport formulas”, Coastal Engineering Proceedings 1 (33)

- J Mil-Homens, CJEM Fortes, AA Pires-Silva, “An evaluation of wave propagation simulations over a barred beach with a Boussinesq-type model”, Ocean Engineering 37 (2), 236-251

- J Mil-Homens, “Modelação Numérica da Propagação Marítima com Modelos de Resolução de Fase” (in Portuguese), LNEC, MSc Thesis

- J Mil-Homens, CJEM Fortes, “Linear and Non-linear Wave Model Performance Evaluated with Ponta Delgada Harbour Physical Model Data”, Poster, WAVES 2005, Madrid, Spain

- J Mil-Homens, CJEM Fortes, AA Pires-Silva, “Modelling Wave Propagation over a Barred Beach with the FUNWAVE Model”,IMAM2005, Lisbon

- J Mil-Homens, CJEM Fortes, AA Pires-Silva, ‘Comparação de Modelos Numéricos na Simulação da Propagação de Ondas Sobre Um Perfil de Praia do Tipo Barra-Fossa" (in Portuguese), 4as Jornadas Portuguesas de Engenharia Costeira e Portuária, Azores